Quantum Entanglement and Quantum Causal Analysis

Bin Yi

Supervisor: Prof. Sougato Bose

Department of Physics
University College London

A dissertation submitted in partial fulfilment for the degree of
Doctor of Philosophy

University College London March 2023

Declaration

I hereby declare that except where specific reference is made to the work of others, the contents of this dissertation are original and have not been submitted in whole or in part for consideration for any other degree or qualification in this, or any other university. This dissertation is my own work and contains nothing which is the outcome of work done in collaboration with others, except as specified in the text and Acknowledgements.

Bin Yi
March 2023

Acknowledgements

There are many people I wish to thank during my research career.

First, I would like to thank Professor Anthony J. Leggett, who brought me into scientific research when I was undergraduate. Over the past 8 years, Prof. Leggett has been encouraging and guiding me throughout.

Also, I am lucky to have Professor Sougato Bose as my PhD supervisor, to whom I am very grateful. Prof. Bose respects students' research freedom and provides full support over the execution. I have had a great experience during the course of my 3 years in UCL.

I would also like to thank my parents, Guiping Yi and Shanghui Zheng for their constant encouragement and financial support. Without them I would not be where I am today.

I also owe a great debt of gratitude to Professor Sixun Huang, who lectured me mathematics for physics wholeheartedly. We also had inspiring discussions about information science.

Finally, I would like to thank Professor X.San Liang for his knowledge and helping with my writings; Professor Urbasi Sinha, Professor Dipankar Home and Professor Anupam Mazumdar for helpful discussions and collaborations in the PhD projects.

Abstract

In this thesis, I consider two broad areas: the generation and verification of entanglement between large masses, and the analysis of causality in quantum dynamics. While the former is an extension of quantum mechanics in hitherto unexplored regimes such as for large masses and gravity, the latter provides a tool to probe quantum mechanics in complex networks.

The first part of the thesis introduces a new methodology, namely, "spatial qubits", to the study of non-classicality of macroscopic objects. Essentially, it allows one to treat a continuous variable system as an effective qubit. This offers us a way to detect the entanglement between a spin and a path in a Stern-Gerlach apparatus, which has never been verified to date. We offer a way to observe it. It also enables one to observe the entanglement between two neutral large masses induced by the Casimir interaction. This works in a regime of non-Gaussian states of the two masses, and can evidence the quantum nature of macroscopic forces. As a separate application, we apply the same technique to witness the quantum nature of gravity via a table-top experiment. This approach has the advantage of not requiring ancillary degrees of freedom such as spins, as well as not requiring a precise closure of an interferometer, to evidence the entanglement. However, here we find it necessary to prepare a highly position squeezed state of a mechanical system.

The other part of the thesis adopts concepts from classical causal analysis to the quantum regime. In particular, we generalize the notion of Liang-Kleeman information flow to quantum networks. The key feature of this theory is that an intervention is applied to the system and then the resulting changes on the target are observed. Causal influence is then quantified by relevant quantum entropic quantities such as the von Neumann entropy and quantum relative entropy. The presence of entanglement in the quantum domain uniquely manifests itself through some counter intuitive flows of information which we exemplify in small networks.

Impact statement

Quantum physics has revolutionized information science. After all, information is encoded in physical systems. The law of information is therefore intimately related to the underlying physical systems, which are fundamentally quantum.

The first part of this thesis pertains to the usage of a freely evolving massive object as a quantum bit, named qubit. This will be a door opener in the sense that it enables one to probe the very boundaries of quantum mechanics in a very simple way – whether massive objects such as nanocrystals obey things such as quantum contextuality. It is also applicable to witness entanglement generated between two such massive objects via their Casimir interaction. The massive spatial qubit methodology is also applied to witness the quantum nature of gravity. Though the scheme is yet very challenging to realize with state of art technology, the methodology provides a witness of quantum nurtured gravity purely through position measurements. Thus the impact of this part ranges from fundamental (quantumness verification) to potentially to applied (new types of qubits).

The second part of the thesis addresses causality quantification in quantum dynamics of many interacting quantum systems from an information theoretical perspective. Though there are several measures of correlations in quantum systems, most notably entanglement, and how these propagate, "causation" is not "correlation". There was no true measure of causation to date. Here a widely applied concept from classical dynamical systems is adapted to fill the gap. Several simple examples have been worked out in this preliminary work. The formalism quantifies causation with respect to von Neumann entropy. A more general formalism with respect to quantum relative entropy is also worked out. This is a first type of work generalizing a concept widely used in the context of classical networks to a quantum setting. This information flow-based approach is applicable to a wide range of topics in quantum physics from both fundamental and practical aspects. Its impact could be on analyzing causality in large scale quantum networks or potentially within quantum circuits.

List of publications

1. Yi, Bin, and Sougato Bose. "Quantum Liang Information Flow as Causation Quantifier." Physical Review Letters 129.2 (2022): 020501.

2. Bin Yi, Urbasi Sinha, Dipankar Home, Anupam Mazumdar, Sougato Bose. "Massive Spatial Qubits for Testing Macroscopic Nonclassicality and Casimir Induced Entanglement". arXiv:2106.11906 (2021)

3. Bin Yi, Urbasi Sinha, Dipankar Home, Anupam Mazumdar, Sougato Bose. "Spatial Qubit Entanglement Witness for Quantum Natured Gravity". arXiv:2211.03661

4. Bin Yi, Sougato Bose. "Causal analysis with respect to quantum relative entropy" (in preparation).

Table of contents

Chapter 1

Introduction

The development of quantum information science began in the early 20th century when quantum mechanics revolutionized physics. Why does physics have anything to do with information? After all, information is encoded in the state of some physical system, and computation is carried out on physical devices. Information theory was initially developed with classical physics. However, the universe is fundamentally quantum. How does quantum theory shed light on the nature of information? One important aspect is that in quantum theory, non-commuting observables can not be determined simultaneously. Therefore, acquiring any information from a physical state would unavoidably disturb the system. Such a limit does not exist in classical systems. The non-commutation relation also leads to the non-cloning principle which states that quantum information can not be copied perfectly, while classical information does not have such a restriction. The deep way in which quantum information differs from its classical counterpart was revealed by John Bell in 1964. He showed that the statistics predicted by quantum mechanics is inconsistent with any local hidden variable theory[19]. Quantum information can be stored in nonlocal correlations such as entanglement, which has no classical analogue. The study of quantum information as a coherent discipline culminated in the late 20th. Many of the central results in classical information theory can be extended to the quantum regime, including: compression of information and bounds on information transmission through noisy channels. This thesis consists of two parts. Part 1 focuses on a novel type of encoding of qubits. A new methodology of encoding qubit with a massive spatial test mass is presented. Chapter 2 gives an outline of this methodology, and applies it to test micro-macro entanglement and witness the quantum nature of the Casimir interaction. Chapter 3 applies this methodology to test the quantum nature of gravity and discusses its challenges. Part 2 focuses on information transmission. Chapter 4 presents a conception of information flow-based causality analysis and demonstrated with several

simple networks. Chapter 5 generalizes the causality analysis with respect to relative entropy and exemplified with ergodic versus non-ergodic model.

1.1 Physics of information

In this section, we review several milestones in history shaping our understanding of how physical systems place constraints on the transmission of information.

Landauer's principle

In 1961, Rolf Landauer first proposed that to erase one bit of information, a minimum possible amount of energy is required, known as the Landauer limit:

$$E = k_B T \log 2 \tag{1.1}$$

where T is the temperature of the heat bath, k_B is the Boltzmann constant. Landauer limit indicates that erasure of information is always dissipative. Any logically irreversible manipulation of information is accompanied by an increase in entropy of the entire system, involving the information processing device and the surrounding environment. From another perspective, if some information of a physical system is leaked to the environment, becoming inaccessible, then heat is generated and we are no longer able to extract useful work from that system. Following Landauer's principle, if a logical computation is reversible, that is, no information is lost during the process, then it maybe implemented without energy dissipation. Hence, considerable effort has been put into reversible computing.

Reversible computation

In 1973, Charles Bennett discovered that any logical computation can be performed with reversible steps. For instance, the NAND gate has two input bits and one output bit, which is irreversible. According to Landauer's principle, a minimum energy of $k_B T \log 2$ is needed to perform the computation because one bit of information is erased. However, the NAND gate can be replaced by reversible Toffoli gate in which all the information about the input is preserved:

$$(x, y, z) \to (x, y, z \oplus x \wedge y). \tag{1.2}$$

The Toffoli gate on 3 bits flips the third bit if the first two bits both take the value of 1 and do nothing otherwise. In the case where $z = 1$, it becomes the NAND gate of x and y. This

reversible computation can be performed, in principle, with 0 dissipation. One may question whether we have only delayed the energy cost to the end of the protocol because we generate useless information in bits during the process. Bennett showed that a reversible computation returns an answer to a logically reversible operation at the end of a computation and then reverse all the computation process and recover to its initial configuration. No information needs to be erased, hence, no energy cost.

To carry out reversible computation, one requires exquisite control of the physical process such that no uncertainty about the physical state is generated during the logical operation. All the energy would be recovered and ready to be reused for subsequent operations after each round, preventing dissipation into the environment in the form of heat. The motivation to improve the computational energy efficiency of computers beyond the Landauer limit drives research on reversible computing technologies. In practice, the Landauer limit is still far below the energy consumption of today's computers. But as computing hardware continues to reduce in size, reversible computation maybe the only viability to break the Landauer's limit and prevent the hardware from overheating.

Maxwell's demon

The second law of thermodynamics states that entropy of an isolated system never decreases. It implies that two physical systems with different temperature, when brought together and allowed to exchange heat with one another while isolated from the rest of the universe, would eventually evolve into thermal equilibrium with same temperature. In 1867, Maxwell proposed a paradox. In the thought experiment, one container is divided into two parts filled with same type of gas and same temperature. An imaginary demon sits on top of a trapdoor between the two partitions. If a high speed molecule fly from left to right, the demon would open the trapdoor and let it pass. If a slow-moving molecule fly from right to left, the demon would also open the trapdoor. Therefore, the left partition cools while the right partition heats up, without inputting energy. This conclusion clearly violates the second law of thermodynamics.

Motivated from the insights of Landauer, Bennett resolved the paradox in 1982. The explanation is that the demon must collect and store information of the molecules' speed. The recorded information is associated with some entropy and must be included in the calculation of the entire system's entropy. If the demon's memory is finite, the gas cannot be cooled without limit. If we erase the demon's memory and restore the demon's state to its initial condition, energy input is needed to compensate for the cooling achieved, as guaranteed by Landauer's limit.

The aforementioned work demonstrates that the study of communication and information is unalienable from the laws of physics. Understanding physical systems' behavior provides not only technological basis for computational devices, but also insights for information theory itself.

1.2 Classical Shannon Theory

Before we delve into the quantum regime, in this section, we review the key concepts from classical information theory. In 1948, Claude Shannon solved two central problems that serves as the benchmark of classical information theory:

1. Noiseless coding theorem: How much can a given message be compressed?
2. Noisy channel coding theorem: At what rate can reliable communications take place over noisy channel?

Both problems regard redundancy: How much redundancy in a message can be extracted out? How much redundancy must be incorporated in communication to fight against errors during transmission? Shannon demonstrated that entropy provides an appropriate quantification of redundancy in communication.

Noiseless coding theorem

File formats such as JPEG, ZIP, GIF, etc. are commonly used in today's telecommunication. They all have compression algorithms for the output source. Intuitively, one would expect that that compression algorithms can not reduce the output source to arbitrary small size. Shannon's theory of data compression proves this intuition.

A message consists of a string of letters. We shall consider the ideal situation in which each letter is selected *identically and independently* from an ensemble with probability distribution:

$$\{x_i, p(x_i)\}. \tag{1.3}$$

Each letter takes a value x_i with probability $p(x_i)$. A n-letter message is therefore associated with a probability:

$$p(x_1, x_2, ...x_n) = \prod_{=1}^{n} p(x_i). \tag{1.4}$$

Now we may ask, for an arbitrary n-letter message, can we convey the same message but with a shorter string of letters? The answer is yes. We shall start from binary scenario in which each letter is either 0 or 1 with probability p and $1-p$ respectively, where p takes

value in between 0 and 1. When n is large, we can apply the law of large numbers and obtain an asymptotic solution. Typical strings would contain about np of 0 and $n(1-p)$ of 1. The number of typical strings is given by the binomial coefficient $\binom{n}{np}$. Applying Stirling's formula to approximate factorials, we obtain:

$$\begin{aligned} \log \binom{n}{np} &= \log\left(\frac{n!}{(np)!\,(n-np)!}\right) \\ &\simeq nS(p), \end{aligned} \tag{1.5}$$

where

$$S(p) = -p\log p - (1-p)\log(1-p) \tag{1.6}$$

is the binary Shannon entropy. Adopting the convention of logarithms with base 2, the number of typical strings is therefore $2^{nS(p)}$. In the asymptotic limit $n \to \infty$, the probability that a message does not fall into the typical set goes to 0. Therefore, to encode a n-letter message, the codeword necessarily distinguishes $2^{nS(p)}$ number of messages. A codeword containing less than $nS(p)$ bits of information would unavoidably omit part of the message. For binary strings, as long as $p \neq 1/2$, the message's string length can be shortened without loss. Shannon's key observation is that not all strings of letters needs to be coded, but only the typical ones.

The binary scenario can be easily extended to incorporate the case where the letters sample from a k-letter alphabet. The number of typical strings is

$$\sim 2^{-nS(p(x))}, \tag{1.7}$$

where

$$S(X) = -\sum_x p(x)\log_2 p(x) \tag{1.8}$$

is the Shannon entropy of the ensemble $X = \{x, p(x)\}$. A letter sampling from this ensemble contains $S(X)$ bits of information on average and a n-letter message can be compressed to about $nS(X)$ bits.

One may ask if this compression rate is optimal, that is, is this the best we can do? The answer is yes. The formal proof of optimality is outside the scope of this thesis, but we shall briefly highlight the common approach to prove a coding theorem in information theory, being classical or quantum. The formal proof of coding theorem typically consists of two parts: *direct coding theorem* and the *converse theorem*.

The statement of the direct coding theorem is given by (as stated by Wilde [177]):

If the rate of compression is greater than the entropy of the source, then there exists a coding scheme that can achieve lossless data compression in the sense that it is possible to make the probability of error for incorrectly decoding arbitrarily small

The proof of the direct coding theorem generally relies on the concept of typical sequences as the length of the sequence becomes infinite. The statement of the converse theorem is given by [177]:

If there exists a coding scheme that can achieve lossless data compression with arbitrarily small probability of decoding error, then the rate of compression is greater than the entropy of the source.

Proof of the converse theorem typically appeals to information inequalities that bounds the relevant entropic quantities in the coding constructions.

Noisy channel coding theorem

The second problem in classical information theory is the transmission of information over noisy channel. We shall start from a simple example−bit-flip channel. The channel flips the input state with probability p and do nothing with probability $1-p$. Again, we assume that the channels are distributed independently and identically. If we use the channel as it is, the scheme only works if the bit-flip error does not occur. To improve communication quality, we may introduce some level of redundancy into the encoding process. For instance, we may encode a logical bit with 3 identical physical bit: $0 \to 000$, $1 \to 111$. At the receiving end, the decoder performs a majority vote. If two or more bits returns the same value, then the value is adopted.

Output	Probability
000	$(1-p)^3$
001,010,100	$p(1-p)^2$
011,110,101	$p^2(1-p)$
111	p^3

Table 1.1 The first column gives all possibilities of 3 "0" bit passing through bit-flip channel independently. The second column gives the corresponding probabilities

If the sender encodes logical bit "0", the possible physical bits at the output of bit-flip channels are 000,001,010,100,011,110,101,111 respectively. 000,001,010,100 would be decoded as "0", otherwise "1". This 3-bit majority vote scheme apparently reduces the possibility of error when p is small, compared with the no coding scenario. The cost is that the rate of transmission drops from 1 to 1/3. This simple example shows that there is a

trade-off between the transmission rate and the error probability. If we simply increase the number of encoding bit in the majority vote scheme, the error approaches 0 asymptotically, but so do the transmission rate. The question is then: can we code information in such a way that the error probability approaches 0 but the communication rate converges to a finite value asymptotically?

Shannon's channel coding theorem

The theorem provides an affirmative answer to the above question. For k data bits encoded on n physical bits carried by the channel, the rate of transmission is defined as:

$$R = k/n. \tag{1.9}$$

To achieve reliable communication under noisy channel, one needs to encode the message such that the number of bits flipped to change one codeword to another is maximized. For input message of length n, the bit-flip channel flips about np number of bits. The number of typical erroneous output strings is about $2^{nS(p)}$, occupying an error space of the input string. If the error space of any two input codewords overlap significantly, then decoding error would occur. Reliable communication can then be achieved if the codewords are far apart from each other so that their error space does not overlap. The condition of reliable transmission is then

$$2^n \geq 2^{nS(p)}2^k \tag{1.10}$$

or

$$1 - S(p) \geq R, \tag{1.11}$$

which simply states that the error space of all encoded message strings must be smaller than the total number of output message bits. The channel capacity per channel denoted C in this example is therefore:

$$C(p) = 1 - S(p). \tag{1.12}$$

Similar to the noiseless coding theorem, one needs to prove that the channel capacity is optimal, that is, the rate $R = C(p)$ is achievable asymptotically. Shannon's insight is that this rate can be achieved with random coding in the limit $n \to \infty$. Here, we will not delve into the proofs in detail, but to give a brief sketch. Consider a total of 2^{nR} random codewords generated by sampling from a uniform binary distribution for a single bit (0 and 1 occurs both with probability 1/2). The codewords transmit to the receiver through the use of n channels. The receiver then calculates the error space for each codeword, which consists of $2^{nS(p)}$ number of strings. The receiver decodes the message if only one codeword exist in

the space slightly larger than the error space$2^{nS(p)+\varepsilon}$, otherwise decodes arbitrarily. An error occurs when the error space containing the message's codeword contains another codeword. The error space contains a fraction of all the strings:

$$f = \frac{2^{n(S(p)+\varepsilon)}}{2^n}. \tag{1.13}$$

Due to the random uniform distribution, the probability of containing any other codeword other than the sent message in the target error space is f. The probability of containing any invalid codewords is therefore:

$$2^k f = 2^{-n(C(p)-\varepsilon)}, \tag{1.14}$$

where ε can be as small as we need. If we choose R slightly less than $C(p)$ of our choice, the decoding error vanishes as n goes to infinity. Hence, the rate $R = C(p)$ can be achieved asymptotically.

Shannon's choice of random coding greatly simplifies the mathematical analysis of the error probability. Shannon's breakthrough idea was to concentrate on the expectation of the average error probability with respect to the random code, rather than the average error probability itself.

The aforementioned binary example can be extended to a more general setting where the noisy channel is characterized by a conditional probability $p(y|x)$ when letter x is sent and letter y is received. We may sample the random codewords from a distribution $X = x, p(x)$. Following the same logic of reasoning, the optimal rate of transmission, achievable with negligible error probability, is given by:

$$R = I(X;Y), \tag{1.15}$$

where $I(X;Y)$ is the mutual information between X and Y defined as:

$$I(X;Y) = S(X) + S(Y) - S(XY). \tag{1.16}$$

$Y = y, p(y)$ is the output ensemble and $XY = (x,y), p(x,y)$ is the joint ensemble. This result demonstrates that the mutual information $I(X;Y)$ quantifies the information gained about X when accessible to Y. It is the maximum rate at which information can be transmitted over the channel reliably. The channel capacity is obtained by maximizing over the input ensemble X:

$$C = \max_X I(X;Y). \tag{1.17}$$

Now it is only a function of the noisy channel, characterized by the conditional probability $p(y|x)$.

Classical Causal analysis

Causal analysis is a sub-field of statistics unveiling the connection between cause and effect. Causal models are generally pertaining to probabilistic inferences about causal relationships from statistical data. The studies typically consists of sequences in time, a dynamical mechanism that governs the evolution of the sequences, certain correlation measures and action to eliminate the possible common causes. Judea pearl characterizes causal models in terms of 3 components: A set of internal variables which are determined by factors within the system, a set of external variables which are determined by factors outside the system and a set of structural equations that describes the dependence of internal variables on external variables. Causal analysis has found applications in climate change, economics, signal processing and machine learning, etc. In this thesis, we shall briefly introduce two most relevant causal measures: Granger causality and transfer entropy.

Granger causality

In 1969, Clive Granger established the first operational definition of causation using tools of probability theory. The essential idea is that causal actions alter the probability of their effects. Clive Granger pointed out that if prior knowledge of one time sequences is able to predict the future of another time series, then causality is witnessed. The intuitive explanation behind Granger causality is straightforward. If predictions of the value of a time series Y based on its own past values, together with the past values of another time series X, is more accurate than using past values of Y alone, then we say random variable X Granger-causes Y. Suppose we have three time series $X(t), Y(t), Z(t)$. We first try to predict $Z(t+1)$ using $X(t)$ and $Z(t)$. Then we incorporate $Y(t)$ to see if the prediction of $Z(t+1)$ is improved. If it does improve, then the past of $Y(t)$ contains information that $X(t)$ or $Z(t)$ does not possess in forecasting $Z(t+1)$. Granger formulated a statistical test to determine whether one variable Granger-causes another and widely accepted in economics. However, it is generally believed that the causality measure is limited. It may produce misleading results when multiple variables are involved. It does not address well with nonlinear causal relations, non-stationary time sequences, existence of rational expectations[125].

Transfer entropy

Transfer entropy, formulated by Schreiber[154] in 2000, measures directed information transfer between joint random sequences. Different from Granger causality, which is framed on prediction, transfer entropy focus on resolution of uncertainty. Given time series $X(t), Y(t), Z(t)$ as before, transfer entropy from Y to X is defined:

$$T_{Y\to X|Z} = S(X_{t+1}|X_t \oplus Z_t) - S(X_{t+1}|X_t \oplus Y_t \oplus Z_t), \tag{1.18}$$

where $S(\ |\ )$ denotes conditional Shannon entropy. The transfer entropy from Y to X is the difference between the entropy of X conditioned on the past of itself and Z, and the entropy of X given additionally the past of Y.

Transfer entropy shows a feature of asymmetry. That is, different classical correlation measures, which are symmetric, transfer entropy excludes the correlations due to common input states or common history. In 2009, it is shown that transfer entropy and Granger causality are equivalent for Gaussian states, substantiating the view point that causality measures are alienable from information [12].

1.3 The language of open quantum systems

In this section, we review the basic postulates of quantum physics and develop the language of open quantum system. Open quantum system refers to the scenario where a system is not isolated, but able to exchange information and energy with the environment. The mathematical formalism is needed when we delve into information/correlation measures of quantum systems. We start from the postulates of quantum physics.

Axiom 1. ***State*** *A quantum state is a ray living in a Hilbert space. It gives complete description of a system.*

A Hilbert space is a vector space over complex numbers. In Dirac's notation, a vector in Hilbert space is denoted $|x\rangle$. It satisfy the following properties

- Linearity: $\langle\phi|(\alpha|\psi_1\rangle + \beta|\psi_2\rangle) = \alpha\langle\phi|\psi_1\rangle + \beta\langle\phi|\psi_2\rangle$
- Positivity: $\langle\phi|\phi\rangle > 0$ for any non-zero $|\phi\rangle$
- Skew symmetry: $\langle\phi|\psi\rangle = \langle\psi|\phi\rangle^*$

A ray is almost identical to a vector $|\psi\rangle$, only differs by a complex scalar. Since an overall phase factor possess no physical significance, that is $|\psi\rangle$ and $e^{i\alpha}|\psi\rangle$ describe the same physical state, we may simply ignore the global phase factor.

Axiom 2. ***Observable*** *Observables in quantum physics are described by self-adjoint operators.*

An observable operator maps quantum state to state:

$$\hat{\mathbf{O}} : |\psi\rangle \rightarrow \hat{\mathbf{O}}|\psi\rangle. \tag{1.19}$$

Observable operators are linear, that is:

$$\hat{\mathbf{O}}(\alpha|\psi\rangle + \beta|\phi\rangle) = \alpha\hat{\mathbf{O}}|\psi\rangle + \beta\hat{\mathbf{O}}|\phi\rangle. \tag{1.20}$$

Further more, the eigenvalues of observable operators are interpreted as physical measurable values, they must be represented by real numbers. So we require that the operators are also self-adjoint:

$$\hat{\mathbf{O}} = \hat{\mathbf{O}}^{\dagger}, \tag{1.21}$$

where $\hat{\mathbf{O}}^{\dagger}$ is the complex conjugate of operator $\hat{\mathbf{O}}$:

$$\langle\phi|\hat{\mathbf{O}}\phi\rangle > 0 = \langle\hat{\mathbf{O}}^{\dagger}\phi|\phi\rangle > 0. \tag{1.22}$$

Self-adjoint operators can be spectral decomposed:

$$\hat{\mathbf{O}} = \sum_i \lambda_i |i\rangle\langle i|, \tag{1.23}$$

where λ_i are eigenvalues of the operator $\hat{\mathbf{O}}$ and $\{|i\rangle\}$ forms a complete orthonormal basis of the eigenstates. Therefore, we have $\hat{\mathbf{O}}|i\rangle = \lambda_i|i\rangle$.

Axiom 3. ***Evolution*** *The dynamical evolution of a closed quantum system is governed by a unitary operator, generated from its Hamiltonian function.*

$$|\phi(t)\rangle = U(t)|\phi(0)\rangle, \tag{1.24}$$

where $U(t)$ is the unitary operator $U(t) = e^{-iHt/\hbar}$ and H is the corresponding Hamiltonian function. The Planck's constant $\hbar$ may be set to 1 for convenience. The Hamiltonian of a system is also an observable operator. So it is self-adjoint. Its eigenvalues are the accessible energy levels of the system. An infinitesimal version of the above equation reads:

$$|\phi(t+\Delta t)\rangle = (I - iH(t)\Delta t)|\phi(t)\rangle. \tag{1.25}$$

This is the Schroedinger equation.

Axiom 4. ***Measurement*** *If a measurement of observable $\hat{\mathbf{O}}$ acts on a physical state $|\phi\rangle$, the outcome is one of the observable's eigenvalue λ_i with probability*

$$p_i = |\langle i|\phi\rangle|^2. \tag{1.26}$$

After the measurement, the state $|\phi\rangle$ collapse to the eigenstate associated with the measured value λ_i. So the post-measurement state is $|i\rangle$.

If the same measurement is conducted on an ensemble of identically prepared states, each described by $|\phi\rangle$, the expectation value of the outcomes is

$$Expectation[\hat{\mathbf{O}}] = \sum_i p_i\lambda_i = \sum_i \lambda_i\langle\phi|i\rangle\langle i|\phi\rangle = \langle\phi|\hat{\mathbf{O}}|\phi\rangle. \tag{1.27}$$

Axiom 5. ***Composite Systems*** *The composite of two Hilbert space $\mathscr{H}_A$ and $\mathscr{H}_B$ of system A and B together, is the tensor product of the two $\mathscr{H}_A \otimes \mathscr{H}_B$*

If system A is prepared in state $|\phi_A\rangle$, system B is prepared in state $|\phi_B\rangle$, the state of the composite system AB is then $|\phi_A\rangle \otimes |\phi_B\rangle$. By the linearity of quantum state, we immediately obtain that if $\{|i\rangle\}$ forms a complete orthonormal basis for $\mathscr{H}_A$ and $\{|j\rangle\}$ forms an orthonormal basis for $\mathscr{H}_B$, then $\{|i\rangle \otimes |j\rangle\}$ is a basis for $\mathscr{H}_A \otimes \mathscr{H}_B$.

Density operator

The stated axioms are formulated in terms of state vectors. Density operator is an alternative formalism, which is mathematically equivalent. One may then wonder what is the point of introducing this additional formalism. The reason is that it is particularly convenient in describing open systems. The entropic quantities in quantum information theory is typically formulated with respect to the density operator description of quantum systems.

We can consider the case where we don't have perfect knowledge of the quantum state, but a classical mixture of various possibilities. To be more precise, let a quantum system described by a set of quantum states $|\phi_i\rangle$, each with probability p_i. The quantum state is described by the set $\{p_i, |\phi_i\rangle\}$. A density state of a quantum system is defined by:

$$\rho = \sum_i p_i|\phi_i\rangle\langle\phi_i|. \tag{1.28}$$

If the density state is exactly known, that is, there is only one term in the summation $\rho = |\phi\rangle\langle\phi|$, it is called a pure state. Otherwise, it is a mixed state because it is a mixture of a set of pure states. If a quantum system is described by a mixture of density states ρ_i, instead

of pure states, it is not difficult to see that the density state describing the system is

$$\rho = \sum_i p_i \rho_i. \tag{1.29}$$

Since the evolution of a quantum state vector is governed by axiom3, a mixture of a quantum state then evolves into a mixture of states with same probability distribution but each state evolves according to a unitary operator. The density state then evolves to:

$$\rho = \sum_i p_i |\phi_i\rangle\langle\phi_i| \rightarrow \rho = \sum_i p_i U|\phi_i\rangle\langle\phi_i|U^\dagger = U\rho U^\dagger. \tag{1.30}$$

The measurement acting on a quantum state vector is governed by axiom4. Translating into the language of density state, we obtain the probability of obtaining a particular outcome λ_j upon measuring $\hat{\mathbf{O}}$ is:

$$p(j) = \sum_i p_i \langle\phi_i|j\rangle\langle j|\phi_i\rangle = Tr[E_j\rho], \tag{1.31}$$

where $E_j = |j\rangle\langle j|$ is the projection operator corresponding to the eigenvalue λ_j.

Properties of the density operator

So far, the formalism of density operator is developed on top of the state vector description and relies on the ensemble interpretation. The density operator representation of quantum physics is equivalent to the state vector-based representation. The characterization based on density operator can be regarded as intrinsic too. Here, we further develop the properties of density operators.

A density operator must satisfy three conditions: it must have trace =1, positively defined in sense of Eq. 1.33 and self-adjoint. For a density operator ρ

$$Tr[\rho] = \sum_i p_i Tr[|\phi_i\rangle\langle\phi_i|] = \sum_i p_i = 1. \tag{1.32}$$

The positive requirement can also be easily proven. Take arbitrary state $|\psi\rangle$

$$\langle\psi|\rho|\psi\rangle = \sum_i p_i \langle\psi|\phi_i\rangle\langle\phi_i|\psi\rangle \geq 0, \tag{1.33}$$

where $\langle\psi|\phi_i\rangle\langle\phi_i|\psi\rangle$ is the probability of projecting state $|\phi_i\rangle$ onto $|\psi\rangle$, which is greater or equal to 0. The self-adjointness is also obvious from the ensemble formalism:

$$\begin{aligned}\rho^\dagger &= \sum_i p_i(|\phi_i\rangle\langle\phi_i|)^\dagger \\ &= \sum_i p_i|\phi_i\rangle\langle\phi_i| \\ &= \rho. \end{aligned} \tag{1.34}$$

The self-adjointness property of density operator indicates that any density state ρ must have a spectral decomposition

$$\sum_i \lambda_i|i\rangle\langle i|, \tag{1.35}$$

where $\{|i\rangle\}$ forms an orthonormal basis. The positivity and unit trace property of density operator guarantees that $\lambda_i > 0$ and $\sum_i \lambda_i = 1$. Therefore, any valid density operator can be written as an ensemble of orthonormal states $\{\lambda_i, |i\rangle\}$.

Note that the unit trace criteria applies to any density operator, being pure or mixed. But if we look at the trace of density operator squared:

$$Tr[\rho^2] = \sum_i p_i^2. \tag{1.36}$$

It is obviously equal to unit $Tr[\rho^2] = 1$ if ρ is a pure state, since there is only one term in the summation. But less than 1 $Tr[\rho^2] < 1$ if the density operator ρ is mixed. This operation is then a test of whether a density operator is mixed or pure.

Reformulating axioms

Now we are in a position to reformulate the axioms of quantum physics using the language of density operator.

Axiom 1 regards the description of state. For a closed system, its density operator gives a complete description. The density operator lives in the Hilbert space associated with the physical system. It must be positive, self-adjoint and its trace is unity.

Axiom 2 states that observables in quantum physics are described by self-adjoint operators. This statement remains unchanged.

Axiom 3 is about the evolution of quantum state. For a closed system, the time evolution of its density operator is governed by a unitary transformation

$$\rho(t) = U(t)\rho(0)U(t)^\dagger. \tag{1.37}$$

Axiom 4 is relevant to the measurement process. A Quantum measurement of an observable $\hat{\mathbf{O}}$ is represented by a set of projection operators $\{E_i\}$, where $E_i = |i\rangle\langle i|$ and $\{|i\rangle\}$ is the eigenvectors of $\hat{\mathbf{O}}$. The index i refers to a potential outcome of the measurement. The projection operators are complete, that is

$$\sum_i E_i = I. \tag{1.38}$$

The probability of obtaining a result i upon conducting the measurement is the following:

$$p_i = Tr[E_i\rho]. \tag{1.39}$$

At the end of the measurement, the density state collapses to the eigenstate $|j\rangle\langle j|$ associated with the measured outcome j.

Axiom 5 states the Hilbert space of composite physical systems are represented by the tensor product of those of their component systems. If the density operator of two Hilbert spaces $\mathscr{H}_A$ and $\mathscr{H}_B$ is denoted ρ_A and ρ_B, the density operator of their composite system is then $\rho_A \otimes \rho_B$.

One may wonder given the density operator of a composite system ρ_{AB}, how to recover the density state of its components? It is obtained by the partial trace operation defined as follows:

$$Tr_B[|A_1\rangle\langle A_2| \otimes |B_1\rangle\langle B_2|] = |A_1\rangle\langle A_2|Tr[|B_1\rangle\langle B_2|], \tag{1.40}$$

where the partial trace is taken over subsystem B. For a product state $\rho_{AB} = \rho_A \otimes \rho_B$, it is obvious that its partial trace over B gives the density state description of A, $\rho_A = Tr_B[\rho_{AB}]$. But when the density state ρ_{AB} is mixed, why does the partial trace operation still give the correct subsystems' density states?

The answer is that the partial trace operation is the only operation that gives the correct measurement statistics for observing a component system. This is also a crucial step to understand the quantum description of open system. For simplicity, we shall consider bipartite system AB. The density operator of the composite system shall be denoted ρ_{AB} and let $\hat{O}_A$ denotes an observable for measurement on system A. Since we are not doing anything on B, the operation acting on B can be denoted by the identity operator I_B. The overall operation performed on the composite system AB is therefore

$$\hat{O}_{AB} = \hat{O}_A \otimes I_B = \sum_i \lambda_i |i\rangle\langle i|_A \otimes I_B. \tag{1.41}$$

After the second equal sign, we have exploited the spectral decomposition of observable $\hat{O}_A$ and λ_i are the eigenvalues.

The expectation value of the observable $\hat{O}_{AB}$ acting only on subsystem A is

$$\begin{aligned} Expectation[\hat{O}_{AB}] &= Tr[\hat{O}_A \otimes I_B . \rho_{AB}] \\ &= \sum_{j,y} a^*_{jy} \langle j|_A \otimes \langle y|_B (\hat{O}_A \otimes I_B) \sum_{ix} a_{ix} |i\rangle_A \otimes |x\rangle_B \\ &= \sum_{ijx} a*_{jx} a_{ix} \langle j|\hat{O}_A|i\rangle = Tr[\hat{O}_A \rho_A], \end{aligned} \tag{1.42}$$

where we have expanded $\rho_{AB} = |\psi\rangle\langle\psi|_{AB}$ in the basis $\{|i\rangle_A \otimes |x\rangle_B\}$:

$$|\psi\rangle_{AB} = \sum_{ix} a_{ix} |i\rangle_A \otimes |x\rangle_B \tag{1.43}$$

and

$$\rho_A = Tr_B[\rho_{AB}] = \sum_{ijx} a_{ix} a^*_{jx} |i\rangle\langle j|. \tag{1.44}$$

Since the above calculation is general to any observable $\hat{O}_A$, we can then interpret $\rho_A = Tr_B[\rho_{AB}]$ as an ensemble of quantum state containing all the information we can acquire from subsystem A.

Ambiguity of ensembles

The density operators in a Hilbert space form a convex set, that is, a mixed density operator can be expressed as an ensemble of pure states in various ways. The pure states are unique and they are extremal points of the convex set. To see this, consider two density operator ρ_1 and ρ_2, we can construct density operator ρ_3 as a convex linear combination of ρ_1 and ρ_2:

$$\rho_3 = \eta\rho_1 + (1-\eta)\rho_2, \tag{1.45}$$

where η is a real number satisfying $0 \leq \eta \leq 1$. It is easy to check that ρ_3 satisfies the necessary criteria as density operator, that is, it is positive, self-adjoint and has unit trace. Therefore, we have shown that density operators can be expressed as a summation of other density operators in more than one ways. The only exception is pure states. It can be easily proven that if ρ_3 is pure, then ρ_1 must equal to ρ_2. Therefore, pure states consist of extremal set of the density state because they can not be expressed as linear combination of other elements in the convex set of vectors. The any mixed state is not in the extremal set since the spectral decomposition of any mixed state $\rho = \sum_i p_i |i\rangle\langle i|$ consists of more than 1 term in the

summation. A mixed state can be regarded as different linear combinations of pure states, all of which are experimentally indistinguishable if we look at the system alone. In the next section when we discuss mixed state entanglement, we will come back to this point.

Generalized measurement

In the previous section, we have seen how the density operator formalism extends the state vector-based language to describe open systems' state. In this section, we further develop the language of open system by generalizing orthogonal measurement to involve more general quantum operations.

The previously stated axiom 4 is that measurement conducted on an isolated system is described by an orthogonal projection operator. However, if we only look at part of a larger system, the measurement operation acting on the subsystem does not necessarily belong to orthogonal projection operators. Generalized measurement is common in practice. To make an observation, experimentalists have to couple the observable with variables representing the measurement apparatus, which we shall regard as an ancillary system. The coupling between the state of a mircroscopic quantum system and an ancilla, which we may take to be a classical indicator, would then allow us to acquire information of the microscopic quantum system by reading the value of the classical variable.

For simplicity, we shall consider two dimensional systems spanned by $\{|0\rangle, |1\rangle\}$. The result can be easily extended to multi-dimensions. Let the microscopic system of interest labeled by A and the ancillary system labeled by B. Suppose they evolve with the joint Unitary operation:

$$(\alpha|0\rangle + \beta|1\rangle)_A \otimes |0\rangle_B \xrightarrow{U} \alpha|0\rangle_A \otimes |0\rangle_B + \beta|1\rangle_A \otimes |1\rangle_B. \tag{1.46}$$

The ancilla initially prepared in $|0\rangle$ is now coupled to the microscopic system A. If we measure the ancilla in the $\{|0\rangle, |1\rangle\}$ basis, system A is then also projected in the $\{|0\rangle, |1\rangle\}$ basis, leading to an orthogonal projection acting on A. However, if we measure the ancilla in different basis, say $|\pm\rangle = (|0\rangle \pm |1\rangle)/\sqrt{2}$, then the operation acting on A is no longer orthogonal. To see this, we shall write the evolved state in new basis

$$\begin{aligned} & \alpha|0\rangle_A \otimes |0\rangle_B + \beta|1\rangle_A \otimes |1\rangle_B \\ = \; & I/\sqrt{2}|\phi\rangle_A \otimes |+\rangle_B + \sigma_z/\sqrt{2}|\phi\rangle_A \otimes |-\rangle_B, \end{aligned} \tag{1.47}$$

where $|\phi\rangle_A = \alpha|0\rangle + \beta|1\rangle$ is the original state of A, $I = \begin{pmatrix} 1 & 0 \\ 0 & 1 \end{pmatrix}$ is the identity operator, $\sigma_z = \begin{pmatrix} 1 & 0 \\ 0 & -1 \end{pmatrix}$ is the Pauli-Z operator. Therefore, measuring the ancillary system in the $\{|\pm\rangle\}$ basis maps the system A to either $|\phi\rangle_A$ or $\sigma_z|\phi\rangle_A$.

The result can be generalized to multiple dimensions, in general, the evolution of a microscopic system and an ancilla $|\phi\rangle_A \otimes |0\rangle_B$ can be represented as

$$\sum_m M_m|\phi\rangle_A \otimes |m\rangle_B. \tag{1.48}$$

We may write

$$E_m = M_m^\dagger M_m. \tag{1.49}$$

The set $\{E_m\}$ is called positive operator valued measurement (POVM). When a POVM $\{E_m\}$ is performed on an open quantum system with density operator ρ, the probability of obtaining result m is

$$p(m) = Tr[\rho E_m]. \tag{1.50}$$

POVM satisfies the following three properties:

- Completeness: $\sum_m E_m = I$
- Positivity: $\langle\phi|E_m|\phi\rangle \geq 0$ for arbitrary state $|\phi\rangle$
- Hermiticity: $E_m = E_m^\dagger$

The requirement of normalization $|\sum_m M_m|\phi\rangle_A \otimes |m\rangle_B|^2 = 1$ guarantees that

$$\sum_m M_m^\dagger M_m = I. \tag{1.51}$$

The above is the completeness relation of POVMs. Positivity and Hermiticity can also be easily proved in a similar manner.

Quantum channel

So far, we have reviewed how does part of a closed system can be described by density operator and the measurement process can be modeled by positive operator valued measurement. What about evolution? The evolution of a closed system is governed by unitary operator. After tracing out the ancillary systems, how does the open system of interest evolve?

In fact, we already have a solution to this question when we introduced POVM. When the system of interest is described by $\rho_A = |\phi\rangle_A\langle\phi|_A$, the evolved density operator after tracing out the ancillary system is given by:

$$\varepsilon(\rho_A) = \sum_m M_m \rho_A M_m^\dagger, \tag{1.52}$$

where the operators $\{M_m\}$ are the same operators appearing in generalized measurement and satisfy the properties of completeness, positivity and self-adjointness. These operators are called Kraus operators. ε denotes a linear map acting on density operators. It is called a quantum channel. In quantum communication the density state mapping ε can be regarded as a channel that links the sender who sends out the state ρ and the receiver who receives $\varepsilon(\rho)$.

Quantum channels are trace preserving completely positive maps, because it satisfies the following properties:

- Preserve trace: $Tr[\varepsilon(\rho)] = Tr[\rho]$
- Preserve positivity: If $\rho \geq 0$, then $\varepsilon(\rho) \geq 0$
- Preserve Hermiticity: If $\rho = \rho^\dagger$, then $\varepsilon(\rho) = \varepsilon(\rho)^\dagger$
- Linear: $\varepsilon(\alpha\rho_A + \beta\rho_B) = \alpha\varepsilon(\rho_A) + \beta\varepsilon(\rho_B)$

In quantum communication, when the system carrying information is sent through a quantum channel, unavoidable interaction with its environment decoheres the system. That is, the system evolves into a mixture of states. The decoherence process is conveniently described with the open system language.

Decoherence

Decoherence refers to the loss of quantum coherence. For a superposition state, as long as the relative phase exists between different states remain definite, the state is coherent. A definite phase is essential to perform quantum computational tasks. If a system is closed, that is, it does not interact with external systems, coherence would be preserved perfectly. However, when the system is open, that is, we allow it to interact with the environment, the system unavoidably interacts with the environment. The language of open system tells us that the evolution of the system is described by a quantum channel. In general, the system evolves from a pure state to a mixed state. Typically, we do not have access to the environment, we can not measure and obtain information from the environment. Therefore, the dynamics of the system is irreversible. Some information about the system is now lost.

Decoherence places a great challenge to the realization of quantum computers. The execution of quantum information protocols rely on the manipulation of coherent states. How to prevent unnecessary interaction with the environment is essential in quantum computing.

For closed systems, the evolution is described by a unitary transformation. However, we usually find it convenient to describe the evolution with a differential equation, namely, the Schrodinger equation, which is essentially equivalent to the unitary evolution over an infinitesimal time duration. For open systems, the evolution is described by quantum channels. In the scenario where the evolution is Markovian, that is, information loss continuously and never returns, the quantum channel description can be replaced by a differential equation called the master equation.

In this thesis, one of the primary systems under consideration is a mass in a spatial quantum superposition (a quantum superposition of two spatially distinct states). We focus on the exponential decay of the off-diagonal components of our density matrix in the position basis. Position-localization decoherence can be described by the dephasing channel:

$$\langle x_1|\rho(t)|x_2\rangle \propto e^{-\Gamma t}\langle x_1|\rho(0)|x_2\rangle, \tag{1.53}$$

where Γ is the dephasing rate and it is typically a function of the separation $|x_1 - x_2|$. This quantum channel is common to decoherence due to interaction with an environment. The corresponding master equation is given by [144]:

$$\langle x_1|\frac{d\rho(t)}{dt}|x_2\rangle = \frac{i}{\hbar}\langle x_1|[\rho, H]|x_2\rangle - \Gamma(x)\langle x_1|\rho(t)|x_2\rangle, \tag{1.54}$$

where $x = |x_1 - x_2|$ and H is the Hamiltonian and the decoherence rate:

$$\Gamma = \gamma(1 - e^{-\frac{x^2}{4a^2}}). \tag{1.55}$$

The value of the localization strength γ and the localization distance a depends on the nature of the decoherence source. The expression of decoherence rate can be greatly simplified in the following two limits:

$$\Gamma \sim \begin{cases} \Lambda x^2 & x << 2a \\ \gamma & x >> 2a \end{cases}, \tag{1.56}$$

where $\Lambda = \gamma/(4a^2)$. In the short range limit $x << 2a$, the decay rate is proportional to separation squared. In the long range limit $x >> 2a$, the decay rate is a constant independent of the separation. Here we focus on the two main source of decoherence for the spatially

superposed states of masses considered in the thesis: air molecules scattering and black-body radiation.

Air molecules scattering

The thermal wavelength of a typical air molecule is given by[144]

$$\lambda^{air} = 2\pi\hbar/\sqrt{2\pi m k_b T_e}, \tag{1.57}$$

where m is the mass of molecule, T_e is external temperature. Substituting $m \sim 28.97$amu and $T_e \sim 4.5$K gives the localization distance $2a_{air} = \lambda^{air} \sim 0.15nm$. The superposition size considered in this thesis is much larger than $2a_{air}$, the long distance limit applies $x >> 2a$. The decoherence rate is then characterized by the constant parameter γ_{air}. It is given by

$$\gamma_{air} = \frac{16\pi\sqrt{2\pi}PR^2}{\sqrt{3}\bar{v}m}, \tag{1.58}$$

where P is the pressure of the gas, R is the molecule effective radius, $\bar{v}$ is the average velocity of the molecules.

Blackbody radiation

The thermal wavelength for photons is given by [144]

$$\lambda^{bb} = \pi^{2/3}\hbar c/(k_b T_e). \tag{1.59}$$

For external temperature $T_e = 4.5$K, the wavelength $\lambda^{bb} = 2a_{bb} \sim 1mm$. This localization distance is much larger than the superposition size considered in this thesis. Therefore the short range limit $x << 2a$ applies. The localization parameter Λ_{bb} consists of three contributions from scattering, absorption and emission of thermal photons

$$\Lambda_{bb} = \Lambda_{sc} + \Lambda_a + \Lambda_e. \tag{1.60}$$

Each of the component is given by [144]

$$\Lambda_{sc} = \frac{8!\,8\zeta(9)cR^6}{d9\pi}\left(\frac{k_bT_e}{\hbar c}\right)^9 Re\left[\frac{\varepsilon_{bb}-1}{\varepsilon_{bb}+2}\right]^2 \tag{1.61}$$

$$\Lambda_a = \frac{16\pi^5 cR^3}{189}\left[\frac{k_bT_e}{\hbar c}\right]^6 Im\left[\frac{\varepsilon_{bb}-1}{\varepsilon_{bb}+2}\right] \tag{1.62}$$

$$\Lambda_e = \frac{16\pi^5 cR^3}{189}\left[\frac{k_bT_i}{\hbar c}\right]^6 Im\left[\frac{\varepsilon_{bb}-1}{\varepsilon_{bb}+2}\right], \tag{1.63}$$

where ζ is the ζ Riemann function, ε_{bb} is the dielectric constant of the relevant blackbody spectrum. T_e and T_i are external and internal temperature respectively. Among the three contributions, the emission localization parameter dominates because it is usually much harder to cool the bulk temperature of the object than the external temperature.

1.4 Quantum entanglement and Bell-CHSH inequality

Quantum entanglement is at the core of quantum communication. In many protocols, quantum advantage over classical communication is obtained by exploiting quantum entanglement. It is a phenomenon that multi-component systems, for instance a group of particles, interact or generated in a way such that the quantum state of each component can not be described independently, even if they may be separated distantly. Entanglement is a phenomenon unique to quantum physics. There is no such analogous quantity in classical mechanics. The mathematical statement of entanglement of rather simple:

Consider quantum systems A and B living in two different Hilbert space $\mathscr{H}_A$ and $\mathscr{H}_B$. If the state of system A is $|\phi\rangle_A$ and the state of system B is $|\psi\rangle_B$. The composite system is then

$$|\phi\rangle_{AB} = |\phi\rangle_A \otimes |\psi\rangle_B. \tag{1.64}$$

State that can be expressed in the product form is called separable states. Otherwise, it is entanglement. In general, the state of a composite system can be expanded in the basis $\{|i\rangle_A \otimes |j\rangle_B\}$ where $\{|i\rangle_A\}$ spans $\mathscr{H}_A$ and $\{|j\rangle_B\}$ spans $\mathscr{H}_B$:

$$|\phi\rangle_{AB} = \sum_{i,j} a_{ij}|i\rangle_A \otimes |j\rangle_B. \tag{1.65}$$

In general the coefficient a_{ij} can not be separated, leading to entangled state. A simple example in two level system is:

$$\frac{1}{\sqrt{2}}(|0\rangle_A \otimes |1\rangle_B - |1\rangle_A \otimes |0\rangle_B). \tag{1.66}$$

In this case, the state of the composite system can not be represented in a product form. If a measurement in the $\{|0\rangle, |1\rangle\}$ basis is performed on system A, the two outcomes of 0 and 1 both occur with 50% probability.

- If 0 is measured, the system state collapses to $|0\rangle_A \otimes |1\rangle_B$
- If 1 is measured, the system state collapses to $|1\rangle_A \otimes |0\rangle_B$

if the first situation occurs, the state of system B becomes $|1\rangle_B$. That is, measurement in the $\{|0\rangle, |1\rangle\}$ basis would always return 1. If the latter situation occurs, then measurement on system B would always return 0. The result holds regardless of whether A and B are separated distantly or no. We can picture the state of $\{|0\rangle, |1\rangle\}$ as the spin or polarization of particles. When a pair of particles are generated such that their spins or polarization are entangled. If one particle is spin up then the other one is spin down and wise versa. The act of measurement on one particle collapse the entire entangled system instantaneously, altering the measurement result of the other particle. This is the foundation of the EPR paradox proposed by Albert Einstein, Boris Podolsky and Nathan Rosen in 1935.

The EPR paradox is a thought experiment which involves a pair of entangled particles. The particles are distantly separated. If the position of one particle is measured, the position of another particle can then be predicted. Similar for momentum measurements as well. Einstein, Podolsky and Rosen argues that no action taken on one particle can instantaneously affect the other particle because the instantaneous transmission of information is forbidden by the theory of relativity. Therefore, they infer that quantum theory is incomplete, that is, the position and momentum of a particle must have definite values prior to measurements. Along this line of thinking, hidden variable theories were proposed. In 1964, John Bell proposed a statistical measure that tests the validity of hidden variable theories versus quantum mechanics.

Bell inequality

Bell's theorem shows that quantum physics is incompatible with local hidden variable theories. Local refers to the principle that a particle can only be influenced by its surroundings and interactions must occur through a mediator, which travels with a speed no greater than

the speed of light. Hidden variable theories represent the theories which assume that the physical observables of a system is predetermined and not affected by how one performs the measurement. The hidden variable theories regard the probabilistic predictions of quantum theory as a result of ignorance of the predetermined hidden variables, hence quantum theory is incomplete. John Bell found out that if we consider a pair of entangled particles and then perform measurement on the particles locally, hidden variable theories would then impose a mathematical constraint on the outcomes of how the measurements are correlated. In other words, quantum mechanics' prediction of the measured correlations would differ from those predicted by hidden variable theories.

Consider two parties Alice and Bob, who performs two sets of measurements A_1, A_2 and B_1, B_2. Each measurement results in either $+1$ or -1. Here we assume that 1. the physical observables a_1, a_2, b_1, b_2 are predetermined, that is, they exist independent of whether it is being measured or not; and 2. locality, that is, Bob's choice of measurement has no impact on Alice's result and vice versa. Consider the following combination of measured observables:

$$a_1 b_1 + a_1 b_2 + a_2 b_1 - a_2 b_2. \tag{1.67}$$

You can convince yourself easily that the combination can only takes the value of either $+2$ or -2. Therefore if the same experiment is conducted with the same setting multiple times, the expectation value of the measured set must be no greater than 2:

$$\langle A_1 B_1 \rangle + \langle A_1 B_2 \rangle + \langle A_2 B_1 \rangle - \langle A_2 B_2 \rangle \leq 2. \tag{1.68}$$

This is called Bell-CHSH inequality. As we shall see later that Quantum mechanics give a different bound on the inequality.

Consider an initial state prepared in maximally entangled state:

$$|\psi\rangle = \frac{1}{\sqrt{2}}(|0\rangle_A \otimes |1\rangle_B - |1\rangle_A \otimes |0\rangle_B) \tag{1.69}$$

and let the measurement represented by:

$$\begin{aligned} A_1 &= \sigma_z, A_2 = \sigma_x \\ B_1 &= -\frac{\sigma_x + \sigma_y}{\sqrt{2}}, B_2 = -\frac{\sigma_x - \sigma_y}{\sqrt{2}}, \end{aligned} \tag{1.70}$$

where σ_x and σ_z are Pauli-X and Pauli-Z operators respectively. The eigenvalues of all the measurements A_1, A_2, B_1, B_2 are either -1 or 1. Substituting the maximally mixed initial state

gives:

$$\langle A_1 B_1 \rangle + \langle A_1 B_2 \rangle + \langle A_2 B_1 \rangle - \langle A_2 B_2 \rangle = 2\sqrt{2}. \tag{1.71}$$

Clearly, this result violates Bell-CHSH inequality obtained for local hidden variable theories. In fact the above result bounds the inequality:

$$\langle A_1 B_1 \rangle + \langle A_1 B_2 \rangle + \langle A_2 B_1 \rangle - \langle A_2 B_2 \rangle \leq 2\sqrt{2}. \tag{1.72}$$

The violation of quantum mechanics with Bell-CHSH inequality indicates that local hidden variable theories are incompatible with quantum physics and the only possibility that hidden variable theories could explain the prediction of quantum physics is that they are non-local. That is, the particles, distantly separated, are able to interact instantaneous. Experimental test of Bell inequality started in 1972 with John Clauser and Stuart Freedman. The initial experiment was using photon's polarization for measurement. The signals are then detected by coincidence monitor. The results are of course consistent with quantum mechanics and eliminated the possibility of local hidden variable theories.

Entanglement witness Following Bell's theorem, entanglement witness has been studied to distinguish entangled state from separable state. Entanglement witnesses are functionals of density matrix. The task is to find necessary and sufficient conditions for the existence of entanglement in noisy quantum state. For low dimensional bipartite state, it is known that positivity of partial transposition provides a necessary and sufficient condition for separability. But it fails for mixed multipartite state. In 2001, a more general formalism of entanglement witness based on linear maps positive on product states is introduced [82] to characterize mixed state entanglement. Note that entanglement witness is by no means a quantification of entanglement, but to test separability.

An observable W is an entanglement witness if and only if

$$Tr[W\rho] \geq 0, \tag{1.73}$$

for all separable state ρ.

The relevant entanglement witness considered in this thesis include

$$I \otimes I + \sigma_x \otimes \sigma_z + \sigma_y \otimes \sigma_y \tag{1.74}$$

$$I \otimes I - \sigma_x \otimes \sigma_x - \sigma_y \otimes \sigma_z - \sigma_z \otimes \sigma_y. \tag{1.75}$$

Implementation of this entanglement witness on bipartite state requires Pauli-X, Y, Z measurement.

Stern-Gerlach apparatus A typical method to entangle the spin degree of freedom and spatial degree of freedom is to send a spin embedded mass through a Stern-Gerlach apparatus. Spin embedded mass is sent through inhomogeneous magnetic field, which may be generated from a set of permanent magnets or current carrying wires, the magnetic field gradient exerts a spin-dependent force on the test mass. Consider a spin embedded nano-crystal, say a diamond with a single spin-1 nitrogen-vacancy center. The spin's symmetry axis is aligned along x axis and a uniform magnetic field gradient $\frac{dB}{dx}$ is applied. The corresponding Hamiltonian is

$$H = \frac{p^2}{2m} - g.\mu_B \frac{dB}{dx}\sigma_z.x, \tag{1.76}$$

where μ_B is the Bohr magneton, g is the Lande g factor, σ_z is Pauli-Z operator and p, x are momentum, position operator respectively.

The second term in the Hamiltonian $g.\mu_B \frac{dB}{dx}\sigma_z.x$ entangles the spin degree of freedom and spatial degree of freedom. Depends on the spin state of the system, the test particle can be deflected along either $x+$ or $x-$ direction before striking a detector screen. The schematic diagram is shown in Fig. 1.1.

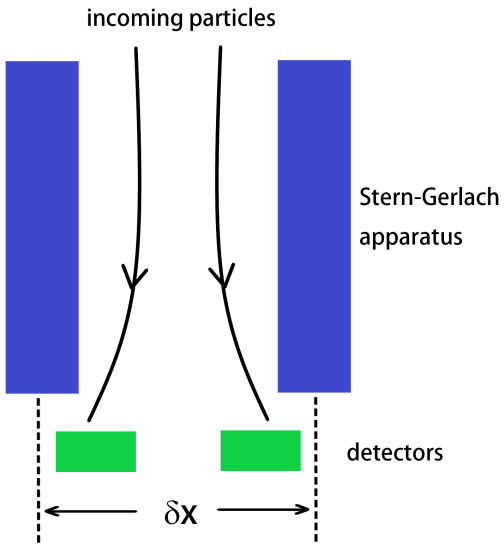

Fig. 1.1 **Stern-Gerlach apparatus**

1.5 Quantum bits

As introduced in the classical information section, bit is the building block of classical computation. In Quantum communication, a quantum bit or qubit for short is the fundamental

concept. Similar to the classical bit, which takes the value of either 0 or 1, a quantum bit is a linear combination of a two level system:

$$|\phi\rangle = \alpha|0\rangle + \beta|1\rangle, \tag{1.77}$$

where α and β are complex numbers denoting probability amplitude. The $|0\rangle$ and $|1\rangle$ state form the computational basis. A qubit state is therefore a unit vector in 2-dimensional Hilbert space. A classical bit can only take the value of either 0 or 1. For a qubit, on the other hand, can be a superposition of $|0\rangle$ and $|1\rangle$ state.

When multiple qubits are present, the system is then spanned by a tensor product of $|0\rangle$ and $|1\rangle$ state. For instance, a two qubit system would be spanned by $|00\rangle, |01\rangle, |10\rangle, |11\rangle$. A two qubit state can then be expressed as

$$|\phi\rangle = a_{00}|00\rangle + a_{01}|01\rangle + a_{10}|10\rangle + a_{11}|11\rangle. \tag{1.78}$$

As illustrated previously, multipartite quantum system can be entangled. Such quantum systems possess correlations that are not present in classical systems. These quantum correlations can exploited to perform information processing tasks such as quantum teleportation and super-dense coding. We will explore these protocols later.

Manipulation of classical bit in classical computer is typically implemented with electrical circuits made from transistors. The state of art technology in semi-conductor enables integrated circuits with billions number of transistors on each chip. The manipulation of quantum bit is then implemented with quantum gates. Here, we briefly review some simple quantum gates and how they may be realized.

A quantum NOT gate should be able to take the state $|0\rangle$ to $|1\rangle$ and take the state $|1\rangle$ to $|0\rangle$. For a linear superposition state $\alpha|0\rangle + \beta|1\rangle$, the quantum NOT gate should be able to turn it into $\alpha|1\rangle + \beta|0\rangle$. Therefore the quantum operator can be described by a two level matrix. For quantum NOT gate on single qubit, it is equivalent to the Pauli-X matrix represented by:

$$\sigma_x = \begin{pmatrix} 0 & 1 \\ 1 & 0 \end{pmatrix}. \tag{1.79}$$

Note that quantum gates are unitary. For quantum gate denoted U, $U\dagger U = I$. Recall from the axioms of quantum physics, the evolution of a closed system is represented by a unitary operator. Here, quantum gates are modeled by such an evolution. Other non-trivial quantum gates including the Z-gate, which flips the sign of $|1\rangle$ but leaves $|0\rangle$ unchanged. Its matrix

representation is given by:

$$\sigma_x = \begin{pmatrix} 1 & 0 \\ 0 & -1 \end{pmatrix}. \tag{1.80}$$

The Hadamard gate denoted by letter H turns $|0\rangle$ into $(|0\rangle + |1\rangle)/\sqrt{2}$ and turns $|1\rangle$ into $(|0\rangle - |1\rangle)/\sqrt{2}$. Its matrix representation is given by:

$$\sigma_x = \begin{pmatrix} 1 & 1 \\ 1 & -1 \end{pmatrix}. \tag{1.81}$$

Quantum gates that act on multiple qubits are also important. An important theoretical result is that single qubit gates and CNOT gates are universal. It means that any quantum gates operating on multipartite system can be decomposed into CNOT gate and singe qubit gates. A CNOT gate acts on two qubits. It flips the target qubit if the control qubit is in state 1 but leave the target qubit unchanged if the control qubit is in state 0, represented in equations:

$$|00\rangle \to |00\rangle; |01\rangle \to |01\rangle; |10\rangle \to |11\rangle; |11\rangle \to |10\rangle. \tag{1.82}$$

The matrix representation of CNOT gate in the standard basis $\{|00\rangle, |01\rangle, |10\rangle, |11\rangle\}$ is therefore:

$$CNOT = \begin{pmatrix} 1 & 0 & 0 & 0 \\ 0 & 1 & 0 & 0 \\ 0 & 0 & 0 & 1 \\ 0 & 0 & 1 & 0 \end{pmatrix}. \tag{1.83}$$

The unitary property of CNOT gate can be easily checked.

1.6 Quantum Information theory

So far, we have covered how quantum systems can carry information and how quantum characteristics of these systems lead to interesting information protocols such as quantum teleportation, super-dense coding. In this section, we review how concepts in classical Shannon theory can be generalized to the quantum setting. In parallel with its classical counterpart, this section would discuss the aspects:

1. Noiseless coding theorem: How much can quantum information be compressed?
2. Characterization, witness and quantification of quantum entanglement
3. Noisy channel coding theorem: At what rate can reliable communications, being classical or quantum, take place over noisy channel?

The study of quantum information is centered around the manipulation of von-Neumann entropy, the quantum version of Shannon entropy. This thesis focus on the principle issues of quantum information theory. So we will look at information protocols in a asymptotic setting. How does information processing task perform when the number of quantum channels approaches infinity and the same quantum channel and quantum state are identically and independently distributed.

von Neumann Entropy

Classical information theory is largely concerned with the interpretation of Shannon entropy and its relatives. We have seen that Shannon entropy gives the asymptotic incompressible information contained in a sequence and it also gives rise to the rate of reliable information transmission through noisy channels. von-Neumann entropy plays a similar role in quantum information theory. Here we review the mathematical properties of von-Neumann entropy before discussing its information theoretical implications. The definition of von Neumann entropy is given by:

$$S(\rho) = -Tr[\rho \log[\rho]], \tag{1.84}$$

where we have adopted the conventional basis of 2 for the logarithm function. Here the notation of Shannon entropy and von Neumann entropy are not distinguished. Which one applies should be clear by the context of whether being classical (Shannon entropy) or quantum (von Neumann entropy). Recall that density operator ρ can be spectral decomposed:

$$\rho = \sum_i \lambda_i |i\rangle\langle i|. \tag{1.85}$$

Substituting in the spectral decomposition of ρ we obtain

$$S(\rho) = -\sum_i \lambda_i \log[\lambda_i]. \tag{1.86}$$

This is same as the Shannon entropy of the distribution specified by $\{\lambda_i\}$. Therefore, we could interpret von Neumann entropy of a given density state as the Shannon entropy of the distribution specified by the density state eigenvalues. Here, we state without proven the basic properties of von Neumann entropy:

- $S(\rho) = 0$ if and only if ρ is pure. That is, if ρ satisfies $Tr[\rho^2] = 1$
- Given the dimension of the Hilbert space d, $S(\rho) \leq \log d$. The bound saturates when the quantum state is maximally mixed, that is, all the eigenvalues are identical.

- $S(\rho)$ is invariant under a change of basis, that is, given unitary operation U, $S(\rho) = S(U\rho U^\dagger)$. Since the entropy only depends on the eigenvalues of ρ

- $S(\rho)$ is concave. Given a set of positive numbers that sum to one $\sum_i \alpha_i = 1$ and density operators with the same index ρ_i, the following equation holds:

$$S(\sum_i \lambda_i \rho_i) \geq \sum_i \lambda_i S(\rho_i). \tag{1.87}$$

  This is a direct outcome of the convexity of log function.

- $S(\rho)$ is additive for separable states. Given two density state ρ_A, ρ_B that lives in Hilbert space $\mathscr{H}_A$, $\mathscr{H}_B$ respectively, the equation holds:

$$S(\rho_A \otimes \rho_B) = S(\rho_A) + S(\rho_B). \tag{1.88}$$

- For pure bipartite system A,B with state $|\phi\rangle_{AB}$, the entropy of each subsystem equates:

$$S(\rho_A) = S(\rho_B). \tag{1.89}$$

- For any tripartite system A, B, C, $S(\rho_{ABC})$ is strongly subadditive:

$$S(\rho_{ABC}) + S(\rho_B) \leq S(\rho_{AB}) + S(\rho_{BC}). \tag{1.90}$$

  It also implies subadditivity of $S(\rho)$ on bipartite systems:

$$S(\rho_{AC}) \leq S(\rho_A) + S(\rho_C). \tag{1.91}$$

A sharp contrast of quantum entropy and classical entropy is that for classical systems, the Shannon entropy of a joint system is always larger than each subsystem. This is intuitive because we generally expect that we cannot have more information about a subsystem than the whole system. But for quantum systems, for instance, a pure bipartite system $|\phi\rangle_{AB}$, its entropy is zero. But $S(\rho_A) = S(\rho_B) > 0$. How can it be that we know everything about the whole system but uncertain about its subsystem? The answer lies in the quantum entanglement between the subsystems. The information is stored in the correlation of the subsystems. The statement should be clearer when we introduce the quantification of entropy.

Other Entropic measures

Just like the classical case where entropic measures based on Shannon entropy gives answers to classical information processing tasks, for instance, classical mutual information gives a quantification of accessible information through a noisy channel, von Neumann entropy also gives rise to entropic measures that play central role in quantum information processing.

Quantum conditional entropy of a bipartite system is the entropy of the joint system minus the entropy of one subsystem:

$$S(A|B) = S(AB) - S(B), \tag{1.92}$$

where the entropy is evaluated on the density state of the joint system AB ρ_{AB}. This definition is a direct extension of classical conditional entropy.

Coherent information of a bipartite system ρ_{AB} is defined as

$$I(A\rangle B) = S(B) - S(AB). \tag{1.93}$$

You would immediately realize that coherent information is simply the negative of conditional information. Then why do we employ a separate name for this quantity? In classical information theory, conditional entropy is always positive because we are more certain about a subsystem than the entire system. But this is not the case for quantum physics. You can convince yourself that for bipartite maximally entangled state, the entropy of the entire system is 0, but each subsystem is described by a two dimensional maximally mixed state, so $S(A|B) = 0 - 1 = -1$bit. How can it be negative? We have briefly explained earlier as the presence of entanglement stores information in the correlations between subsystems. In this case, the coherent information is positive and gives 1bit. Coherent information deserves its own name because it gives answer to certain information processing tasks. In particular, it gives channel capacity of quantum communication, in which a sender is trying to transmit the entanglement with some inaccessible reference system through noisy quantum channels to the receiver.

Quantum mutual information is a direct extension of classical information. Just like its classical counterpart, quantum mutual information plays a central role in quantifying accessible information through noisy quantum channels. Quantum mutual information of a

bipartite system ρ_{AB} is defined as:

$$I(A;B) = S(A) + S(B) - S(AB). \tag{1.94}$$

From the definition we can directly see its relation with conditional entropy and coherent information:

$$I(A;B) = S(A) - S(A|B) = S(A) + I(A\rangle B). \tag{1.95}$$

Quantum relative entropy Quantum relative entropy act as a "parent" among entropic measures in quantum information theory. Many entropy quantities can be expressed in terms of it. The quantum relative entropy $S(\rho_1||\rho_2)$ between two density operators ρ_1, ρ_2 is defined as

$$S(\rho_1||\rho_2) = Tr\{\rho_1(\log\rho_1 - \log\rho_2)\}. \tag{1.96}$$

The importance of quantum relative entropy is comparable to von Neumann entropy itself. It is useful to review its key properties:

- The quantum relative entropy is non-negative

$$S(\rho_1||\rho_2) \geq 0. \tag{1.97}$$

- Invariant under unitary transformation U

$$S(\rho_1||\rho_2) = S(U\rho_1U^\dagger||U\rho_2U^\dagger). \tag{1.98}$$

- The quantum relative entropy between two density states can not increase under the application of the same quantum channel ε

$$S(\rho_1||\rho_2) \geq S(\varepsilon(\rho_1)||\varepsilon(\rho_2)). \tag{1.99}$$

Quantum relative entropy can be regarded as quantifying how far about two states are in quantum information, though it is not strictly a distance measure. The property that it can not increase under the application of a common quantum channel is relevant to quantum information processing inequality, which states that processing quantum data decreases quantum correlations.

Noiseless coding theorem

The essence of classical noiseless coding theorem is that one only needs to code the typical sequences as the atypical sequences becomes negligible asymptotically. Similarly, the quantum incompressible information is determined by the typical subspace.

Consider messages drawn from an ensemble $\{p_x, |\phi_x\rangle\}$, so each letter is determined by a density matrix

$$\rho = \sum_x p_x |\phi_x\rangle \langle\phi_x|. \tag{1.100}$$

A n-letter message is then determined by the tensor product of each letter's density state

$$\rho^{\otimes n}. \tag{1.101}$$

Recall that density states contain all the information one can obtain from the system regardless of how it is represented in terms of pure states. Note that density states can be spectral decomposed into orthogonal states $\rho = \sum_i \lambda_i |i\rangle\langle i|$. We can then perceive each letter as drawn from a classical probability distribution specified by the eigenvalues $\{\lambda_i\}$. Therefore, the quantum information source is equivalent to a classical source in this basis. Following from Shannon's argument, one immediately realize that the density matrix specified by $\rho^{\otimes n}$ has asymptotically all of its support on the subspace spanned by $(|i\rangle\langle i|)^{\otimes n}$ whose corresponding classical sequences are typical. Therefore, the dimension of the typical subspace asymptotically approaches

$$2^{nS(\rho)}. \tag{1.102}$$

Therefore, the rate at which one can compress quantum information stored in a state ρ without loss of information asymptotically is equal to its entropy $S(\rho)$. The essence is that nearly all message has entire support on the typical subspace, so one only needs to code the typical subspace and ignore the rest.

Entanglement concentration and dilution

Another way to look at von Neumann entropy is that it gives answer to the quantification of quantum entanglement. This feature is unique to quantum information theory. Suppose we have a set of pure bipartite systems, all of which are entangled, how do we know which one of the systems are more entangled than others? We have seen that entanglement can be treated as a resource in quantum information processing tasks. How much of this resource is contained in each entangled pair?

Local operations and classical communication First, we shall note that entanglement can not be generated by local operations and classical communication, abbreviated LOCC. Suppose two parties possess a quantum state independently, so that the composite system is a separable state $\rho_A \otimes \rho_B$. The two parties are allowed to exchange classical messages with each other but can only perform quantum operations on their own site. The evolution of each state is then described by a unitary operator. More generally, the evolution is described by quantum channels. Since classical messages are allowed, we may assume that the quantum channels acting on each state are correlated, denoted by a subscript $\varepsilon_\alpha(\rho_A) \otimes \varepsilon_\beta(\rho_B)$. Regardless of how α and β are correlated, the composite system is always described by a tensor product state, therefore, remains separable. More generally, any quantification of entanglement should possess the feature that it does not increase under LOCC and vanishes for separable state.

Now let us turn back to the quantification of entanglement. Recall that in previous examples of using entanglement as a resource, we have been using maximally entangled state, called ebit. So the key to quantify entanglement is to convert entangled states with LOCC into maximally entangled state, which acts as a choice of currency for comparison. Now the problem becomes identifying the rate at which one can convert a entangled state into a ebit. Consider n pairs of entangled state shared between two parties AB $|\psi\rangle_{AB}^{\otimes n}$, they are to be converted into Bell state $|\phi\rangle_{AB}^{\otimes k}$. The rate of conversion is then

$$R = \frac{k}{n}. \tag{1.103}$$

We can also ask the reverse problem, given k Bell state pairs $|\phi\rangle_{AB}^{\otimes k}$, how many pairs of $|\psi\rangle_{AB}$ can be generated? For pure bipartite state, these two measures, called entanglement dilution an concentration respectively, are equivalent. So the processes are reversible and we may not distinguish between the two rates. For mixed state, the situation is more complicated. But we shall not cover the topic in this thesis due to limited spaces.

The asymptotic rate of conversion for each state $|\psi\rangle_{AB}$ is equal to the entropy of its subsystems.

$$S(\rho_A) = S(\rho_B), \tag{1.104}$$

where $\rho_A = Tr_B[|\psi\rangle_{AB}\langle\psi|_{AB}]$ and similar for ρ_B.

To give a hint of how the conversion may be implemented, consider the entanglement dilution protocol where two parties AB are converting $nS(\rho_A)$ pairs of Bell states into n pairs of $|\psi\rangle_{AB}$ with LOCC. First Alice creates n copies of $|\psi\rangle_{AA'}$ at her own site, hence local operation. She then performs the compression protocol to compress subsystem A' into $nS(\rho_{A'})$ bits. Next, she exploit the pre-shared entanglement of $nS(\rho_A)$ pairs of Bell state and

classical communication channels to perform quantum teleportation, so that subsystem A' is now teleported to B. Bob then decompresses the states. Now Alice and Bob share the state $|\psi\rangle_{AB}^{\otimes n}$ with perfect fidelity asymptotically.

Noisy channel coding theorem

This sections explores that dynamical aspect of Quantum information theory. When a sender and a receiver communicates through quantum channels, the system that encodes the transmitted message interact with the environment. At what rate can reliable communication occur? The result is a direct generalization of Shannon's noisy channel coding theorem. However, as we discussed in the unit protocols of quantum information, entanglement shared between the sender and the receiver acts as a resource. Depends on what communication resource is available and what type of information, being classical or quantum, is transmitted, quantum information theory is richer than its classical counterpart. The typically studied information processing tasks are 1. classical communication, where a sender and receiver are communicating classical messages through quantum channels but without pre-shared entanglement. 2. Entanglement assisted classical communication, where unlimited pre-shared entanglement is available. 3. Quantum communication, where the sender is trying to transmit the entanglement with an inaccessible reference system to the receiver. 4. Entanglement-assisted coherent communication. These protocols maybe regarded as generalizations of the pre-discussed unit protocols. The entanglement assisted classical communication, for instance, is a direct generalization of super dense coding in noisy environment. In this thesis, we will take classical communication over quantum channels as an example to illustrate the basic concepts in noisy channel coding theorem without delve into details.

The information processing protocol for classical communication over quantum channels is as follows: the sender encodes a message into quantum codeword as input. The codeword then transmit through n independently, identically distributed quantum channels. The decoder receives the codeword and performs POVM to determine which message is sent. Let the message to be selected from a set $\{1,.,x,..,M\}$. The sender prepares a quantum state of dimension 2^n encoding the message x, denoted $\rho_{A^n}^x$. The state is then transmitted through n channels denoted ε so that the received state is

$$\varepsilon^{\otimes n}(\rho_{A^n}^x). \tag{1.105}$$

The receiver then performs a set of POVM $\{\Lambda_x\}$ to decode the message. The probability of obtaining the correct message is

$$p = Tr[\Lambda_x \varepsilon^{\otimes n}(\rho^x_{A^n})]. \tag{1.106}$$

The rate of communication is then

$$R = logM/n. \tag{1.107}$$

A rate R is achievable if the probability of obtaining the correct message reaches 1 as n approaches infinity. The classical capacity $C(\varepsilon)$ of a quantum channel ε is the maximum of all achievable rates through quantum channel ε for classical communication.

Here, we state without proven the classical capacity theorem:

The classical capacity of a quantum channel ε is given by the regularization of the Holevo information of the channel

$$C(\varepsilon) = \lim_{n\to\infty} \chi(\varepsilon^{\otimes n})/n, \tag{1.108}$$

where $\chi(\varepsilon)$ denotes the Holevo information of the channel

$$\chi(\varepsilon) = \max_{\rho} I(X;B). \tag{1.109}$$

$I(X;B)$ is the mutual information evaluated with respect to the state

$$\rho_{XB} = \sum_x p_x |x\rangle\langle x|_X \otimes \varepsilon_{A\to B}(\rho^x_A). \tag{1.110}$$

The classical state $\{|x\rangle\langle x|\}$ carries information of the message. It can be regarded as a copy of the message for the sender's reference. The Holevo information gives an upper bound on the accessible classical information. The regularization process refers to averaging over all n channels. In the case where a particular channel ε_i is additive, that is $\lim_{n\to\infty} \chi(\varepsilon_i^{\otimes n})/n = \chi(\varepsilon_i)$, the regularization is no longer needed. In general, quantum channels are superadditive $\lim_{n\to\infty} \chi(\varepsilon^{\otimes n})/n > \chi(\varepsilon)$. This is a reflection that entanglement among the input state could, in general, protect the information from noise. If we restrict to product input state $\rho^x_{A^n} = \rho^{\otimes n}_A$, the channel capacity is then $C(\varepsilon) = \chi(\varepsilon)$.

Proof of the channel capacity theorem again consists of a direct coding theorem and a converse theorem, similar to its classical counterpart. The direct theorem is to show that the regularized Holevo information is achievable by exploiting quantum typicality. The converse

theorem is to prove that the rate is optimal, which make use of random encoding and quantum data processing inequality.

For other information processing tasks, for instance, entanglement assisted classical communication, quantum communication, entanglement-assisted coherent communication, the channel capacity is generally expressed in terms of entropic measures introduced previously including quantum mutual information and coherent information. Hence, we claim that the significance of these entropic measures is that they give operational answers to quantum information processing tasks.

1.7 Quantum field theoretical origin of gravity

Causality is one of the salient features of a local quantum field theory [172]. The causality dictates that separated space-like local operators must commute, which ensures that the measurement at a spacetime point x, cannot influence the measurement at a spacetime point y, if x and y are not causally connected. This property will also hold in interacting theories. It is usually treated as one of the axioms of local quantum field theories [78].

A causal structure of field theory can be probed by the nature of a Feynman *propagator*. By preparing a particle at spacetime point x, we can ask what is the amplitude to find it at point y, and vice versa. For a massless quantum field theory, one can show that the Feynman propagator has a support only within the past and future light cones, and vanishes strictly for space-like separation. Indeed, in a relativistic quantum field theory there is a way to interpret the results; the amplitude for the particle to propagate from $x \to y$ gets canceled by an anti-particle traveling from $y \to x$. The challenges arise in a non-relativistic quantum field theory, where there is no concept of an anti-particle. Indeed, in quantum mechanics we have a conservation of a particle number, which would not have been possible in a relativistic quantum field theory. Nevertheless, even if we are working in a regime of quantum mechanics we are always in a hybrid scenario, where the masses are non-relativistic, but their interaction is mediated by a relativistic quantum field theory. Such examples are abundant, slowly moving charged particles are interacting via massless photon, or non-relativistic massive particles are interacting via massless spin-2 graviton.

Any interacting local quantum field theory possesses an interesting quantum feature, known as quantum entanglement, which measures quantum correlation [34]. In particular, in the S-matrix formulation, for arbitrary initial states, the final states will get entangled by virtue of quantum interaction or via a quantum mediator. These results are also corroborated from a theorem in quantum information theory, which states that local operation and classical communication (LOCC) cannot lead to an increment in the entanglement of two quantum

systems [22]. We would require local operation and quantum communication (LOQC) to entangle the two unentangled quantum states to begin with, which was recently highlighted in the context of both local and non-local quantum field theories of gravity, see [121]. LOQC builds this foundations and basis for testing the quantum nature of a graviton in the lowest order in the scattering diagram, which was recently proposed in a *spin entanglement witness for quantum gravity* [28]. The theoretical and experimental protocol is known as quantum gravity induced entanglement of masses (QGEM). The protocol relies on bringing two quantum masses sufficient close to each other, where other interactions such as electromagnetic interactions can be sufficiently screened, and then study quantum correlations between the two quantum masses to ascertain whether the final states are entangled or not.

The aim of this thesis will be to explore such a hybrid regime, and illustrate how causality will influence quantum properties, such as quantum entanglement. This will be an indirect test to causal propagation of the quantum mediator. In the case of gravity, it will ensure that the graviton propagation between the two sources happen within the causal light cone, and not outside the light cone.

Let us first consider the gravitational action

$$S = \int d^4x\sqrt{-g}\left[\frac{M_p^2}{2}R\right], \tag{1.111}$$

where $M_p \sim 2.4\times 10^{18}$ GeV is the Planck mass. The physical excitations of this action around the Minkowski background has been studied widely. We can compute the second variation of the action, using $g_{\mu\nu} = \bar{g}_{\mu\nu} + h_{\mu\nu}$, where $\mu,\nu = 0,1,2,3$ and. A quick computation can be made by employing the covariant mode decomposition of the metric following Refs. [29]

$$h_{\mu\nu} = h^{\perp}_{\mu\nu} + \bar{\nabla}_\mu A_\nu + \bar{\nabla}_\nu A_\mu + \left(\bar{\nabla}_\mu\bar{\nabla}_\nu - \frac{1}{4}\bar{\eta}_{\mu\nu}\bar{\Box}\right)B + \frac{1}{4}\bar{g}_{\mu\nu}h, \tag{1.112}$$

where $h^{\perp}_{\mu\nu}$ is the transverse and traceless spin-2 excitation, A_μ is a transverse vector field, and B, h are two scalar degrees of freedom. Upon linearization around maximally symmetric backgrounds, the vector mode and the double derivative scalar mode vanish identically, and we end up only with $h^{\perp}_{\mu\nu}$ and $\phi = h - \bar{\Box}B$ [121]. Performing necessary computations (which are indeed straightforward around Minkowski as all derivatives commute), one gets [121]

$$\begin{aligned}\delta^2 S(h^{\perp}_{\mu\nu}) &= \int d^4x\sqrt{-\bar{g}}\frac{1}{2}h^{\perp}_{\mu\nu}\bar{\Box}h^{\perp}_{\mu\nu}\\ \delta^2 S(\phi) &= \int d^4x\sqrt{-\bar{g}}\frac{1}{2}\phi\bar{\Box}\phi,\end{aligned} \tag{1.113}$$

for the tensor component (where the field was rescaled by $M_p/2$ to become canonically normalised), and the scalar component (where the field was rescaled by $M_p\sqrt{3/32}$ to be canonically normalised), respectively.

If we wish to quantise purely gravitational waves, it suffices to quantise just the transverse traceless graviton, $h^{\perp}_{\mu\nu}$. Though perturbative quantization of gravity is fundamentally a non-renormalizable theory, it can be understood as an effective field theory for which the graviton gives a good description in the low energy limit [55].

However, if we wish to understand the covariant virtual graviton propagator, the full graviton propagator is required, which can be written using a similar method to [16], barring the suppressed indices

$$\Pi(k^2) = \frac{\mathscr{P}^{(2)}}{k^2} - \frac{\mathscr{P}^{(0)}}{2k^2}. \tag{1.114}$$

Assuming the massive external particles have zero spin, the Feynman rules for graviton exchange can be computed by the covariant S-matrix $S^{\rm cov}_{fi} = \langle f|S|i\rangle_{\rm cov}$, where $S^{\rm cov}_{fi} = -i8\pi G T^{(1)}_{\mu\nu}\Pi^{\mu\nu\alpha\beta}T^{(2)}_{\alpha\beta}\delta^4(P_{fi})$, where $\delta^4(P_{fi})$ is the four momenta conservation. In the non-relativistic limit it will give us the gravitational potential where we use $S^{\rm cov}_{fi} = i\delta^4(P_{fi})T^{\rm cov}_{fi}$.

$$V(r) = \int d^3k e^{-ik\cdot r} T^{\rm cov}_{fi}(NR) = -Gm_1m_2/r. \tag{1.115}$$

Although, the lowest order potential does not have explicit $\hbar$, the exchange of graviton is a quantum process where both $h^{\perp}_{\mu\nu}$ and scalar ϕ degrees of freedom contribute in virtual exchange of a graviton. The presence of $\hbar$ appears in the gravitational potential $V(r)$ at one-loop in graviton exchange, $\sim 32G^2m_1m_2\hbar/15\pi r^3$. Indeed, by including the spin in the particles, such as fermions in the initial and final states will yield an extra contribution in the metric potential, which is at the lowest order independent of the mass term, i.e. $\propto 2G\vec{S}\times\vec{r}/r^3$, which is further suppressed by the distance between the two masses. Therefore, leading order contribution in G arises from the spin-less components, i.e. Newtonian potential.

Our aim will be to study the scattering amplitude between the two neutral masses, but we will embed an electronic spin inside the neutral masses, and study the lowest order in G and the distance, which is dominated by Gm_1m_2/r in order to compute the entanglement.

Part I

Massive Spatial Qubits

Chapter 2

Massive Spatial Qubits: Testing Macro-Nonclassicality & Casimir Entanglement

In Chapter 2, we present a new tool: massive spatial qubits. An open challenge in physics is to expand the frontiers of the validity of quantum mechanics by evidencing nonclassicality of the center of mass state of a macroscopic object. Yet another equally important task is to evidence the essential nonclassicality of the interactions which act between macroscopic objects. The methodology of encoding qubits in the spatial superposition states of massive objects addresses these two challenges. In particular, we show that if two distinct localized states of a mass are used as the $|0\rangle$ and $|1\rangle$ states of a qubit, then we can measure this encoded spatial qubit with a high fidelity in the σ_x, σ_y and σ_z bases simply by measuring its position after different duration of free evolution. This technique can be used to reveal the irreducible nonclassicality of the spin-centre of mass entangled state of a nano-crystal implying macro-contextuality. Further, in the context of Casimir interaction, this offers a powerful method to create and certify non-Gaussian entanglement between two neutral nano-objects. The entanglement such produced provides an empirical demonstration of the Casimir interaction being inherently quantum.

2.1 Motivation

It is an open challenge to witness a nonclassicality in the behavior of the center of mass of a massive object [102, 7]. While there are ideas to observe nonclassicalities of ever more massive objects [27, 5, 120, 25, 38, 145, 146, 144, 151, 170, 26], the state of art

demonstrations have only reached up to macro-molecules of 10^4 amu mass [66, 58]. Such demonstrations would test the limits of quantum mechanics [52, 137, 15, 127, 131, 173], would be a stepping stone to witness the quantum character of gravity [28, 121, 119, 116, 165], and would open up unprecedented sensing opportunities [123]. Identifying new tools to probe macroscopic nonclassicality (by which here we mean in terms of large mass) is thus particularly important. Here we propose and examine the efficacy of precisely such a tool: a mechanism to read out a qubit encoded in the spatial degree of freedom of a *free (untrapped) mass* (a purely spatial qubit). A principal merit of this scheme is that *measuring* the spatial qubit operators σ_x, σ_y and σ_z exploits solely the free time evolution of the mass (Hamiltonian $H = \hat{p}^2/2m$), followed by the detection of its position. As the mass is not controlled/trapped by any fields during its free evolution, decoherence is minimized.

As a first application, we show that our tool enables the verification of an irreducible nonclassicality of a particular joint state of a spin (a well established quantum degree spin) and the center of mass of a macroscopic object, whose quantum nature is yet to be established. To this end, we use the state produced in a Stern-Gerlach apparatus which is usually written down as an *entangled* state of a spin and the position [56, 79, 88, 116, 118, 147]. Such Stern-Gerlach states have been created with atoms with its spatial coherence verified after selecting a specific spin state [114, 118]. However, there are, as yet, no protocols to verify the *entanglement* between the spin of an object in a Stern-Gerlach experiment and the motion of its center of mass in a way which can be scaled to macroscopic objects. We show that this can be accomplished via the violation of a Bell's inequality in which the spin and the positions of the mass are measured. This violation will also prove the nonclassicality of a large mass in terms of quantum contextuality [1, 80].

Next, we propose a second application once the quantum nature of the center of mass degree of freedom of macroscopic objects is assumed (or established in the above, or in some other way). This application has import in establishing the quantum nature of the *interactions* between macroscopic objects. We show how our spatial qubit methodology can enable witnessing the entanglement created between two neutral nano-crystals through their Casimir interaction. This has two implications: (a) It will empirically show that the extensively measured Casimir interaction [100, 181, 180] is indeed quantum (e.g., is mediated by virtual photons similar to [134, 101] – if photons are replaced by classical entities they would not entangle the masses [28, 121, 119, 86, 99]). (b) As the entangled state is generated by starting from a superposition of localized states, it is non-Gaussian. While there are ample methods for generating [140, 98, 174] and testing [155] Gaussian entanglement of nanocrystals, there is hardly any work on their non-Gaussian counterparts.

We are constructing our methodology by combining ideas from two different quantum technologies: photonic quantum information processing and the trapping and cooling of nano-crystals. In the former field a qubit can be encoded in the spatial mode of a single photon by passing it through an effective Young's double slit [162]. These qubits, called Young qubits, and their d-level counterparts [67, 150], have been exploited in quantum information [95, 143]. On the other hand, we have had a rapid development recently in the field of levitated quantum nano-objects [38, 145, 11] culminating in their ground state cooling and the verification of energy quantization [49, 163]. While several schemes for verifying quantum superposition of distinct states of such objects have been proposed to date, in these schemes, either the x, y and z motions are measured as infinite dimensional systems [144, 17, 184] rather than being discretized as an effective qubit, or never measured at all (only ancillary systems coupled to them are measured [151, 170]). Here we adapt the idea of Young qubits from photonic technologies to massive systems. Note that a very different encoding of a qubit in the continuous variables of a harmonic oscillator was proposed long ago for quantum error correction [71], which is not suited to an untrapped nano-crystal.

2.2 Qubit Encoding and its Measurement in all Bases:

Our encoding is intuitive: $|0\rangle$ and $|1\rangle$ states of a qubit are represented by two spatially separated (say, in the x direction) non-overlapping wavepackets whose position and momenta are both centered around zero in the other two commuting (y and z) directions. Explicitly, these states (writing only the x part of their wavefunction) are

$$|0\rangle \equiv \frac{1}{\sqrt{\sigma_d}\pi^{1/4}} \int_{-\infty}^{\infty} \exp[-\frac{(x+d/2)^2}{4\sigma_d^2}]|x\rangle dx, \tag{2.1}$$

$$|1\rangle \equiv \frac{1}{\sqrt{\sigma_d}\pi^{1/4}} \int_{-\infty}^{\infty} \exp[-\frac{(x-d/2)^2}{4\sigma_d^2}]|x\rangle dx, \tag{2.2}$$

with $d >> \sigma_d$. These states are schematically depicted in Fig. 2.1 in which only the x direction is depicted along with their evolution in *time*. For simplicity, we will omit the acceleration due to the Earth's gravity (as if the experiment is taking place in a freely falling frame), which can easily be incorporated as its effect commutes with the rest. Thus we only consider 1D time evolution in the x direction. In this chapter, we will only require two states: (a) a state in which a spin embedded in a mass is entangled with the mass's spatial degree of freedom in the state $|\phi^+\rangle = \frac{1}{\sqrt{2}}(|\uparrow,1\rangle + |\downarrow,0\rangle)$ for our first application, and (b) the spatial

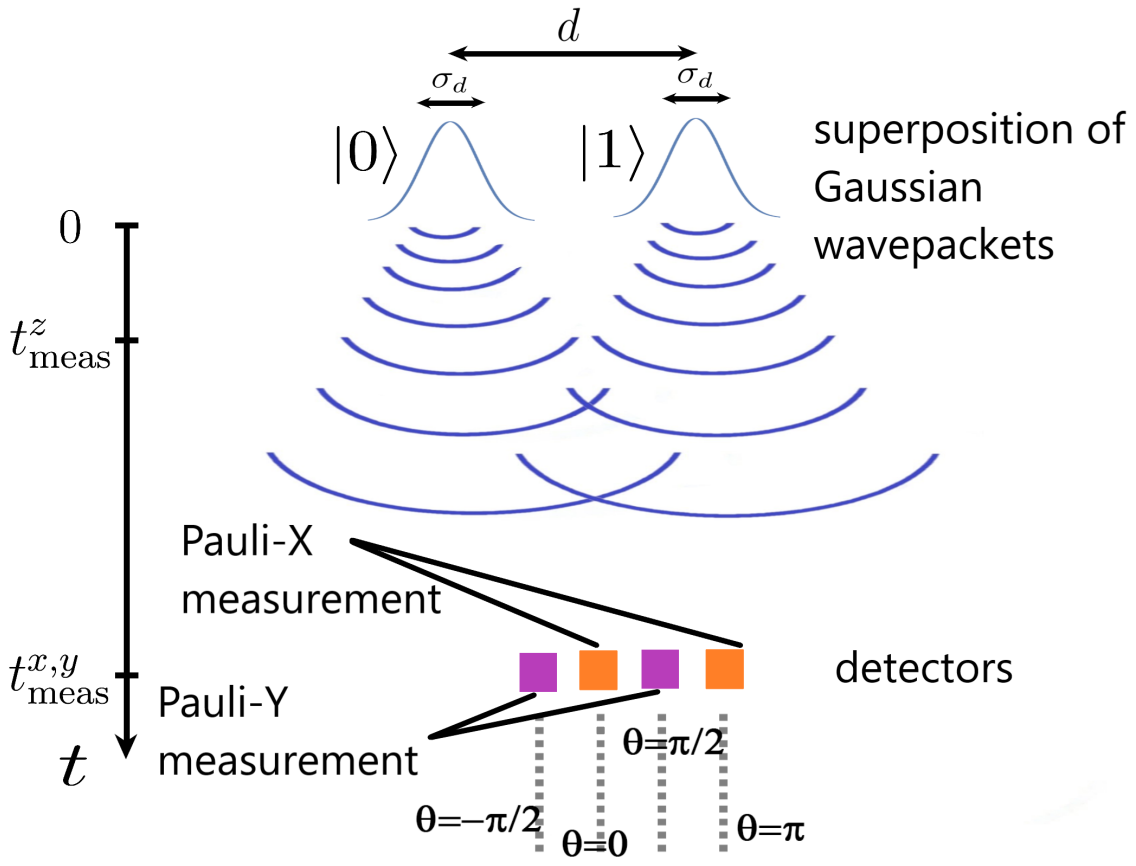

Fig. 2.1 **Spatial detection for σ_x, σ_y measurements:** a pair of detectors (color: orange) located at phase angle $\theta = 0, \theta = \pi$ perform σ_x measurement. The detectors (color: purple) at $\theta = \pi/2, \theta = -\pi/2$ perform σ_y measurement.

qubit state $|+\rangle = \frac{1}{\sqrt{2}}(|0\rangle + |1\rangle)$ as a resource for our second application. Preparation of the above adapts previous proposals and will be discussed with the respective applications.

We now outline our central tool: the method of measuring the above encoded spatial qubit in various bases. The spatial detection can be performed by shining laser light onto the test masses [68, 168]. The Rayleigh scattered light field acquires a position dependent phase shift. The scheme is limited only by the standard quantum limit [68] (quantum back action) of phase measurement when a *large number of photons* are scattered from the mass. The resolution scales with the number n of scattered and detected photons as $\lambda/\sqrt{n}$, hence, the power collected at the detector (see Eq. 13 of Ref [168]), and the detection time (as long as this is lower than the dynamical time scale, it is independent of whether the particle is trapped/untrapped). Thus the detection time should be as much as one needs for the required resolution, but much less than the time span of the experiment. By the above methodology, for a 60nm diameter silica particle, the detection resolution can reach 200 ± 20 fm/$\sqrt{\text{Hz}}$ with laser power $\sim 385\mu$W at the detector, at environmental pressure ~ 0.01mbar [168]. Thus for an integration time of $\sim 4\mu s$, the resolution reaches ~ 1Å, which corresponds to just $\sim 10^8$ photons. The whole measurement is μs, any noise of frequency lower than MHz will not affect it (simply remains constant during each measurement run). Moreover, lower frequency noise causing variation between, say, groups of runs, could be measured efficiently by other proximal sensors and taken into account. Also note that the spatial detection is performed at the very end of the protocol, so the question of back action on further position measurements does not arise.

Due to the spreading of the wavepackets along y and z directions, when we determine whether the object is in a given position $x = x_0$ at some measurement time t, we are essentially integrating the probability of detecting it over a finite region $\Delta y(t)$ and $\Delta z(t)$. The operator $\sigma_z = |0\rangle\langle 0| - |1\rangle\langle 1|$ is trivial to measure, as we simply shine a laser centered at $x = d/2$ much before the wavepacket states $|0\rangle$ and $|1\rangle$ have started to overlap (at a time $t^z_{\text{meas}} << d(2\sigma_d m)/\hbar$; the error in σ_z measurement as a function of t^z_{meas} is described in the appendix; timing errors $\delta t << t^z_{\text{meas}}$ have very little effect). If light is scattered, the state is $|0\rangle$, otherwise $|1\rangle$.

To measure the spatial qubit σ_x and σ_y operators, we need a large enough time $t^{x,y}_{\text{meas}} \geq d(2\sigma_d m)/\hbar$ so that the wavepackets of the $|0\rangle$ and $|1\rangle$ states have spread out enough to significantly overlap with each other and produce an interference pattern. Moreover, due to the free propagation, we would expect the measurement time $t^{x,y}_{\text{meas}}$, final position x and the transverse wave vector k_x are related by: $x = \frac{\hbar k_x t^{x,y}_{\text{meas}}}{m}$ (detecting at a position x after the interference effectively measures the initial superposition state of $|0\rangle$ and $|1\rangle$ in the $|k_x\rangle$ basis). Noting the momentum representation of the qubit states $|n\rangle =$

$\int \left\{ \sqrt{2}\sigma_d \exp[\frac{ik_x d}{2} - k_x^2\sigma_d^2] \exp[-ink_x d]|k_x\rangle \right\} dk_x$ $(n = 0, 1)$, the probability to detect the object at a position x for any initial qubit state $|\psi\rangle$ is now obtained:

$$P(x) = |\langle\psi|k_x\rangle|^2 \propto \left| \exp[\frac{ik_x d}{2} - k_x^2\sigma_d^2]\langle\theta|\psi\rangle \right|^2, \tag{2.3}$$

where $|\theta\rangle = |0\rangle + |1\rangle e^{i\theta}$ in which the parameter $\theta = k_x d = \frac{xmd}{\hbar t^{x,y}_{\text{meas}}}$ (we will call θ the phase angle). Therefore, finding the object in various positions x is in one to one correspondence with positive operator valued measurements (POVM) on the spatial qubit, with the relevant projection on the state being, up to a normalization factor, as $|\theta\rangle\langle\theta|$. σ_x measurements can therefore be implemented by placing a pair of position detectors (which will, in practice be, lasers scattering from the object) at positions corresponding to phase angle $\theta = 0, \theta = \pi$; Similarly, σ_y measurements can be achieved by placing detectors at $\theta = \pi/2, \theta = -\pi/2$ (Schematic shown in Fig. 2.1). For minimizing the time of the experiment, we are going to choose $t^{x,y}_{\text{meas}} = d(2\sigma_d m)/\hbar$. The efficacy of the σ_x and σ_y measurements as a function of the finite time $t^{x,y}_{\text{meas}}$ for various ratios $\sigma_d : d$ is discussed in the appendix.

2.2.1 Young type qubit as beam splitter

Our experimental setup serves the same purpose as a Mach-Zehnder interferometer in probing contextuality [1], in which a particle pass through beam splitters and which path information defines a spatial qubit. In our approach, Young type double slit acts effectively as a lossy beam splitter [2]. A cubic beam splitter has two input and two output. The transformation matrix from the former to the latter ports is described by a two-by-two unitary matrix. The initial states $|0\rangle$ and $|1\rangle$ act as the two input. By placing a pair of detectors in the interference plane, we project the input states onto a different basis, parameterized by phase angle θ. For instance, conducting Pauli-Y operation requires placing two detectors at phase angle $-\pi/2$ and $\pi/2$ respectively. The effective beam splitter therefore transforms the system from a superposition of $|0\rangle$ and $|1\rangle$ to the basis spanned by $|0\rangle - i|1\rangle$ and $|0\rangle + i|1\rangle$. The transformation matrix is therefore $\frac{1}{\sqrt{2}}\begin{pmatrix} 1 & i \\ 1 & -i \end{pmatrix} = \frac{1}{\sqrt{2}}\begin{pmatrix} 1 & i \\ i \times e^{-i\pi/2} & 1 \times e^{-i\pi/2} \end{pmatrix}$, equivalently, a 50:50 beam splitter followed by a phase shifter with angle $-\pi/2$.

2.3 Application: Nonclassicality of the Stern-Gerlach state:

As a first application of this spatial qubit technology, we consider an extra spin degree of freedom embedded in a mesoscopic mass. We now imagine that the mass goes through a

Stern-Gerlach apparatus. The motion of the mass relative to the source of the inhomogeneous magnetic field (current/magnets) is affected in a spin dependent manner due to the exchange of virtual photons between the source and the spin (Fig. 2.2) resulting in an entangled state of the spin and position of the nano-object as given by $|\phi^+\rangle = \frac{1}{\sqrt{2}}(|\uparrow,1\rangle + |\downarrow,0\rangle)$, as depicted as the output of the preparation stage in Fig. 2.2. It could also be regarded as an intra-particle entanglement (an entanglement between two degrees of freedom of the same object), which has been a subject of several investigations [1, 75, 9].

To measure the spin-motion entanglement in $|\phi^+\rangle$, we have to measure variables of spin and spatial qubit. Here we specifically want to estimate the action of measuring one of these qubits on the quantum state of the other. During this measurement, the inhomogeneous magnetic field causing the Stern-Gerlach splitting is simply switched off so that spin coherence can be maintained using any dynamical decoupling schemes as required [10]. Alternatively, one can also use more pristine nano diamond with less surface defects. As shown in Fig. 2.2, after a required period of free evolution $t^{x,y}_{\text{meas}}$, measurements of the spatial qubit operators are made; the light shone on the object should not interact at all with the embedded spin degree of freedom if it is completely *off-resonant* with any relevant spin transition. Immediately after measuring the spatial qubit, the spin degree of freedom is directly measured in various bases. The latter could be implemented, for example, with a NV center spin qubit in a nano-diamond crystal, where the spin state is rotated by a microwave pulse, which corresponds to basis change, followed by a fluorescence measurement by shining a laser resonant with an optical transition [76]. The implementation would require cryogenic temperature of the diamond [187, 171]. So the spin coherence time is much greater than the experimental time scale [10]. As the spin measurement is very efficient, we only need to consider the resolutions $\delta x, \delta t$ of the spatial qubit measurements so that the effective spatial Pauli X and Y operators are then projections onto a mixed state with phase angle ranging from $\theta - \frac{\delta\theta}{2}$ to $\theta + \frac{\delta\theta}{2}$ with $\delta\theta = \frac{md}{\hbar t^{x,y}_{\text{meas}}}\delta x - \frac{xmd}{\hbar (t^{x,y}_{\text{meas}})^2}\delta t$. For purposes of coherence, which continuously decreases with time, it is best to choose time of the order of the minimum allowed time for overlap of the wavepackets, i.e., choose $t^{x,y}_{\text{meas}} = d(2\sigma_d m)/\hbar$ so that $\delta\theta = \frac{\delta x}{2\sigma_d} - \frac{x\hbar}{4\sigma_d^2 md}\delta t$. The approximate Pauli matrices are then:

$$\begin{aligned}
\tilde{\sigma}_x &= \frac{1}{\delta\theta}\begin{pmatrix} 0 & \int_{\theta-\frac{\delta\theta}{2}}^{\theta+\frac{\delta\theta}{2}} e^{-i\theta} d\theta|_{\theta=0} \\ \int_{\theta-\frac{\delta\theta}{2}}^{\theta+\frac{\delta\theta}{2}} e^{i\theta} d\theta|_{\theta=0} & 0 \end{pmatrix} \\
&= \frac{1}{\delta\theta}\begin{pmatrix} 0 & -ie^{i\frac{\delta\theta}{2}} + ie^{-i\frac{\delta\theta}{2}} \\ -ie^{i\frac{\delta\theta}{2}} + ie^{-i\frac{\delta\theta}{2}} & 0 \end{pmatrix},
\end{aligned}$$

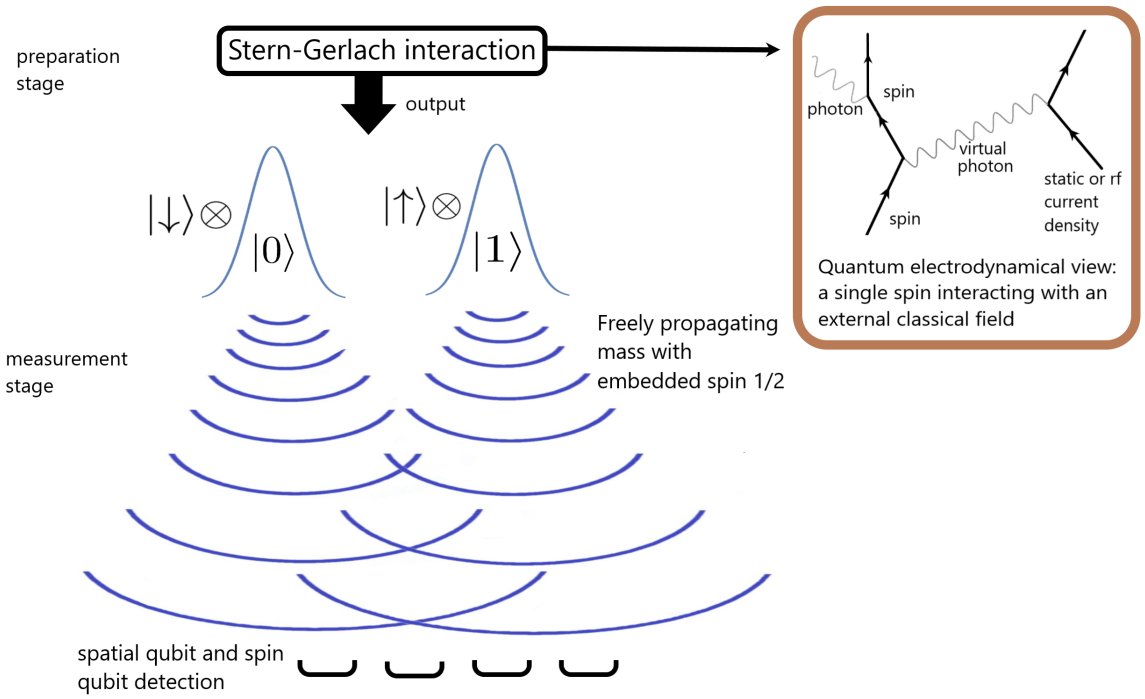

Fig. 2.2 **Detection scheme for the entanglement of spin and center of mass of a Stern-Gerlach state:** A spin bearing nano-object is measured to be in a set of zones of size δx, where the size is set by the strength and duration of lasers scattered from the object, which serves to measure the spatial qubit. Within each spatial zone a suitable method is used to measure the spin in different bases, for example by rotating the spin states by microwave pulses followed by fluorescence of certain states under excitation by a laser of appropriate frequency.

and similarly, $\tilde{\sigma}_y = \frac{1}{\delta\theta}\begin{pmatrix} 0 & -e^{i\frac{\delta\theta}{2}}+e^{-i\frac{\delta\theta}{2}} \\ e^{i\frac{\delta\theta}{2}}-e^{-i\frac{\delta\theta}{2}} & 0 \end{pmatrix}$. To verify the entanglement we have to show that the spin-motion entangled state violates the Bell-CHSH inequality $\mathscr{B} = |\langle AB\rangle + \langle AB'\rangle + \langle A'B\rangle - \langle A'B'\rangle| \leq 2$ with variables [46] $A = \tau_x + \tau_y$ and $A' = \tau_x - \tau_y$ operators of the spin (τ_x and τ_y are spin Pauli matrices) and $B = \tilde{\sigma}_x$ and $B' = \tilde{\sigma}_y$ operators of the spatial qubit. The expected correlation can be calculated (see appendix) to give $\mathscr{B} = |2\sqrt{2}f(\delta\theta)| \leq 2\sqrt{2}$ where $f(\delta\theta) = \frac{2}{\delta\theta}Re[ie^{i\delta\theta/2}] = \frac{2}{\delta\theta}cos(\frac{\pi+\delta\theta}{2})$. To obtain a violation of the CHSH inequality the upper bound of $\delta\theta$ can be calculated:$|f(\delta\theta)| = \frac{1}{\sqrt{2}}, \delta\theta \approx 2.783$.

For realization, consider a $m \sim 10^{-19}$ kg (10^8 amu) spin-bearing mass cooled to a ground state in $\omega \sim 100$ kHz trap [144, 49, 163] so that its ground state spread is $= \sqrt{\frac{\hbar}{2m\omega}} \sim 1$ Å. At time $t = 0$ the embedded spin is placed in a superposition $1/\sqrt{2}(|\uparrow\rangle + |\downarrow\rangle)$, and the mass is released from the trap. The wave packet then passes through an inhomogeneous magnetic field gradient $\sim 10^5$ Tm^{-1} [116]. Due to the Stern-Gerlach effect, the mass moves in opposite directions corresponding to $|\uparrow\rangle$ and $|\downarrow\rangle$ spin states, and, in a time-scale of $t_{\rm prep} \sim 50\mu$s, evolves to a $|\phi^+\rangle$ state with a separation of $d = 25$nm between the $|0\rangle$ and

$|1\rangle$ spatial qubit states [170, 28, 123, 165, 116] (all lower m and d are also possible as they demand lower t_{prep} and $\partial B/\partial x$). To keep the spin coherence for t_{prep}, dynamical decoupling may be needed [10]; it is possible to accomodate this within our protocols-one just needs to change the direction of the magnetic field as well in tandem with the dynamical decoupling pulses which flip the spin direction [179]. During the above t_{prep}, the $|0\rangle$ and $|1\rangle$ wavepackets spreads from $\sigma_d \sim 1$ Åto ~ 5 Å. The ratio $\sigma_d/d \sim 1/50$ is within the validity regime of a high fidelity spatial qubit σ_x and σ_y measurement as discussed by us if performed at time $t^{x,y}_{\text{meas}} \sim \frac{2\sigma_d m d}{\hbar} \sim 1$ ms.

According to our results above, in order to obtain a CHSH inequality violation, one has to measure to within $\delta x \sim 2\sigma_d \delta\theta \sim 1$ Å resolution. To achieve this resolution, firstly, we have to ensure that during the whole duration of our protocol, the acceleration noise has to be below a certain threshold so as to not cause random displacement greater than 1Å. Given $t^{x,y} \sim 1$ms is the longest duration step, the acceleration noise needs to be $\sim 10^{-4} ms^{-2}$. Next comes the measurement step where light is scattered from the object, which also needs to measure to the required resolution. This is possible as there are feasible techniques that give resolutions of 0.1 pm/$\sqrt{\text{Hz}}$ [68, 168] for position measurements by scattering light continuously from an object. In fact, we would need to scatter light only for a μs to achieve our required resolution. Adopting the scheme in [168], the resolution can be achieved by scattering light continuously from the object for $\sim 4\mu$ s, which is $2-3$ orders of magnitude smaller than the experimental time span. On the other hand if the timing accuracy δt of $t^{x,y}_{\text{meas}}$ is kept below ~ 0.1ms (also easy in terms of laser switching on/off times), there is a negligible inaccuracy in θ.

Note that as shown in the appendix, dephasing between the spatial states $|0\rangle$ and $|1\rangle$ at a rate γ simply suppresses the CHSH violation by a factor $e^{-\gamma t}$, which could be a new way to investigate decoherence of the mass from various postulated models [52, 137, 15, 127, 131, 173] and environment.

The decoherence of the spatial degree of freedom results from background gas collision and black-body radiation. Adopting the formulae from Ref [144], for our realization, the contribution to γ from background gas reaches $\sim 167.2\text{s}^{-1}$ at pressure $\sim 10^{-10}$Torr. Black-body radiation induces decoherence at a rate of $\sim 274.9\text{s}^{-1}$ at internal temperature ~ 50K. On the other hand, the spin degree of freedom, which may be encoded in NV centers of nano-diamond crystal, reaches a coherence time of ~ 0.6s at liquid nitrogen temperature 77K [10]. Therefore, achievable pressure and temperature make the coherence time sufficient for the realization of our protocol (same estimates hold for the protocol of the next section).

As *both* the spin and the mass are measured, it characterizes the entanglement of the given state *irrespective* of the dynamics from which the state was generated, as opposed to previous

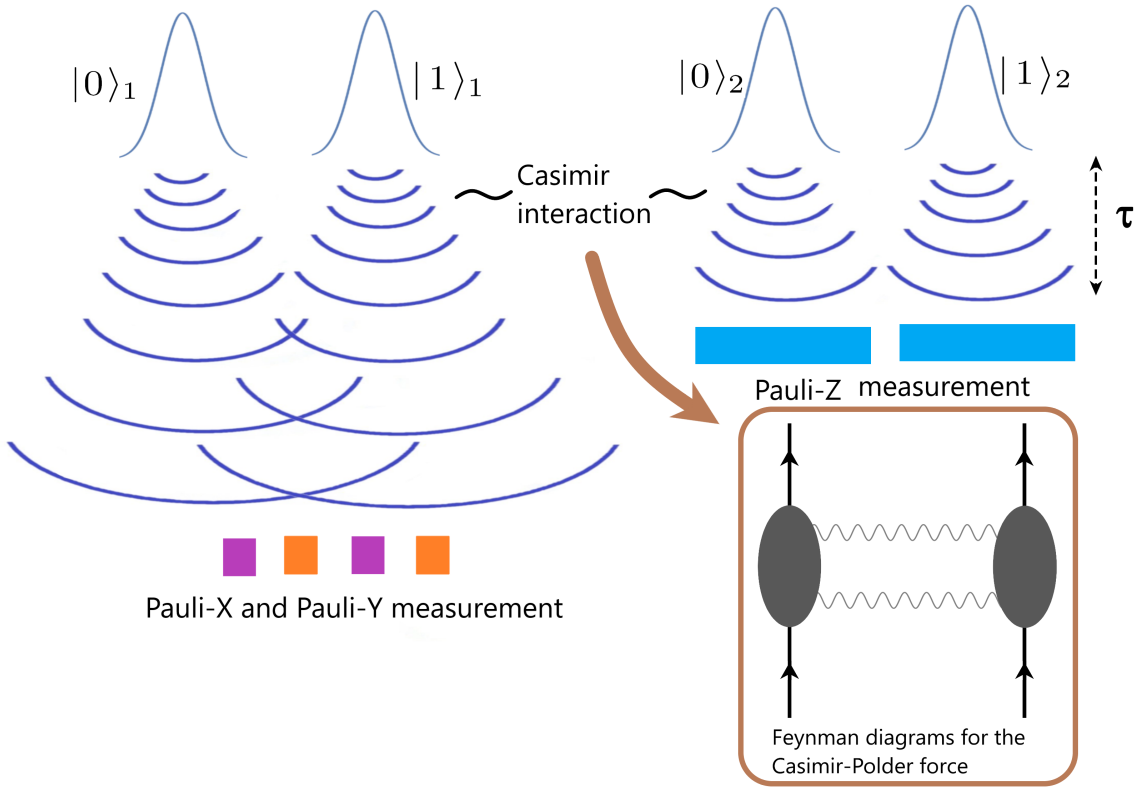

Fig. 2.3 **Application in witnessing Casimir induced entanglement:** Two masses, each prepared in a superposition of two states, act as two qubits $\frac{1}{\sqrt{2}}(|0\rangle_1+|1\rangle_1)\otimes\frac{1}{\sqrt{2}}(|0\rangle_2+|1\rangle_2)$. The system freely propagates and undergoes mutual interactions for a time τ. This interaction induces entanglement which can be witnessed from correlations of spatial qubit Pauli measurements. For example, in the figure, σ_x, σ_y measurements on test mass 1 and σ_z measurements on test mass 2 are depicted. Casimir interaction induced by virtual photons as quantum mediators is shown [59].

protocols which rely on a reversible nature of the quantum dynamics [27, 5, 120, 25]. As opposed to single object interferometry [144, 17, 184], here the CHSH violation explores decoherence of the mass in multiple bases – not only how the $|0\rangle\langle 1|$ term of the spatial qubit decays (position basis), but also whether, and, if so, how, $|+\rangle\langle -|$ decays (where $|-\rangle = |0\rangle - |1\rangle$) – a novel type of decoherence of even/odd parity basis. Moreover, as the total spin-motional system is quantum 4 state system, the CHSH violation can also be regarded as a violation of the classical notion of non-contextuality [80, 1, 31].

2.4 Application: Casimir interaction induced entanglement:

Neutral unmagnetized untrapped masses, ideal for the preservation of spatial coherence, can interact with each other via the Casimir interaction [165] (gravity can cause observable effects in reasonable times only for masses $> 10^{-15} - 10^{-14}$ kg [28, 165]). Two such masses

(mass m, radius R) indexed 1 and 2 are each prepared in the spatial qubit state $|+\rangle$ (the superposition size, separation between states $|0\rangle$ and $|1\rangle$, being d) while the distance between the centers of the superpositions is D (Fig. 2.3). In a time τ, the Casimir interaction evolves the system to

$$\frac{e^{i\phi}}{\sqrt{2}}[|0\rangle_1\frac{1}{\sqrt{2}}(|0\rangle_2+e^{i\Delta\phi_{01}}|1\rangle_2)+|1\rangle_1\frac{1}{\sqrt{2}}(e^{i\Delta\phi_{10}}|0\rangle_2+|1\rangle_2)],$$

where $\phi=k\frac{R^6}{D^7}\tau,\Delta\phi_{01}=k\frac{R^6}{(D+d)^7}\tau-\phi,\Delta\phi_{10}=k\frac{R^6}{(D-d)^7}\tau-\phi$, in which $k=\frac{23c}{4\pi}(\varepsilon-1)^2/(\varepsilon+2)^2)$, where ε is the relative permittivity of the material of the masses. On top of the above evolution, we assume a local dephasing ($|0\rangle\langle 1|_i\rightarrow e^{-\gamma\tau}|0\rangle\langle 1|_i$) for both particles ($i=1,2$) (this can generically model all dephasing [165, 164]). To verify the induced entanglement, one can make spatial qubit measurements up to uncertainties parametrized by $\delta\theta$ as outlined previously and then estimate the entanglement witness [41] $W=I\otimes I-\tilde{\sigma}_x\otimes\tilde{\sigma}_x-\tilde{\sigma}_z\otimes\tilde{\sigma}_y-\tilde{\sigma}_y\otimes\tilde{\sigma}_z$ where $\tilde{\sigma}_x$ and $\tilde{\sigma}_y$ are as discussed before, and we take $\tilde{\sigma}_z=\int_{-\infty}^{0}|x\rangle\langle x|dx-\int_0^{\infty}|x\rangle\langle x|dx$. If $\langle W\rangle=Tr(W\rho)$ is negative, the masses are entangled. We find

$$\begin{aligned}\langle\tilde{W}\rangle=&1-\frac{1}{2}e^{-2\gamma t}g^2(\delta\theta)(1+\cos(\Delta\phi_{10}-\Delta\phi_{01}))\\&-e^{-\gamma t}g(\delta\theta)(\sin(\Delta\phi_{10})+\sin(\Delta\phi_{01})),\end{aligned}\tag{2.4}$$

where $g(\delta\theta)=\frac{2}{\delta\theta}\cos(\frac{\pi-\delta\theta}{2})$.

We are going to consider the Stern-Gerlach mechanism to first prepare the state $|\phi^+\rangle$, and use that to prepare $|+\rangle$. We consider a $R\sim 20$ nm, $m\sim 1.17\times 10^{-19}$ kg mass, and consider it to have been trapped and cooled it to its ground state ($\sigma_d\sim 1$ nm) in a 1 kHz trap [184]. We then release it, and subject it to a magnetic field gradient of 5×10^4 Tm^{-1} [116] for $t\sim 100\mu$s so that a Stern-Gerlach splitting of $d\approx 50$ nm develops while there is insignificant wavepacket spreading (σ_d remains ~ 1 nm). At this stage, a microwave pulse may be given to rotate the spin state so that the $|\phi^+\rangle$ state evolves to $|0\rangle(|\uparrow\rangle+|\downarrow\rangle)+|1\rangle(|\uparrow\rangle-|\downarrow\rangle)$. A subselection of the $|\uparrow\rangle$ spin state via deflection through another Stern-Gerlach, then yields the state $|+\rangle$ [114, 118]. Alternatively, by performing a Controlled-NOT with the spatial qubit as the control and the spin as the target (again, performed quite accurately by a microwave pulse [184]), $|\phi^+\rangle$ gets converted to $|+\rangle|\downarrow\rangle$ so that the spatial part is our required state. For $D\approx 2.1\mu$m, then $\Delta\phi_{10}=\phi_{10}-\phi\approx 0.17$, $\Delta\phi_{01}=\phi_{01}-\phi\approx -0.14$ after $\tau\sim 0.012$s of entangling time, which gives a negative witness $\langle W\rangle\sim -0.0064$.

Note here that the form of witness operator compels one to measure both the $\tilde{\sigma}_x\otimes\tilde{\sigma}_x$ operator and the other two operators on the *same entangled state*. $\tilde{\sigma}_z$ measurement is also done at $t^z_{\text{meas}}=\tau$. This is about 0.1 of the overlapping time $\sim\frac{d(2\sigma_d m)}{\hbar}$ so that the fidelity

of the σ_z measurement is very high (see appendix). We then require $t^{x,y}_{\text{meas}} - t^{z}_{\text{meas}} << \tau$ so that the extra entanglement generated due to interactions after the $\tilde{\sigma}_z$ measurement and before the $\tilde{\sigma}_x/\tilde{\sigma}_y$ measurements is negligible. This, in turn, requires us to *speed up* the development of spatial overlap between the qubit states due to wavepacket spreading after the $\tilde{\sigma}_z$ measurement, which can be accomplished by squeezing both of the wavepackets in position after the time t^{z}_{meas}. After 0.01 s of flight, the wavepacket width $\sigma_d \sim 1$ nm expands to ~ 10 nm. Thus we have to squeeze the state by 2 orders of magnitude to $\sim 1 \times 10^{-10}$ m, so that it expands to ~ 100 nm, where overlapping occurs, in the next 0.001.s The fidelity of XY measurement here is very high (see appendix). The slight delay in $\sigma_{x/y}$ measurement (0.001s later than the σ_z measurement) would cause only a $\sim 5\%$ error in the witness magnitude. Note that in order to achieve the required squeezing, two appropriate periods of unitary evolution in harmonic potentials of $\omega_1 \sim$1 MHz and $\omega_2 \sim 0.1$ MHz would suffice (n repeated changes between ω_1 and ω_2 separated by appropriate periods of harmonic evolution will squeeze by the factor $(\omega_1/\omega_2)^n$ [90]); if this potential was applied as an optical tweezer then it will hardly cause any decoherence $\gamma_{\text{squeeze},j} \sim \omega_j 10^{-5}$ [38]. We additionally need to ensure, for reasons described earlier, the acceleration noise needs to be kept below $10^{-6} ms^{-2}$. The whole procedure described above could be one of the earliest demonstrations of non-Gaussian entanglement between neutral masses. It would also demonstrate the nonclassical nature of the Casimir interaction, namely that it is mediated by quantum agents (virtual photons) as in the inset of Fig. 2.3.

2.5 Summary

We have shown how to measure a qubit encoded in a massive object by position detection. We have shown how this can be applied to: (a) stretch the validity of quantum mechanics rules to the center of mass of nano-objects – demonstrating quantum entanglement between spin and center of mass, which has never before been tested for macroscopic objects, (b) entangle spatial qubits encoded in two such objects, extending non-Gaussian quantum technology, (c) prove empirically the quantum coherent nature of the Casimir force. Indeed, in the *same* open-minded way that one asks whether quantum mechanics continues to hold for macroscopic masses [102, 7], one can question whether those interactions between such masses which are extensive in nature (grow as volume/area/mass) *continue* to be mediated by a quantum natured field so as to be able to entangle the masses. In comparison with standard approaches for probing the nonclassicality for smaller masses, we avoid a Mach-Zehnder interferometer – only requiring the preparation of an original spatial superposition. This is advantageous because of the difficulty of realizing beam-splitters for nano-objects (tunneling

probability $\propto e^{-\frac{\sqrt{2mV}}{\hbar}\Delta x}$ getting extremely small), and also for avoiding interactions with mirrors and beam splitters which can cause decoherence. (we exploit a two-slit experiment as a beam-splitter [2]). Our methodology can be quantum mechanically simulated with cold atoms, where other methods to encode qubits in motional states have been demonstrated [61], before they are actually applied to nano-objects.

Chapter 3

Spatial Qubit Entanglement Witness for Quantum Effects Of Gravity

Evidencing the quantum nature of gravity through the entanglement of two masses has recently been proposed. Proposals using qubits to witness this entanglement can afford to bring two masses close enough so that the complete $1/r$ interaction is at play (as opposed to its second order Taylor expansion), and micron sized masses separated by 10-100 microns (with/without electromagnetic screening) suffice to provide a $\sim 0.01 - 1$ Hz rate of growth of entanglement. Yet the only viable method proposed for obtaining qubit witnesses so far has been to employ spins embedded in the masses, whose correlations are used to witness the entanglement developed between masses during interferometry. This comes with the dual challenge of incorporating spin coherence preserving methodologies into the protocol, as well as a demanding precision of control fields for the accurate completion of spin aided (Stern-Gerlach) interferometry. Here we show that if superpositions of distinct spatially localized states of each mass can be created, whatever the means, simple position correlation measurements alone can yield a spatial qubit witness of entanglement between the masses. We find that a significant squeezing at a specific stage of the protocol is the principal new requirement (in addition to the need to maintain spatial quantum coherence) for its viability.

3.1 Motivation

The quantumness of gravity is an open question due to a lack of empirical evidence. A lot of research is performed in the setting of semi-classical gravity, in which matter and non-gravitational fields are treated quantum mechanically, while gravity is treated classically. A substantial community argues that gravity can be classical as quantum physics break

down at macroscopic level, where gravitational effects become evident [137, 52, 15, 14]. Various proposals have been made to avoid quantizing gravity, at the cost of introducing extra stochastic terms [87, 132] – but these are not ruled out by any current experiment such as measuring forces precisely. Therefore, testing the quantum nature of gravity experimentally is an open problem. Even if its quantumness is accepted from the point of view several existing successful theories [133, 89], its *verification* is still open.

In 2017, Bose and collaborators proposed a protocol to test whether the nature of gravity is quantum [28] (see also recorded online talk of 2016, where the same protocol is presented [1]). Two spatial superposition state of masses *can not entangle* via classical channel [21] (see also [119]). Locality in quantum field theory circumvents the non-local interaction between the two superposed test masses [121]. Entanglement between the masses can only be generated through local operations and *quantum* communication (in fact, quantum communication is *necessary* for operator valued interactions, [29] which in turn is necessary for the coherent interaction that generates entanglement). On the other hand, once quantum communication is proven through a witnessing of gravitationally generated entanglement, this unambiguously certifies the presence of off-shell/virtual graviton as this is the only way to get a continuous deterministic operator valued interaction [121, 29]. Alternatively, the witnessed entanglement can also be regarded as evidencing the quantum superposition of geometries inherent in superposition states of each mass [45, 44].Moreover, from logical arguments, the quantum nature of the Newtonian component of the gravitational field automatically has a bearing on the quantum nature of other components [18, 48, 36, 4].

The original proposal exploits spin-embedded masses [28]. Stern-Gerlach interferometers (SGIs) are used to prepare the spatial superpositions depend on embedded spins so that the motional and spin degree of freedom is entangled. The test masses then freely evolve subject to gravitational interaction. At the end of the proposed protocol, the Stern-Gerlach apparatus is exploited again to bring the superposition components back to the center. Spin correlations between the test masses then evidence the entanglement generated through the gravitational interaction during propagation. Alternatively, it has also been proposed to witness the gravitational entanglement growth between two initial delocalized gaussian states by position and momentum correlations [140, 98, 175] (see also [24, 36, 4] for similar entanglement via gravity between light and matter or between optical fields). However, a two-qubit witness for entanglement is applicable to a situation where masses are brought as close to each other as their delocalization (spatial superposition scale), so that the entanglement itself has a faster growth rate (~ 1 Hz) even for smaller (micron sized) masses.

It is challenging to complete SGIs as an exact overlap has to be attained in both position and momentum of the wavepackets in the two interferometric arms [57, 114], although this

has been achieved very recently for small atomic interferometers [116]. Moreover, the spin can bring in an extra avenue of decoherence requiring extra dynamical decoupling procedures which could potentially complicate the interferometry even more requiring further dynamical decouplings [10, 179]. Although exceptionally long spin coherence have been shown, and these are the subject of qubits in quantum computers, it may be worthwhile to look for witnessing of the entanglement without spins. This may even be the case where we actually use spin dependent forces (Stern-Gerlach) to create the initial superposition. However, we do not worry about also completing the interferometry by appropriate matching of forces in the two arms. On the other hand, without spins, the advantage of two-qubit witnesses for quantum entanglement seems to disappear. We thus here look at the potential of using position measurements themselves to infer states of “spatial qubits"(which have been called Young qubits in photonic systems [162, 94, 150, 67]) and use that as witness for evidencing gravitational entanglement. We find that aside the usual coherence requirements to be satisfied for maintaining the quantum superpositions [28, 165], which is unavoidable in any scheme, a spatial qubit witnessing of gravitational entanglement is possible if a challenging squeezing requirement can be met.

The spatial qubit methodology [183] encodes qubit in the spatial degree of freedom of a freely propagating test mass. The readout of the information stored in the qubit can be implemented by placing sets of spatial detectors at appropriate positions. Correlations generated between two such spatial qubits during evolution can then be tested by spatial detection. One advantage of this approach is its simplicity: free propagation followed by spatial detection. An interferometer with beam splitting elements such as Mach-Zhender, looks highly unfeasible because of the large mass that has to tunnel through such a system. Of course, a Stern-Gerlach interfrometer is possible, but this requires a spin, as well as exquisite control in completing the interferometry. Both these requirements are completely avoided if spatial qubits are used. However, it in general requires the application of an additional squeezing operator. In this chapter, we apply this methodology to witness quantum natured gravity.

3.2 Spin entanglement witness setup

Ref. [28] presents an approach to witness quantum effects of gravity (See Fig. 3.1 below). The scheme consists of two spin embedded test masses initially in spatially localized states, say, in respective traps. The test masses labeled $j = 1, 2$ pass through a set of Stern-Gerlach (SG) interferometers so that the spatial degree of freedom entangles with the spin degree of

freedom to prepare

$$|\psi_0\rangle = (|L,\uparrow\rangle_j + |R,\downarrow\rangle_j)/\sqrt{2}(j=1,2), \tag{3.1}$$

with states $|L\rangle$ and $|R\rangle$ being separated by d, and the distance between the midpoint of each superposition ($\sim$ initial separation between the masses) being D. Next, let the coherent superposition state propagate for a time τ by switching off the magnetic field of the SG apparatus. If gravity were quantum, gravitational interaction can induce, through relative phases among the superposition components, an entanglement between the masses (classical gravity as mediator would not give an operator valued interaction [29], and hence will be unable to entangle the two masses). The final step refocuses the SG apparatus to bring the spatial superposition back to the center so that the final spin state reads

$$\begin{aligned}\frac{e^{i\phi}}{\sqrt{2}} \quad & [|\uparrow\rangle_1 \frac{1}{\sqrt{2}}(|\uparrow\rangle_2 + e^{i\Delta\phi_{\uparrow\downarrow}}|\downarrow\rangle_2) \\ & + |\downarrow\rangle_1 \frac{1}{\sqrt{2}}(e^{i\Delta\phi_{\downarrow\uparrow}}|\uparrow\rangle_2 + |\downarrow\rangle_2)],\end{aligned} \tag{3.2}$$

where $\phi = \frac{Gm_1m_2}{\hbar D}\tau, \Delta\phi_{\uparrow\downarrow} = \frac{Gm_1m_2}{\hbar(D+d)}\tau - \phi, \Delta\phi_{\downarrow\uparrow} = \frac{Gm_1m_2}{\hbar(D-d)}\tau - \phi$. This is generically an entangled state as soon as $\frac{1}{\sqrt{2}}(|\uparrow\rangle_2 + e^{i\Delta\phi_{\uparrow\downarrow}}|\downarrow\rangle_2) \neq \frac{1}{\sqrt{2}}(e^{i\Delta\phi_{\downarrow\uparrow}}|\uparrow\rangle_2 + |\downarrow\rangle_2)$. By measuring spin correlations, one can then verify the entanglement induced during the propagation time τ. That can only arise from the exchange of quantum coherent mediators. If gravity is the only interaction present, one can then conclude that gravity is quantum. To prevent unwanted electromagnetic interactions between the masses, we will assume the placement of a screening plate between them as will be discussed later. Of course, there is the question of efficacy of this screening mechanism, as well as decoherence induced by it, which will be subject of future investigations.

To produce observable relative phase, the original proposal in Ref. [28] considers massive objects with $m \sim 10^{-14}kg$. The required mass is restricted by the minimum distance between the two masses $D-d$. At micro-meter scale, Casimir-Polder force, which is another source of interaction between neutral objects, becomes dominant over gravitational interaction. A minimum distance $D-d \sim 100\mu m$ is necessary to ignore influence from Casimir-Polder interaction. Later, a revised scheme based on Casimir screening [165] relaxes the parameters to $D \sim 47\mu m$, $d \sim 23\mu m$ by placing a conducting plate, which acts as a *Faraday cage*, between the test masses to screen the mutual electromagnetic interaction. On the other hand, to test the spin entanglement witness also requires a delicate balancing of magnetic field gradient to bring the superposition components back to the center. In the revised scheme, the test mass $m \sim 10^{-15}$ kg and the total accumulated phase during interaction time $\tau \sim 1s$ is of order of 0.01rad.

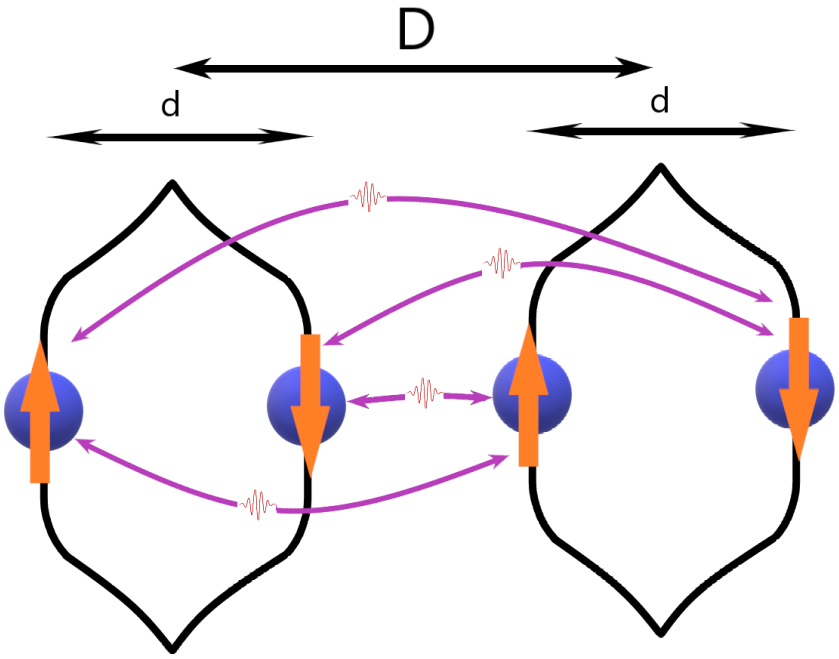

Fig. 3.1 **Schematic diagram: traveling of quantum coherent mediators.** Two test masses, each in superposition state and embedded with spin, are separated by distance D. quantum interactions induce relative phase among different superposition components through the exchange of quantum mediators.

3.3 Massive spatial qubit methodology for Witnesssing Gravitational Entanglement

In this chapter, we investigate the viability of testing the quantum nature of gravity with recently developed methodology: massive spatial qubit. This approach treats freely evolving spatially superposed masses as qubits, which does not call for spins. Therefore, it may relax the criteria for witnessing the quantum aspect of gravity. The schematic diagram is shown in Fig. 3.2. Two test masses m_1, m_2, each prepared in spatial superposition of two well separated Gaussian states $|L\rangle$ and $|R\rangle$, are placed adjacent to each other then freely evolve, under their own Hamiltonian, as well as undergo a joint phase evolution under their mutual gravitational interaction as shown in Fig. 2.2. The propagation of each individual wavepacket is modeled as the spreading of a Gaussian wavepacket due to free evolution. Each spatial superposition $\frac{1}{\sqrt{2}}(|L\rangle + |R\rangle)$ of test mass can be treated as a state of a qubit with the two qubit states identified with $|L\rangle$ and $|R\rangle$.

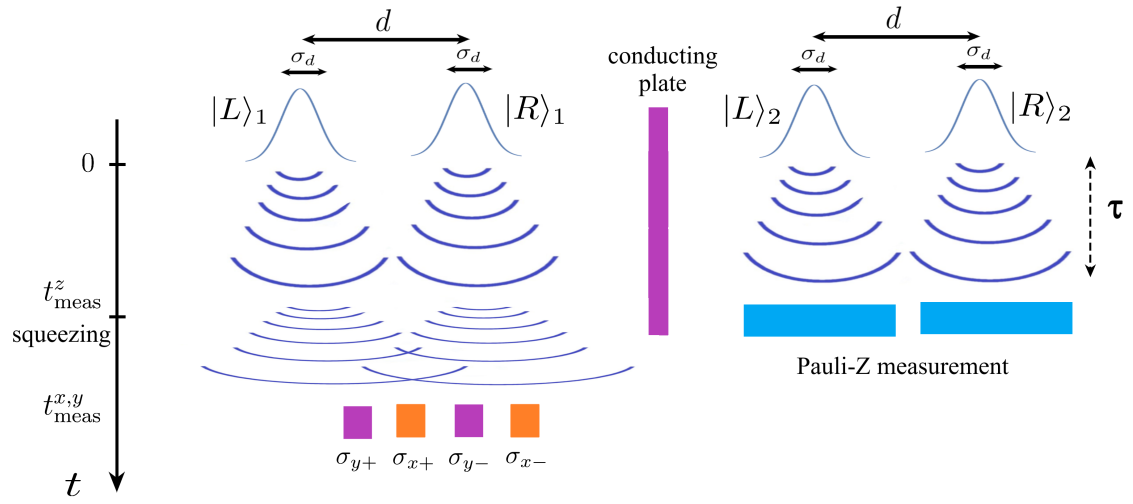

Fig. 3.2 **Testing quantumness of gravity with massive spatial qubits** This interaction induces entanglement which can be deduced from spatial qubit Pauli measurements. To evaluate the entanglement witness W, we conduct spatial qubit measurements on both masses and evaluate the correlations. For example, in the figure, Pauli-X, Pauli-Y measurements on test mass 1 and Pauli-Z measurements on test mass 2 are depicted. An additional conducting plate is inserted between the masses for electromagnetic shielding

3.3.1 Witnessing the quantum nature of gravity:

If quantum gravitational interaction is the only source of interaction, relative phase induced among the superposition components then reads (Please see the appendix for a more detailed treatment taking into account the traveling time of coherent mediators):

$$|\psi(t=0)\rangle = \frac{1}{\sqrt{2}}(|L\rangle_1+|R\rangle_1)\frac{1}{\sqrt{2}}(|L\rangle_2+|R\rangle_2) \tag{3.3}$$

$$\begin{aligned}\rightarrow |\psi(t=\tau)\rangle &= \frac{e^{i\phi}}{\sqrt{2}}[|L\rangle_1\frac{1}{\sqrt{2}}(|L\rangle_2+e^{i\Delta\phi_{LR}}|R\rangle_2)\\ &+ |R\rangle_1\frac{1}{\sqrt{2}}(e^{i\Delta\phi_{RL}}|L\rangle_2+|R\rangle_2)].\end{aligned} \tag{3.4}$$

It is true that the creation of a superposition of two localized states (a highly non-Gaussian state) is a *pre-requisite* for being able to use spatial qubits (we will not delve into that issue here in detail, but mention some possibilities in the next section). Here we concentrate on *how* to read-out spatial qubits in absence of (in this context impractical) beam-splitter elements, and thereby witness the entanglement of two masses without resorting to spins. Pauli measurements, which readout the encoded information, can be performed by placing spatial detectors at particular locations. Any entanglement induced during the propagation process can be witnessed by the correlations between two spatial qubits. All of Pauli-x,y

and z measurements are involved in obtaining these correlations. Pauli-z measurement $\sigma_z = |L\rangle\langle L| - |R\rangle\langle R|$ reads the probability amplitude of the encoded spatial qubit state, which has to be performed *before* $|L\rangle$ and $|R\rangle$ have spread so much as to be confused with each other (i.e., spread to about $\sim d$). On the other hand, Pauli-x measurements project on to states $\frac{1}{\sqrt{2}}(|L\rangle \pm |R\rangle)$ and Pauli-y measurements project on to states $\frac{1}{\sqrt{2}}(|L\rangle \pm i|R\rangle)$, which are only discernible in the interference plane as shown in Fig. 2.2, which implies that they are performed *after* each of $|L\rangle$ and $|R\rangle$ have spread to a length d so that they can overlap. At the interference plane, the probability of detecting the test mass at position x is given by:

$$P(x) = |\langle\psi|k_x\rangle|^2 \propto \left|\exp[\frac{ik_x d}{2} - k_x^2\sigma_d^2]\langle\theta|\psi\rangle\right|^2, \tag{3.5}$$

where $|\theta\rangle = |0\rangle + |1\rangle e^{i\theta}$, $\theta = k_x d$ and $k_x = \frac{xm}{\hbar t^{x,y}_{\text{meas}}}$ is the transverse wavevector. Projection of the spatial qubit state along σ_{x+}, σ_{x-} (σ_{y+}, σ_{y-}) can then be implemented by placing spatial detectors corresponds to $\theta = 0, \pi(-\pi/2, \pi/2)$ respectively. Thus the Pauli-x,y and Pauli-z measurements would normally have to be performed at different times t^z_{meas} (before spreading) and $t^{x/y}_{meas}$ (after spreading).

3.3.2 Squeezing requirement

The masses have to entangle sufficiently first. This inevitably requires a time of τ over which the gravitational interaction should act between them. This is the earliest time *any* measurement can occur as we want to measure the two masses after they are entangled. Thus we set $t^z_{meas} = \tau$, being careful that hardly any spreading of the wavepackets $|L\rangle$ and $|R\rangle$ happens in time τ. However, we want to measure Pauli-x,y on the *same* state, i.e., the state evolved up to time τ as the gravitational interaction cannot be switched off. This demands that we must also measure Pauli-x,y at (or very nearly) the same time. So we need to induce some process at τ so that the wavepackets immediately spread to $\sim d$ and overlap to interfere. This requires the application of an additional squeezing operator to the masses immediately after time τ. This localizes the wavefunctions so much (each of $|L\rangle$ and $|R\rangle$ are now highly squeezed) that in subsequent free evolution for $t^{x,y}_{meas} - t^z_{meas}$ they spread rapidly to overlap and interfere. Thus the extra squeezing at τ enables us to meet the criterion: $t^{x,y}_{meas} \sim t^z_{meas} = \tau$, so that both the Pauli-z and the Pauli-x,y measurements are essentially performed on the same entangled state of the two masses.

The spread of wavepackets scales approximately inversely proportional to its initial width $\sigma_d(0)$: $\sigma(t) \sim \frac{\hbar t}{m\sigma_d(0)}$. Therefore, application of squeezing operator at τ, squeezes width of the wavepacket and speeds up subsequent spreading. This technique can be accomplished by

passing the test masses through local Harmonic potentials with jumps between frequencies. More precisely, n sudden switches between frequencies ω_1 and ω_2, with a quarter period of harmonic evolution in each frequency, squeezes the wavepackets spatially by a factor $(\omega_1/\omega_2)^n$ [85, 142]. As, for the squeezing, we have to expend a quarter period of time $\pi/2\omega_j$ in each frequency ω_j, this inevitably requires a time

$$t_{squeeze} = n(\pi/2\omega_1 + \pi/2\omega_2). \tag{3.6}$$

On the other hand, the amount of squeezing depends on satisfying $t^{x,y}_{meas} \approx t^{z}_{meas} = \tau$. We want the $t_{squeeze}$ to be a negligible time-scale in comparison to the other times of the problem as the gravitational entanglement is always happening (we cannot stop it). Thus n, ω_1, ω_2 must be so chosen that

$$t_{squeeze} << t^{x,y}_{meas} \approx t^{z}_{meas} = \tau. \tag{3.7}$$

Squeezing thus places significant demands on this protocol.

3.3.3 Casimir screening imposed constraints

To shield the system from unwanted electromagnetic interaction, one places a conducting plate between the test masses to act as a *Faraday cage*. For simpicity we assume that the placement of a perfect conductor completely blocks the Casimir interaction between test masses. The Casimir screening scheme introduces additional Casimir force between the plate and test masses. The plate-mass Casimir interaction is now the dominant force at very small scale and places constraints on the system. The screen is closest to one of the components of the superposition ($|R\rangle$ for the mass to the left of the screen and $|L\rangle$ for the mass to the right of the screen). We do not want this component to be pulled so close to the screen that it prevents the overlap between the two components of each mass in order to enable the Pauli-x,y measurements. Thus we require that the spread of wavepackets (which we *exploit* in our scheme) dominates over the displacement due to Casimir force. This places a new constraint on minimum separation of a mass and the conducting plate. The Casimir force between a plate and sphere is given by[37]

$$F_{ca} = -\frac{3\hbar c}{2\pi}\left(\frac{\varepsilon - 1}{\varepsilon + 2}\right)\frac{R^3}{s^5}, \tag{3.8}$$

where ε is the dielectric constant of test masses, R is the radius of test masses and $s = \frac{D-d}{2}$ is the mass-plate separation.

We require that the spread of wavepacket dominates over the displacement due to Casimir force by at least one order of magnitude:

$$0.1\sigma_d(t_1) \geq D_{ca}, \tag{3.9}$$

where $\sigma_d(t)$ is the width of the propagating wave packets, t_1 is the total time before the wavepackets overlap. Thus, in terms of the notation of the previous part of the chapter, $t_1 \sim t^{x,y}_{meas} - t^{z}_{meas} - t_{squeeze}$, as that is the time over which the wavepacket expands after squeezing (We know that this spread is required to be of the order of the slit separation d for the overlap to happen; moreover, actually $t_1 << t^{x,y}_{meas}, t^{z}_{meas}, t_{squeeze}$).

Classical treatment of Casimir force gives an estimate of its resulting displacement on test masses given by:

$$D_{ca} = -\frac{9\hbar c}{16\pi^2}\left(\frac{\varepsilon-1}{\varepsilon+2}\right)\frac{1}{\mu s^5}, \tag{3.10}$$

where μ is the density of test mass.

On the other hand, the spread of Gaussian wave packet $\sigma_d(t)$ scales linearly with time by a factor of $\frac{\hbar}{\sigma_d m}$. Since wave overlaps at a time $t \sim 2m\sigma_d d/\hbar$, the width of wavepackets spread is of same order as the slit separation $\sigma_d(t_1) \sim d$. In the original setup, d and $\frac{D-d}{2}$ are on the same scale. We may then take $\sigma_d(t_1) \sim d \sim s$. The above parameter domain is satisfied for mass density $\mu \sim 3 \times 10^3 kg/m^3$, $\varepsilon = 5.7$, and the minimum plate-mass separation $s \sim 12\mu m$.

3.3.4 Induced phase

With the same mechanism as in [28], we can prepare initial state given by Eq. 3.3. Taking $D \sim 40\mu m, d \sim 10\mu m$, for mass $m \sim 10^{-15} kg$, gravitational interaction, if quantum, would induce relative phase $\Delta\phi \sim 1 \times 10^{-2} rad$ after $\tau \sim 3s$ of entangling time. To certify the induced relative phase, we estimate the entanglement witness [40]

$$W = I \otimes I - \sigma_x \otimes \sigma_x - \sigma_z \otimes \sigma_y - \sigma_y \otimes \sigma_z. \tag{3.11}$$

The expectation value $\langle W \rangle = \mathrm{Tr}(W\rho)$ would be negative, if the two masses are entangled. Using Eq. 3.4 for the state, and phases $\Delta\phi_{LR} = \Delta\phi_{\uparrow\downarrow}, \Delta\phi_{RL} = \Delta\phi_{\downarrow\uparrow}$ from below Eq. 3.2, the expected witness measure at $\tau \sim 3s$ is ~ -0.0065.

3.3.5 Initial state preparation

Witnessing the quantum nature of gravity through qubit correlations requires preparation of superposition state of large spatial splitting $d \sim 10 - 100\mu m$ of a micron scale mass ,

$m \sim 10^{-15} - 10^{-14}$kg [28, 165]. This is considerably beyond what has already been realized (e.g., 10^{-25}kg mass over $0.5m$ [96], or 10^{-22}kg mass over 0.25μm [6], [58]). However, there are several proposed schemes to achieve the required superpositions, with criteria in terms of temperature, pressure, acceleration/vibration noise well identified.

The protocol starts from preparing a mass in a pure quantum state in a harmonic trap, typically the ground state. This mass may or may not have a spin embedded in it (the protocol of creating the initial state $\frac{1}{\sqrt{2}}(|L\rangle + |R\rangle)$ will depend on that). We imagine these objects to be levitated in low frequency static magnetic traps [103, 186, 124, 169]. Feedback cooling can be achieved by first shining light towards the particle. Scattered photons, which carries information of the particle's position, are collected by photo-diode detector. For example, from detecting n scattered photons, the position of a particle gets determined to the accuracy of $\lambda/\sqrt{n}$, where λ is the wavelength of the scattered light [69]. This information is then used as feedback to cool the motion of the micro-sphere via an external damping force. Essentially, the information gathering rate from detecting scattered photons must overtake the entropy increase rate of the object from undetected scatterings (photons, atoms) and noises from the environment. Using the feedback cooling principle, a mechanical oscillator as massive as 10kg has been prepared close to its ground state, the center-of-mass motion of which is cooled down to tens of nano-Kelvin [176], which involved to measuring position to the uncertainty of $\sim 10^{-20}\text{m}/\sqrt{\text{Hz}}$. Cryogenic diamagnetic levitated micro-mechanical oscillator has also been realized with very low (μ Hz) dissipation rate [103, 186]. For test mass $m \sim 10^{-15}$kg in a trap with frequency $\sim \mathscr{O}(10-100)$Hz, its ground state spread is $\sim \mathscr{O}(0.1-1)$nm. As this uncertainty being much larger than the precision to which position has been localized recently in feedback cooling [176], it is reasonable to suppose that feedback cooling to nearly the ground state is also imminent for the above systems (for example, will require $n \sim 10^8$ scattered photons to be detected, with undetected photons being much lower, in a time scale over which no collisions with air molecules take place). Following the above stage either spinless or spinful methods can be used to create the superposition.

If we have a spin embedded in the mass, a popular avenue to create a small superposition ($\leq$ 100nm) is to use the Stern-Gerlach effect [151, 184, 170, 28, 179]. The test mass in an initially pure localized state $|C\rangle$ (say, the ground state) is prepared with its spin in a state $\frac{1}{\sqrt{2}}(|\uparrow\rangle + |\downarrow\rangle)$ (by microwave pulses), and the trap is suddenly switched off. The spin state undergoes spatial splitting due to an inhomogeneous magnetic field gradient so that the system evolves as

$$\frac{1}{\sqrt{2}}(|\uparrow\rangle + |\downarrow\rangle)|C\rangle \rightarrow \frac{1}{\sqrt{2}}(|L\uparrow\rangle + |R\downarrow\rangle). \tag{3.12}$$

A subsequent measurement of the spin in a different basis, say, the $|\pm\rangle$ basis, and, for example, getting the $|+\rangle$ outcome, will prepare the mass in the spatial superposition

$$\frac{1}{\sqrt{2}}(|L\rangle + |R\rangle). \tag{3.13}$$

Care must be taken so that the spin measurement does not reveal the position of the mass itself to a better precision than the $|L\rangle$ and $|R\rangle$ difference. However, we now require to amplify this superposition as we require (in the case where there is a screening of electromagnetic interactions) a spatial splitting of $\sim 10\mu$m, while the diamagnetism induced by the magnetic field gradient used for the splitting, restricts the splitting [136, 122]. Interestingly, the superposition could be *amplified* using a current carrying wire providing a diamagnetism induced repulsion between wire and each split component [189]. Alternatively, spins may be subject to nonlinear gradients to accumulate a velocity difference before catapulting to a large size [188]. With magnetic field gradient $\sim 10^3 Tm^{-1}$, the desired separation of $10\mu m$ can be obtained after $\sim$ 1s of flight time [188]. It is easy to verify that during such intervals of time, the wavepacket spread remains in the $\sim \mathscr{O}(0.1-1)$nm regime. During these protocols, spin coherence does not need to be retained during the amplifications (diamagnetic repulsion/catapulting) the electronic spin does not play an active role. So, just before the amplification stage, one could map it to much more coherent nuclear spins, or alternately, simply measured in a different basis as noted above, to obtain directly the $\frac{1}{\sqrt{2}}(|L\rangle + |R\rangle)$ state. noted above so as to have only a spatial superposition. Moreover, for the application herewith (using spatial qubits) we do not need to complete an interferometer – only create the large splitting superposition, which removes a significant challenge.

It is possible that even without spins the state $\frac{1}{\sqrt{2}}(|L\rangle + |R\rangle)$ can be produced as far as $\sim 1\mu$m sized distances between $|L\rangle$ and $|R\rangle$ are concerned. For example, the first few stages of the on-chip interferometer of Ref. [138] based on coherent inflation and a $\hat{x}^2$ (position^2) measurement can be used (till the superposition is generated). One can then, in principle, combine with an diamagnetic repulsion aided further spatial splitting of the $|L\rangle$ and $|R\rangle$ terms [189] so as to reach $\sim 10\mu$m size.

3.3.6 Decoherence

During propagation, background gas collision and black body radiation unavoidably decoheres quantum coherence of the superposition state. Adopting the model in [144], air molecule collision decoheres the 10^{-15}kg test mass at a rate of $\sim 0.776 s^{-1}$ under pressure $\sim 10^{-15}$Torr. Blackbody radiation arises from emission, absorption and scattering of thermal photons. The emission localization parameter typically dominates because the internal

temperature is usually larger than the external temperature. If internal temperature can be cooled down to $T_i = 4$K, black body radiation decoheres the test mass at a rate of $\sim 0.72s^{-1}$, which corresponds to $\sim$ 10s of coherence time. The required cooling to keep coherence of the superposition state is challenging with state of art technology.

3.3.7 Squeezing challenges

Take initial width ~ 0.4nm, the wavepacket expands to ~ 0.85nm after 3 seconds of flight. We will then have to squeeze the state by about 7 orders of magnitude to 1.5×10^{-16}m, so that it expands to $\sim 20\mu m$ in the next $0.03s$, where interference occurs.

Optical squeezing is the most common technique for microscopic objects. However, momentum recoil due to photon scattering induce decoherence and heating on the levitated objects, the rate of which scales with the object size [141, 129, 38]. For large mass $\sim 10^{-15}$kg, this approach becomes infeasible, the coherence time is only $\sim 10^{-6}$s. Alternatively, one may adopt diamagnetic trapping for squeezing [103, 186, 124, 169]. Diamagnetic trapping typically operates at much lower frequencies compare to its optical counterpart, therefore, making it advantageous to hold large masses. Potential energy per unit volume of a diamagnetic mass in trapped in magnetic field reads:

$$U \approx -\frac{\chi_m}{2\mu_0} B^2 + \rho g r, \tag{3.14}$$

where χ_m is the mass magnetic susceptibility, μ_0 is the magnetic permeability in vacuum, g is the gravitational acceleration, B is induction of the magnetic field when the particle is absent and r is the vertical displacement.

The mechanical frequency is therefore:

$$\omega_m = \sqrt{\frac{\chi_m}{\mu_0}} \frac{\partial B}{\partial r}, \tag{3.15}$$

where $\frac{\partial B}{\partial r}$ is the field gradient.

To control the motional superposition state during the squeezing procedure, the thermal decoherence rate $\gamma_{th} = \bar{n}\gamma$ needs to be suppressed, where γ is the mechanical dissipation rate and $\bar{n} = \frac{k_B T}{\hbar \omega_m}$ is the average phonon number. To keep coherence during n periods of quarter oscillations, the dissipation rate must, therefore, satisfy the following relation:

$$\gamma < \frac{\hbar \omega_m^2}{n k_B T}. \tag{3.16}$$

In order to achieve the required squeezing, 7 times of successive changes between two periods of harmonic potentials of 100Hz and 1000Hz would suffice. The environmental temperature can be kept at $\sim 10mK$ with commercial dilution refrigerator. The dissipation rate then must be kept below micro-hertz $\gamma < 1\mu$ Hz.

For solid state systems, the main contribution to dissipation is the direct coupling between the system and the substrate. Ultra-low dissipation of micro hertz has been reported with diamagnetic levitated objects, where permanent magnets are used for trapping. In [186], where the levitated mass is similar to our scheme, damping rate of μHz is achieved at pressure $\sim 3\times 10^{-7}Torr$ and room temperature. The major contribution of damping came from background gas collision, which scales linearly with pressure. Dissipation due to gas collision could be significantly reduced by lowering temperature and pressure. Comparing with the condition to keep coherence during the propagation stage, one finds that the required level of vacuum is much less demanding during the squeezing stage.

However, permanent magnet based scheme maybe unfeasible for squeezing since successive changes of trapping potential are required. Alternatively, one may use magnetic field generated by current-carrying coil, which introduces an additional type of dissipation due to field fluctuation. One has to consider specific current sources for that and we do not go to that technicality herewith. Moreover, there could be other sources of random forces at given times $\delta F(t)$. Thus we herewith estimate the constraint those forces have to satisfy. Although the magnetic field noise will be switched off after attaining the required squeezing, and free spreading of wavepacket under propagation will ensue, we assume some random force noise being always present and constrain it (this will surely be an overestimate as far as forces from magnetic field noise are concerned). Random forces will give a decoherence rate of

$$\Gamma \sim \frac{S_{FF}(\Omega)d^2}{\hbar^2}, \tag{3.17}$$

where $S_{FF}(\Omega) = \int \delta F(0)\delta F(t)e^{i\Omega t}dt$ is the force noise spectrum at the frequency $\Omega \sim 1/\tau$ of our experiment, and d is the spatial splitting of each superposition. Keeping $\Gamma < 1$Hz gives us the constraint that random force noise should be kept below $\sqrt{S_{FF}} \sim 10^{-29}\mathrm{N}/\sqrt{\mathrm{Hz}}$. Note that although this may sound challenging, faster frequency noise does not affect the experiment particularly, while noise at this Hz frequency should be determinable by precision measurements over a long duration of 1s to be taken into account in the experiment. Note that this requirement is not unique to the spatial qubit method. Rather in the spatial qubit method we are using free propagation for a large fraction of the time when, at least randomness in superposition creating/delocalizing forces will be inactive.

3.4 Summary

We have analyzed the feasibility of applying the massive spatial qubit methodology to witness the quantum nature of gravity. This will enable a *spinless* witnessing of the gravitational entanglement growth between two masses ($\sim 10^{-15}$ kg each), essentially through position measurements on masses, but *still* using qubit-qubit correlations to measure the entanglement. The core property used here is the spreading of a free quantum wavepacket which brings two initially localized states $|L\rangle$ and $|R\rangle$ to interfere so that observables such as $\sigma_x = |L\rangle\langle R| + |R\rangle\langle L|$ can be measured from the interference pattern. It is expedient work within the remit of a *Faraday* shielding scheme so as to block unwanted electromagnetic interactions between two masses, so that the masses can be brought closer and still interact only gravitationally. But here the necessity for the wavepacket spreading to dominate over the Casimir force of the Faraday screen to its nearest component arises. This, in turn, implies a minimum distance to the screen, which, in turn, dictates a minimum separation $d \sim 10\mu$m between $|L\rangle$ and $|R\rangle$ to have a significant entanglement growth rate. This minimum d then also necessitates a wavefunction spreading from a very localized width σ_d of each of $|L\rangle$ and $|R\rangle$ rapidly to $\sim d$ in an extremely short time-scale, so that the spatial qubit σ_z and σ_x measurements are accomplished at nearly the same time (on the same entangled state of the two masses). This is turn, necessitates squeezing the width immediately after significant gravitationally generated entanglement is attained between the masses (at a time τ). The requirements and a method for achieving this squeezing is described along with the challenges (it requires position squeezing of the wavepacket by 7 orders of magnitude). As long as the above can be met, and spatial superpositions can be generated (for which one may use spins or other spinless methods), the evidencing through a qubit-qubit entanglement witness can take place purely through position measurements.

Part II

Quantum Liang Information Flow as Causation Quantifier

Chapter 4

Quantum Liang Information Flow as Causation Quantifier

In Chapter 3, we focus on the aspect of information transmission and causality. Liang information flow is a quantity widely used in classical network theory to quantify causation, and has been applied widely, for example, to finance and climate. The most striking aspect here is to freeze/subtract a certain node of the network to ascertain its causal influence to other nodes of the network. Such an approach is yet to be applied to quantum network dynamics. Here we generalize Liang information flow to the quantum domain using the von-Neumann entropy. Using that we propose to assess the relative importance of various nodes of a network to causally influence a target node. We exemplify the application by using small quantum networks.

4.1 Motivation

The significance of information flow lies in its logical association [106] with the important notion of causation [72, 135, 157, 111, 23, 154]. Historically, various measures of classical information flow were proposed e.g., [72, 167, 154, 111, 30, 158, 161, 33]. Nonetheless, limitations were pointed out e.g., [74, 156, 161], the most severe being an incorrect reflection of causality. In 2005, Liang and Kleeman found a law for two-dimensional classical systems [111]. Later on, the dimensionality and determinism limitations were overcome, and eventually Liang was able to link information flow to causality and establish a universally applicable formalism within the framework of classical dynamical systems [111, 104–106, 109, 110]. This series of works puts the notion of information flow and causation on a rigorous footing, as Liang(2016) [106] argued: "Information flow and causality can be derived *ab initio*." The

formalism has been validated with various benchmark cases [106], and successfully applied to many realistic problems: glaciology [166], neuro-science [84], El Niño-study[105] and prediction [112], precipitation-soil moisture interaction[73], global climate change [159, 53], economics [113], etc.

The discussion of causality in quantum physics goes back to the paradigmatic Bell experiment [19]. Causal structure places constraints on the correlations that can be generated in any classical hidden variable theories, which quantum physics violates [63, 8, 43, 148, 70]. Motivated by the possible relation between causality and correlations (Liang just put this relation in a mathematical formula [105, 106], various attempts have been made to estimate causal influences in certain quantum environments [65, 77, 39, 47, 64, 13, 178, 2]. The quantification of causal effects in quantum regime sheds new light on quantum communication [60, 139] and helps understanding information flow in quantum processors [51, 50]. Usually, correlation functions of Heisenberg picture evolving operators are used to ascertain casual influences, but caution should be exercised since correlation does not imply causation [105, 106].

Surprisingly, the straightforward approach to ascertaining causality that an experimentalist will naturally employ, i.e., to subtract a given component from a network and examine its influence, remains unexplored. Motivated by that, we hereafter adopt Liang's methodology to quantify causal influence in quantum systems. As opposed to all the approaches mentioned above in the quantum context, here one detaches or freezes a certain subsystem of a network (sender) in order to ascertain its causal influence on other subsystems (target). The change of a target element's von Neumann entropy, which possess various interpretations [130], then gives the information flow from the sender.

4.2 Classical information flow-based causality analysis

Liang information flow quantitatively defines causality. The series of work starts with the investigation of bi-variate deterministic systems and is originally based on a heuristic argument [111]. Later on, the formalism is put on a rigorous footing and generalized to stochastic and multi-variate systems [104, 106, 110]. To present this fundamental idea in its simplest form, we will focus on bi-variate autonomous system with equation of motion given by:

$$\frac{d\mathbf{x}}{dt} = \mathbf{F}(\mathbf{x}) \tag{4.1}$$

where $\mathbf{x} = (x_1, x_2) \in \Omega$ and the sample space Ω is a direct product of subspace $\Omega_1 \otimes \Omega_2$. $\mathbf{X} = (X_1, X_2)$ is the random variable of subsystem 1 and 2. $\{\mathbf{X}, t\}$ is assumed a stochastic process

and the joint probability density distribution at time t is denoted $\rho(x_1,x_2,t)$. $\mathbf{F}=(F_1,F_2)$ may be interpreted as the force acting on the system. Shannon entropy of this system is given by:

$$S_{(classical)}(t) = -\int_{\Omega} \rho log(\rho) dx_1 dx_2 \tag{4.2}$$

Substitute Eq. 4.1 into Eq. 4.2, one obtains the time rate change of entropy, provided that ρ vanishes at boundaries[111]:

$$\frac{dS_{(classical)}}{dt} = E(\nabla \cdot \mathbf{F}) \tag{4.3}$$

The right hand side is the expectation value of the divergence of force $\mathbf{F}$. The physics revealed by Eq. 4.3 is that the expansion and contraction of the phase space governs the change of entropy.

The probability distribution of a subsystem, say subsystem 1, can be obtained by taking the marginal density $\rho_1(x_1,t) = \int_{\Omega_2} \rho(x_1,x_2,t) dx_2$. Its entropy can be calculated:

$$\frac{dS_{1(classical)}}{dt} = -\int_{\Omega} \rho [\frac{F_1}{\rho_1} \frac{\partial \rho_1}{\partial x_1}] dx_1 dx_2 \tag{4.4}$$

Liang and Kleeman identified that the entropy change of subsystem 1 given by Eq. 4.4 can be decomposed into two parts: the evolution due to X_1 alone, with effect from subsystem 2 excluded, denoted as $\frac{dS_{1\not2(classical)}}{dt}$. Another part is the influence from X_2 through the coupling with external force. Through heuristic reasoning based on the interpretation of Eq. 4.3, Liang and Kleeman argue that if subsystem 1 evolves on its own, the entropy change of subsystem 1 would depend only on $\partial F_1/\partial x_1$:

$$\frac{dS_{1\not2(classical)}}{dt} \equiv E(\frac{\partial F_1}{\partial x_1}) = \int_{\Omega} \rho \frac{\partial F_1}{\partial x_1} dx_1 dx_2, \tag{4.5}$$

In 2016, Liang [106] showed that the above result Eq. 4.5 can be derived by treating x_2 as a fixed parameter at time t, rather than a variate. Consider the mapping $\Phi : \mathbf{x}(t) \mapsto \mathbf{x}(t+\Delta t)$, which acts as follows:

$$\begin{cases} x_1(t+\Delta t) = x_1(t) + F_1(x_1,x_2,...,x_n)\Delta t \\ x_2(t+\Delta t) = x_2(t) + F_2(x_1,x_2,...,x_n)\Delta t \\ \qquad\qquad \vdots \\ x_n(t+\Delta t) = x_n(t) + F_n(x_1,x_2,...,x_n)\Delta t \end{cases}, \tag{4.6}$$

the modified mapping $\Phi_{\not 2}$ with x_2 frozen as a parameter during the time interval Δt is:

$$\begin{cases} x_1(t+\Delta t) &= x_1(t)+F_1(x_1,x_2,...,x_n)\Delta t \\ x_2(t+\Delta t) &= x_2(t) \\ x_3(t+\Delta t) &= x_3(t)+F_3(x_1,x_2,...,x_n)\Delta t \\ \quad\vdots & \\ x_n(t+\Delta t) &= x_n(t)+F_n(x_1,x_2,...,x_n)\Delta t \end{cases}, \tag{4.7}$$

$\rho_{1\not 2}(t+\Delta t)$ denotes the density of x_1 under the modified mapping $\Phi_{\not 2}$ and $S_{1\not 2(classical)}$ is its Shannon entropy.

The rate of information flow from X_2 to X_1 is then:

$$\begin{aligned} T_{2\to 1} &= \frac{dS_{1(classical)}}{dt} - \frac{dS_{1\not 2(classical)}}{dt} \\ &= -\int_\Omega \rho[\frac{F_1}{\rho_1}\frac{\partial \rho_1}{\partial x_1}+\frac{\partial F_1}{\partial x_1}]dx_1dx_2 \end{aligned} \tag{4.8}$$

This formula verifies what Liang refers to as *the principle of nil causality*:

If F_1 is independent of x_2, then the information flow from 2 to 1 vanishes: $T_{2\to 1}=0$.

If $T_{2\to 1}$ is negative (positive), the interpretation is that system 2 is making system 1 more (less) certain. Note that the information flow formalism Eq. 4.8 is asymmetric, that is $T_{2\to 1}\neq T_{1\to 2}$. When the information flow from 2 to 1 vanishes, that from 1 to 2 maybe non-zero. The asymmetry feature distinguishes the information flow formalism with classical correlation measures.

It should be pointed out that the evaluation of Eq. 4.8 requires full knowledge of the dynamics. In [105], Liang showed that $T_{2\to 1}$ can be estimated with local statistics. The maximum-likelihood estimator of Eq. 4.8 is shown to be a combination of some sample covariances, which greatly facilitates the implementation of the causality analysis.

This formalism has been widely applied to realistic schemes [105, 159, 73, 166, 84]. Among them, we will briefly mention its application to a network consisting of Stuart-Landau oscillators [109], a typical model for many biological phenomena [160]. The magnitude of Liang information flow quantifies the influence of individual components to produce the collective behavior of the whole system. The direct addition of individual contributions does not equal the cumulative information flow, demonstrating its collective property. Moreover, the node with greatest information flow is verified to be the most crucial as its suppression

leads to shut down of the entire network. Surprisingly, such a node may be sparsely connected, rather than a center of network. The information-flow based causality analysis successfully explains why small defects at local node could severely damage structural integrity.

4.2.1 Classical closed bivariate system

The classical model considered in Eq. 4.1 is dissipative. System 1 and 2 exchanges energy with the environment through external force $\mathbf{F}$. If system 1 and 2 is closed, the divergence of force $\mathbf{F}$ vanishes: $\nabla \cdot \mathbf{F} = 0$. As a result, Eq. 4.3, Eq. 4.5 becomes: $dS_{(classical)}/dt = E(\nabla \cdot \mathbf{F}) = 0$, $dS_{12(classical)}/dt = E(\frac{\partial F_1}{\partial x_1}) = 0$, therefore,

$$T_{2\to 1} = \frac{dS_{1(classical)}}{dt} \tag{4.9}$$

Eq. 4.9 is completely in agreement with the quantum formalism obtained for initially mixed bipartite system.

4.3 Quantum Generalization: Definition

Consider a multi-partite system with a density operator state ρ, evolving under a generic unitary operator $U(t)$. The evolution leads to an entropy change of its subsystems as initial uncertainties can flow between the subsystems as well as when they get correlated quantum mechanically with each other (an open system is also addressed here by tracing out the ancillary degrees of freedom). Following Liang's methodology, we decompose the time rate of change of the von Neumann entropy of a subsystem A, dS_A/dt, into two parts: $T_{B\to A}$, the rate of information flow from subsystem B to A, and $\frac{dS_{A\not B}}{dt}$, the entropic evolution rate of subsystem A with the influence from B excluded:

$$T_{B\to A} = \frac{dS_A}{dt} - \frac{dS_{A\not B}}{dt}. \tag{4.10}$$

S is the von Neumann entropy given by $S = -\mathrm{Tr}(\sigma \log \sigma)$ for arbitrary state σ. $S_{A\not B} = S(\rho_{A\not B}) = S[\varepsilon(t)_{A\not B}\rho_A(0)]$, where $\varepsilon(t)_{A\not B}$ is a map denoting the evolution of A with B frozen. We will discuss the definition and properties of $\varepsilon(t)_{A\not B}$ in the following section. If we consider time evolution as a discrete mapping during interval Δt, the cumulative information flow is then formulated in terms of the change of entropy ΔS:

$$\mathbb{T}_{B\to A} = \int T_{B\to A} dt = \Delta(S_A - S_{A\not B}). \tag{4.11}$$

Note that the von Neumann entropy, hence the information flow formalism, possess various interpretations [130]. Particularly distinct from the Shannon entropy, the von Neumann entropy quantifies the entanglement within a pure bipartite quantum system. $S_{A\not B}$ (or S_A) can then be interpreted as the entanglement between A and the rest of the universe with (or without) B frozen. The term $(S_A - S_{A\not B})$ that appears in Eq. 4.10, 4.11 is then the difference of these two entanglement measures, in units of ebits. $\mathbb{T}_{B\to A}$ then quantifies the causal influence of B on A in the sense of how much it causes the entanglement of A with the rest of the universe to change. Similarly, other interpretations, such as the uncertainty of a given state, also apply here.

4.3.1 Evolution of subsystem A with B frozen

Since $\varepsilon(t)_{A\not B}$ is a mapping of states, it can be interpreted as a quantum channel acting on subsystem A [130]: $\rho_A(0) \overset{\varepsilon(t)_{A\not B}}{\to} \rho_{A\not B}(t)$. We further require that $\varepsilon(t)_{A\not B}$ corresponds to a physical process, therefore it can be obtained from taking the partial trace of the full system, which evolves unitarily. For tripartite system ρ_{ABC}:

$$\rho_{A\not B}(t) = \mathrm{Tr}_{BC}\{U_{A\not BC}(t)\rho_{ABC}(0)U^{\dagger}_{A\not BC}(t)\} \tag{4.12}$$

for some unitary operator $U_{A\not BC}$.

4.4 *The principle of nil causality* in quantum regime

We define the evolution mechanism with a subsystem frozen in terms of tensor product of unitary operations acting on the frozen part and other parts of the system respectively:

$$U_{A\not BC}(t) = \mathscr{V}_{AC} \otimes \mathscr{W}_B \tag{4.13}$$

where $\mathscr{V}_{AC}$ and $\mathscr{W}_B$ are unitary operators acting on subsystems AC and B respectively. Frozen mechanism of the form Eq. 4.13 guarantees what Liang referred to as *the principle of nil causality* [106]:

$T_{B\to A} = 0$ if the evolution of A is independent of B, that is, the unitary evolution operator $U_{ABC}(t)$ takes separable form $\mathscr{M}_A \otimes \mathscr{N}_{BC}$ or $\mathscr{O}_{AC} \otimes \mathscr{Q}_B$.

For tripartite system, if $U_{A\not BC}(t)$ takes the form of Eq. 4 ($\mathscr{V}_{AC} \otimes \mathscr{W}_B$), then the statement of causality is satisfied, that is, $T_{B\to A} = 0$ when A evolves independent of B.

If $U_{ABC} = \mathscr{M}_A \otimes \mathscr{N}_{BC}$, the evolution of A is solely determined by unitary operator $\mathscr{M}_A$. Excluding B from the joint evolution of subsystem BC, denoted $\mathscr{N}_{\not BC}$, has no effect on A. Therefore, $\rho_A(t) = \rho_{A\not B}(t) = \mathscr{M}_A \rho_A(0) \mathscr{M}_A^\dagger$. By the unitary invariance of von-Neumann entropy, $\frac{dS_A}{dt} = \frac{dS_{A\not B}}{dt} = 0$, thus $T_{B\to A} = 0$.

If $U_{ABC}(t) = \mathscr{O}_{AC} \otimes \mathscr{Q}_B$, it is already of the form given in Eq. 4.13. Therefore, excluding B or not has no impact on the joint evolution of system AC. That is,

$$\begin{aligned} \rho_A(t) &= \mathrm{Tr}_{BC}\{U_{ABC}(t)\rho_{ABC}(0)U_{ABC}^\dagger(t)\} \\ &= \mathrm{Tr}_C[\mathscr{O}_{AC}\rho_{AC}(0)\mathscr{O}_{AC}^\dagger] \\ &= \mathrm{Tr}_{BC}\{U_{A\not BC}(t)\rho_{ABC}(0)U_{A\not BC}^\dagger(t)\} = \rho_{A\not B}(t) \end{aligned}$$

Therefore, $T_{B\to A} = \frac{dS_A}{dt} - \frac{dS_{A\not B}}{dt} = 0$.

This results obtained above can be easily extended to multi-dimensions. Whether the converse proof also holds remains an open question.

Therefore, the causal structure of space-time in physics is embedded in the formalism. If quantum operations, conducted at 4-dimensional coordinates x and y, are space-like separated, hence non-causal, then the operations acting at x do not affect the state located at y and vice versa. The quantum operations at x and y commute and the joint evolution is in product form. Thus the quantum Liang information flow from one coordinate to another vanishes.

Bipartite system

Consider a bipartite state ρ_{AB} under unitary evolution $U_{AB}(t)$. Comparing with Eq. 4.13, $U_{A\not B}$ takes the form $\mathscr{V}_A \otimes \mathscr{W}_B$ in 2 dimensions. Since von Neumann entropy is invariant under a unitary change of basis, $\rho_{A\not B} = \mathscr{V}_A \rho_A(0) \mathscr{V}_A^\dagger$ and $\frac{dS_{A\not B}}{dt} = 0$. Therefore, the rate of information flow from B to A: $T_{B\to A} = \frac{dS_A}{dt}$. Similarly,$T_{A\to B} = \frac{dS_B}{dt}$. If the initial state $\rho_{AB}(0)$ is pure, that is, the system is closed, by Schmidt decomposition, ρ_A and ρ_B share the same set of eigenvalues. Since closed bipartite system is symmetric, $S_A(t) = S_B(t)$ and $T_{B\to A} = T_{A\to B}$. In general, if the initial state $\rho_{AB}(0)$ is mixed, which can arise from entanglement with some external system, then we no longer have the symmetry $T_{A\to B} \neq T_{B\to A}$. Consider CNOT gate with controlled qubit A and target qubit B acts on the initial state $\rho_{AB}(0) = (1/2|0\rangle\langle 0|_A + 1/2|1\rangle\langle 1|_A) \otimes |0\rangle\langle 0|_B$, the system evolves to $1/2|0\rangle\langle 0|_A \otimes |0\rangle\langle 0|_B + 1/2|1\rangle\langle 1|_A \otimes |1\rangle\langle 1|_B$. The cumulative information flow for this discrete mapping $\mathbb{T}_{B\to A} = \Delta S_A = 0$ and $\mathbb{T}_{A\to B} = \Delta S_B = 1$bit. The asymmetric quantum information flow obtained for initially mixed bipartite system parallels its classical counterpart. For multi-partite system $\rho_{ABCD\cdots}$, the information flow from the rest of a closed system towards a particular unit, say A, is equivalent to the bipartite scenario: $T_{BCD\cdots\to A} = \frac{dS_A}{dt}$, $\mathbb{T}_{BCD\cdots\to A} = \Delta S_A$.

Multipartite system

Evaluation of the information flow in a multipartite system requires a method to fix $\mathscr{V}_{AC}$ in Eq. 4.13. Here we demonstrate this with a tripartite system ρ_{ABC}. We define the evolution of A with B frozen by replacing the interaction terms relevant to B in the Hamiltonian with the identity operator. For simplicity, consider the evolution operator generated from a time-independent Hamiltonian H, $U(t) = e^{-iHt}$, with $\hbar$ set to unity. For instance, let:

$$H_{ABC} = H_{0A} + H_{0B} + H_{0C} + \mathscr{A} \otimes \mathscr{C} + \mathscr{B} \otimes \mathscr{C} \tag{4.14}$$

where H_{0i},with $i = A,B,C$, is the free Hamiltonian. $\mathscr{A},\mathscr{B}$ and $\mathscr{C}$, which occur in the interactions, are hermitian operators acting on subsystems A,B and C respectively. The evolution mechanism with B frozen is then: $U_{A\not{B}C} = e^{-iH_{A\not{B}C}t}$, where

$$H_{A\not{B}C} \equiv H_{0A} + H_{0C} + \mathscr{A} \otimes \mathscr{C} + I_B \tag{4.15}$$

$U_{A\not{B}C}$ is clearly of the product form given in Eq. 4.13, with $\mathscr{W}_B = I$ and $\mathscr{V}_{AC}$ generated by hermitian operator $H_{0A} + H_{0C} + \mathscr{A} \otimes \mathscr{C}$. The meaning of $U_{A\not{B}C}$ is then:

evolution of the system if subsystem B is removed from the original evolution mechanism.

The operational meaning of the frozen mechanism guarantees that this definition is basis (observable) independent. Now, we are equipped with the tools needed to evaluate quantum Liang information flow.

4.5 Application: multi-qubit spin system

Consider a multi-qubit spin chain. The interaction Hamiltonian between any two interacting qubits i, j is given by [185]:

$$H_{spin,ij} = \eta_{ij}(\sigma_{+i}\sigma_{-j} + \sigma_{-i}\sigma_{+j}) \tag{4.16}$$

where $\sigma_{\pm}$ can be expressed in terms of Pauli matrices $\{\sigma_{x,y,z}\}$, $\sigma_{\pm} = \frac{1}{2}(\sigma_x \pm i\sigma_y)$, η_{ij} represents the coupling strength. The interaction Hamiltonian for 3 interacting qubits, labeled A, B, C, of the form Eq. 4.14 is given by:

$$H_{int,ABC} = \eta_{AC}(\sigma_{+A}\sigma_{-C} + \sigma_{-A}\sigma_{+C}) + \eta_{BC}(\sigma_{+B}\sigma_{-C} + \sigma_{-B}\sigma_{+C}) \tag{4.17}$$

For simplicity, η has scaled value with respect to unit relative coupling strength of frequency dimensions. Time t is scaled inversely to unit relative coupling strength.

4.5.1 Relative coupling strength variation

We here investigate the cumulative information flow $\mathbb{T}$ from A,B to C with different coupling strengths; the classical counterpart is seen in [108]. We set the initial state of the sending qubits A, B being maximally mixed while the receiving qubits C pure: $\rho(0) = I_A \otimes I_B \otimes |0\rangle\langle 0|_C$. So the sending qubits are competing to propagate uncertainty towards the target qubit. The Hamiltonian with one qubit frozen, say A, is obtained by erasing the terms involving qubit A in Hamiltonian Eq. 4.17:

$$H_{int,\not{A}BC} = \eta_{BC}(\sigma_{+B}\sigma_{-C} + \sigma_{-B}\sigma_{+C}) + I_A. \tag{4.18}$$

The evolution of $\rho_{\not{A}\not{B}C}$ is defined similarly by removing hermitian terms relevant to qubits A,B altogether. Therefore, $\Delta S_{\not{A}\not{B}C}$ vanishes and the joint cumulative information flow from AB to C is: $\mathbb{T}_{AB\to C} = \Delta S_C$. Set $\eta_{AC} = 1$, $\eta_{BC} = 3$, at time $t \sim 0.49$, the entropy of C reaches its maxima of 1 bit for the first time. This is the maximum uncertainty qubit C can receive, determined by its dimension. For the purpose of illustration, we compare the cumulative information flow from different sending qubits before this capacity is reached. The early time behavior of cumulative information flow $\mathbb{T}_{AB\to C}(t)$, $\mathbb{T}_{A\to C}(t)$, $\mathbb{T}_{B\to C}(t)$ is plotted in figure 4.1a.

From Fig. 4.1a, we notice that: The cumulative information flow from B to C is greater than that from A to C: $\mathbb{T}_{B\to C} > \mathbb{T}_{A\to C}$. This formalism is consistent with the intuition that the strongly coupled qubit has greater impact on the target. The direct addition of cumulative information flow from individual qubit A,B is smaller than the joint value: $\mathbb{T}_{B\to C} + \mathbb{T}_{A\to C} < \mathbb{T}_{AB\to C}$ in this example. It means that turning off qubit A and B altogether has more impact on qubit C than the direct addition of turning A,B off one at a time. Similar result is obtained for the early time behavior of a 5 qubit spin chain.

4.5.2 5 qubits

For 5 qubits, labeled A,B,C,D,E, with E in the center and interacting with other qubits independently. To check if stronger coupled sending qubit delivers more information towards the receiving qubit, we set $\eta_{DE} = 1$, $\eta_{CE} = 2$, $\eta_{BE} = 3$, $\eta_{AE} = 4$ and let the initial state of the sending qubits A,B,C,D being maximally mixed and the receiving qubit E pure, so that $\rho_0 = I_A/2 \otimes I_B/2 \otimes I_C/2 \otimes I_D/2 \otimes |0\rangle\langle 0|_E$.

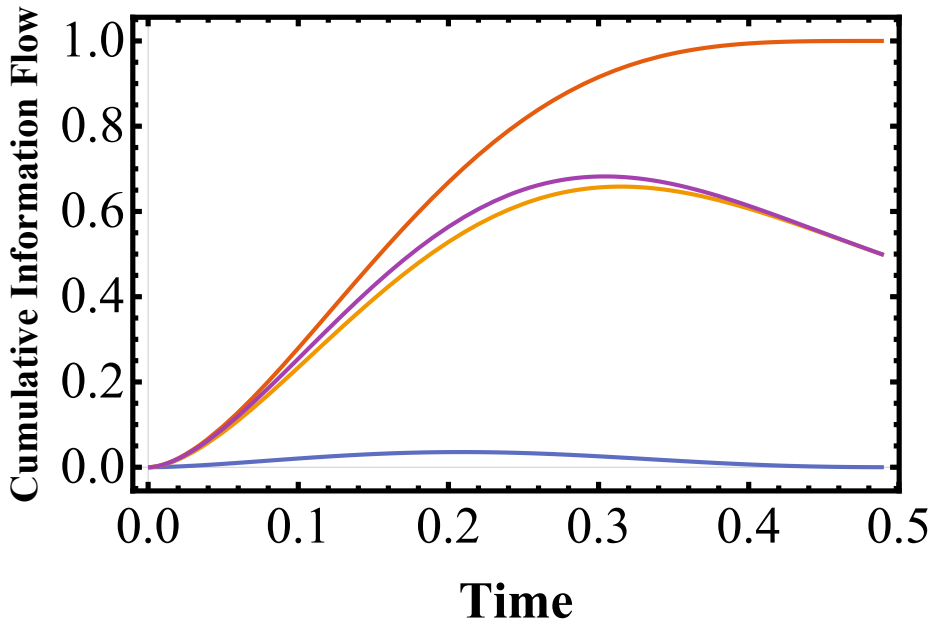

(a)

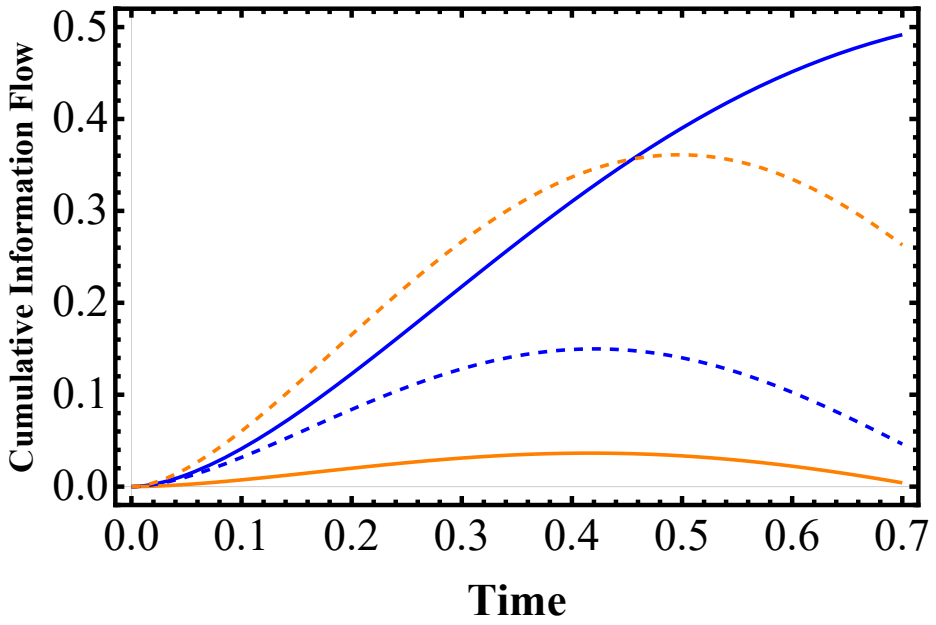

(b)

Fig. 4.1 **3-qubit spin chain** (a) From top to bottom (measured in bits): $\mathbb{T}_{AB\to C}$, $\mathbb{T}_{B\to C}+\mathbb{T}_{A\to C}$, $\mathbb{T}_{B\to C}$, $\mathbb{T}_{A\to C}$. Coupling strength: $\eta_{AC}=1$, $\eta_{BC}=3$. Initial state: $\rho(0)=I_A\otimes I_B\otimes|0\rangle\langle 0|_C$. (b)Blue curves: $\mathbb{T}_{A\to C}$, Orange curves: $\mathbb{T}_{B\to C}$. Solid curves: Initial state $\rho_{0(1)}=I_A\otimes(0.9|0\rangle\langle 0|+0.1|1\rangle\langle 1|)_B\otimes|0\rangle\langle 0|_C$, Dashed curves: Initial state $\rho_{0(2)}=I_A\otimes(0.1|0\rangle\langle 0|+0.9|1\rangle\langle 1|)_B\otimes|0\rangle\langle 0|_C$. Coupling strength: $\eta_{AC}=\eta_{BC}=1$.

Calculation of information flow from the k^{th} qubit to E, where k runs through the sending qubits, requires the evolution mechanism with the k^{th} qubit frozen:

$$H_{spin,\not k}=\sum_{i,i\neq k}H_{spin,iE} \tag{4.19}$$

The joint information flow from A,B,C,D to E is simply the change of S_E:

$$\mathbb{T}_{ABCD\to E} = \Delta S_E \tag{4.20}$$

At time $t \sim 0.26$, the entropy of E reaches its maxima $S_E = 1$bit for the first time. The Information flow from each sending qubit to E is plotted in Fig. 4.2, before the capacity is reached. The stronger coupled qubit delivers more information to E at all time during $t \in [0, 0.26]$:

$$\mathbb{T}_{A\to E} > \mathbb{T}_{B\to E} > \mathbb{T}_{C\to E} > \mathbb{T}_{D\to E} \tag{4.21}$$

At $t = 0.26$, $\mathbb{T}_{A\to E} \sim 0.0731$bits, $\mathbb{T}_{B\to E} \sim 0.0132$bits, $\mathbb{T}_{C\to E} \sim 0.0022$bits, $\mathbb{T}_{D\to E} \sim 0.0001$bits.

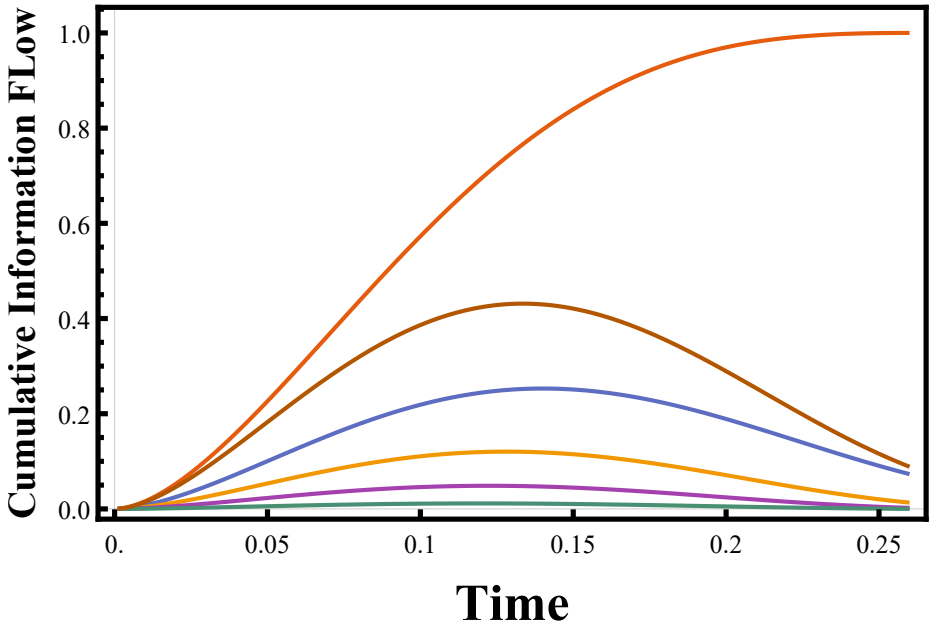

Fig. 4.2 **5-qubit spin chain: Cumulative Information flow towards qubit E (in Bits)** from top to bottom: $\mathbb{T}_{ABCD\to E}$, $\mathbb{T}_{A\to E} + \mathbb{T}_{B\to E} + \mathbb{T}_{C\to E} + \mathbb{T}_{D\to E}$,$\mathbb{T}_{A\to E}$, $\mathbb{T}_{B\to E}$, $\mathbb{T}_{C\to E}$, $\mathbb{T}_{D\to E}$

Similar to the results obtained for 3 qubit system in the main text, here we also observe superadditivity of quantum Liang information flow:

$$\mathbb{T}_{ABCD\to E} > \mathbb{T}_{A\to E} + \mathbb{T}_{B\to E} + \mathbb{T}_{C\to E} + \mathbb{T}_{D\to E} \tag{4.22}$$

4.5.3 Initial configuration dependence

Note that the information flow formalism also depends on the initial configuration. To see how different initial states affect the information flow, set the coupling constant equal: $\eta_{AC} = \eta_{BC} = 1$, with initial state $\rho_{0(1)} = I_A \otimes (0.9|0\rangle\langle 0| + 0.1|1\rangle\langle 1|)_B \otimes |0\rangle\langle 0|_C$ and $\rho_{0(2)} =$

$I_A \otimes (0.1|0\rangle\langle 0| + 0.9|1\rangle\langle 1|)_B \otimes |0\rangle\langle 0|_C$. In both cases, the initial entropy of qubit B is ~ 0.47bit while A is 1 bit. At a first glance, one may be expecting that A is transmitting more uncertainty to C than qubit B. From Fig. 4.1b, we see this is indeed the case for initial state $\rho_{0(1)}$. But when the initial state is switched to $\rho_{0(2)}$, we have $\mathbb{T}_{B\to C} > \mathbb{T}_{A\to C}$. This is because increasing the von Neumann entropy could result from not only classical uncertainty propagation, but also from entanglement generation. The qubit interaction given in Eq. 4.16 entangles state $|10\rangle$ ($|01\rangle$), while it does not act on state $|00\rangle(|11\rangle)$:

$$(\sigma_+\sigma_- + \sigma_-\sigma_+)|00\rangle = 0, \;\; (\sigma_+\sigma_- + \sigma_-\sigma_+)|10\rangle = |01\rangle$$

For initial state $\rho_{0(2)}$, qubit B and C has 90% probability in $|10\rangle_{BC}$ state, the entangling mechanism greatly increases $\mathbb{T}_{B\to C}$ compared to $\rho_{0(1)}$, for which the probability is only 10%. Changing the initial state to $\rho_{0(2)}$ also suppresses $\mathbb{T}_{A\to C}$ due to the growing competition from B.

4.5.4 Quantum super-exchange

Add constant magnetic field along the z-axis with strength $\mathbf{B}$ on the intermediate qubit C so that its energy is lifted by an amount $\mathbf{B}\sigma_z$, while qubits A and B remain unaffected. The total Hamiltonian acting on the system then gains an additional term:

$$H_{additional} = I_A \otimes I_B \otimes \mathbf{B}\sigma_{z(C)} \tag{4.23}$$

Set coupling strength $\eta_{AC} = \eta_{BC} = 1$ and initial state $\rho(0) = I_A \otimes |0\rangle\langle 0|_B \otimes I_C$. We wish to compare information flow from A,C to B with various magnetic field strengths. Note that when $\mathbf{B} = 0$, the dynamics of information flow in the XY model (Eq. 4.16), which is not apriori obvious, can be pictured from Fig. 4.3a. The cumulative information flow is initially from C to B and it reaches a high value of 1 bit before it declines and is overtaken by the cumulative information flow from A to B. As the magnetic field strength increases, super-exchange process [20] between A and B becomes progressively dominant. Thus, we see that information flow from C to B goes down while that from A to B becomes that dictated by an effective weaker super-exchange coupling $\eta_{AC}^2/\mathbf{B}$ between A and B ($\sigma_{+A}\sigma_{-B} + h.c.$) [20].

4.5.5 5-qubit network

Consider a 5-qubit spin system, labeled A,B,C,D,E, with E in the center, we wish to investigate the information flow towards E. The total Hamiltonian for the 5-qubit spin chain

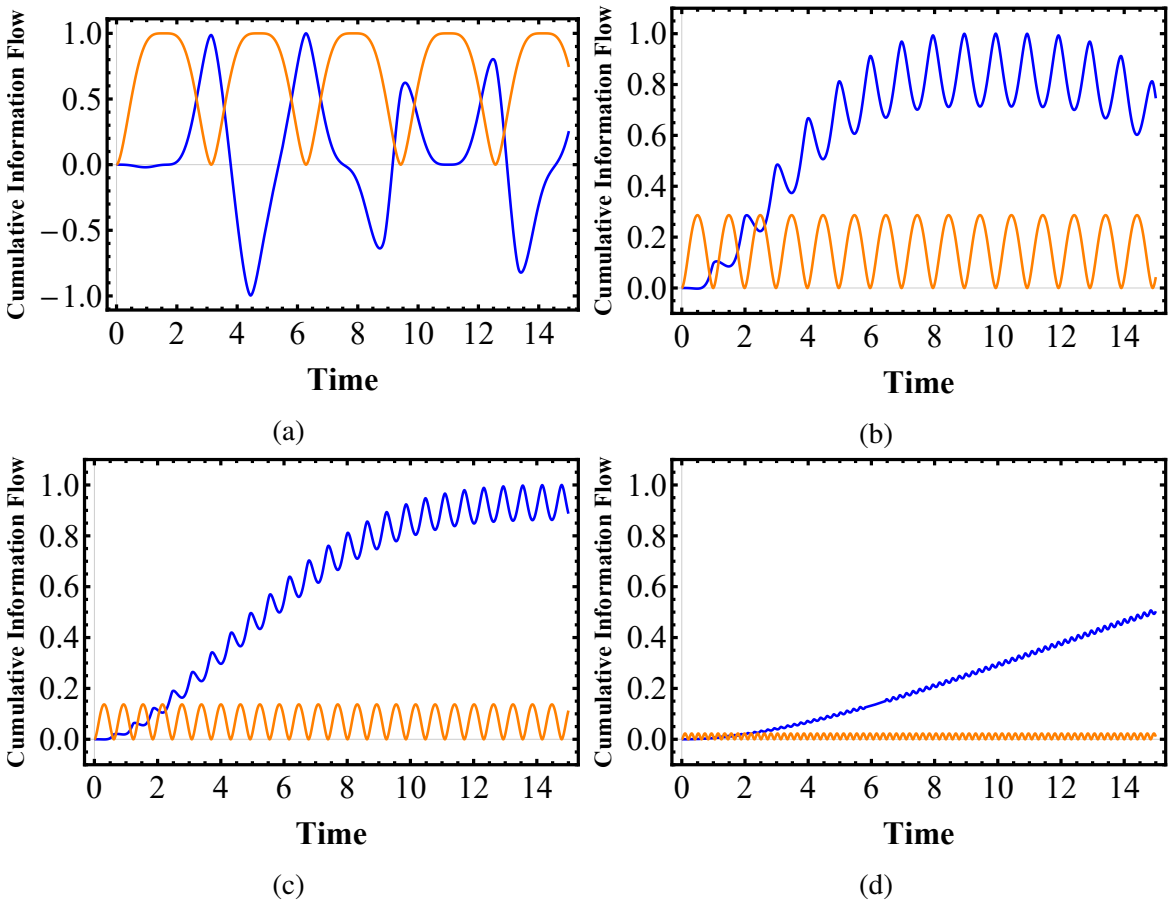

Fig. 4.3 **Quantum super-exchange**: (In bits) Blue curves: $\mathbb{T}_{A\to B}$, Orange curves: $\mathbb{T}_{C\to B}$. In 4.3a, 4.3b, 4.3c, 4.3d, Magnetic field strength set to $\mathbf{B} = 0, 3, 5, 15$ respectively. Coupling strength: $\eta_{AC} = \eta_{BC} = 1$. Initial state: $I_A \otimes |0\rangle\langle 0|_B \otimes I_C$.

is

$$H_{spin,tot} = \sum_i H_{spin,iE} \tag{4.24}$$

with $i = A, B, C, D$. Set all the coupling strength with E identical: $\eta_{DE} = \eta_{CE} = \eta_{BE} = \eta_{AE} = 1$, and initial state of sending qubits A, B, C, D maximally mixed, receiving qubit E pure. At time $t \sim 0.69$, the entropy of E reaches its maximum of 1 bit for the first time. The cumulative information flow from each sending qubit, which is identical $\mathbb{T}_{A\to E} = \mathbb{T}_{B\to E} = \mathbb{T}_{C\to E} = \mathbb{T}_{D\to E}$, is plotted for the time interval $t \in [0, 0.69]$ in Fig. 4.4a.

Now let us add mutual interaction between C, D with a relative coupling strength $\eta_{CD} = 5$ and observe how the information flow towards the central qubit E changes (schematic diagram of the interaction pattern is shown in Fig. 4.5). The total Hamiltonian is now given by:

$$\sum_i H_{spin,iE} + H_{spin,CD} \tag{4.25}$$

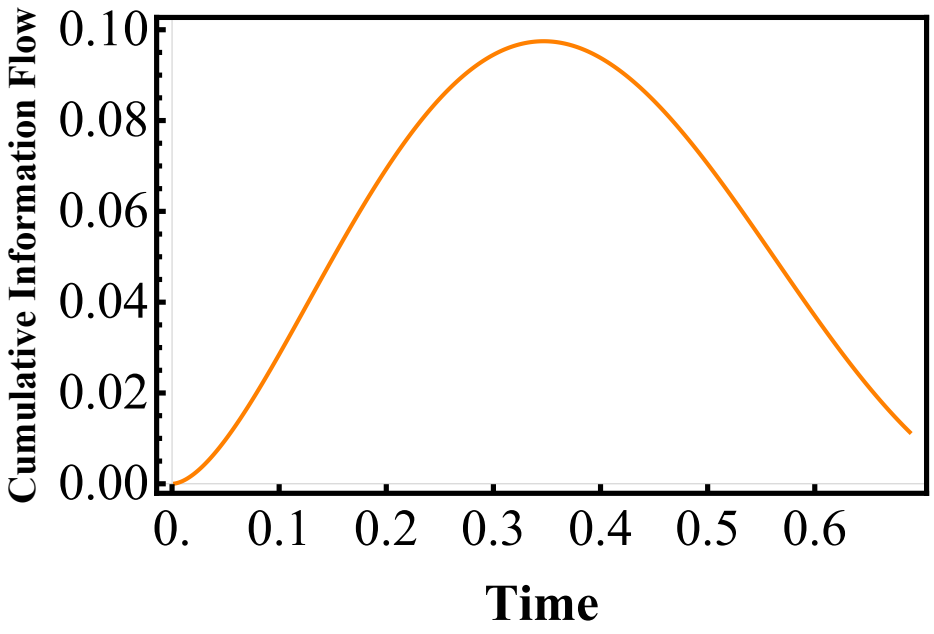

(a)

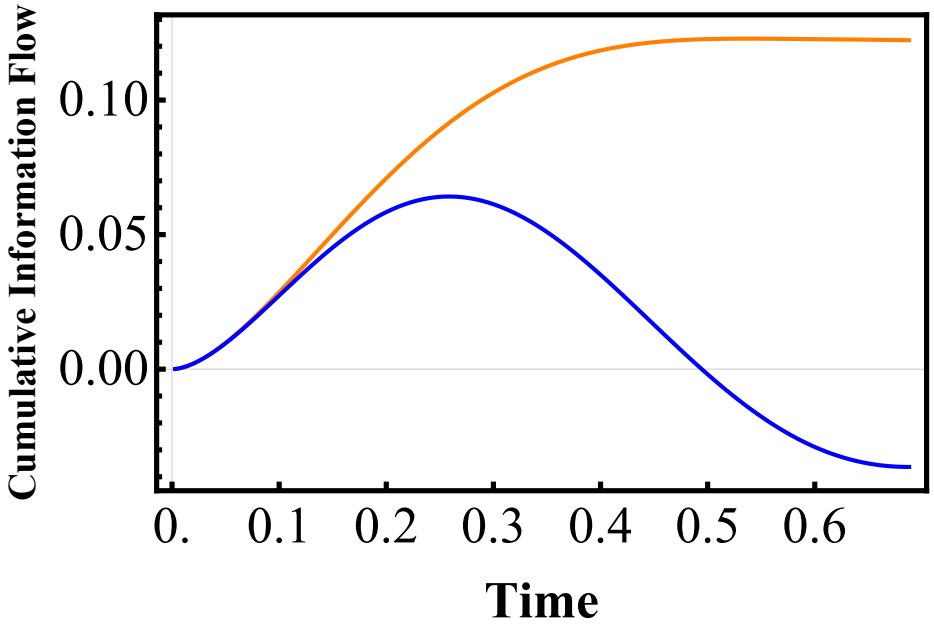

(b)

Fig. 4.4 **5-qubit network** Cumulative information flow (in bits) (a) from any sending qubit towards E with identical coupling strength: $\eta_{DE} = \eta_{CE} = \eta_{BE} = \eta_{AE} = 1$. (b) with additional coupling $\eta_{CD} = 5$. Orange curve: A(or B) to E, Blue curve: C(or D) to E.

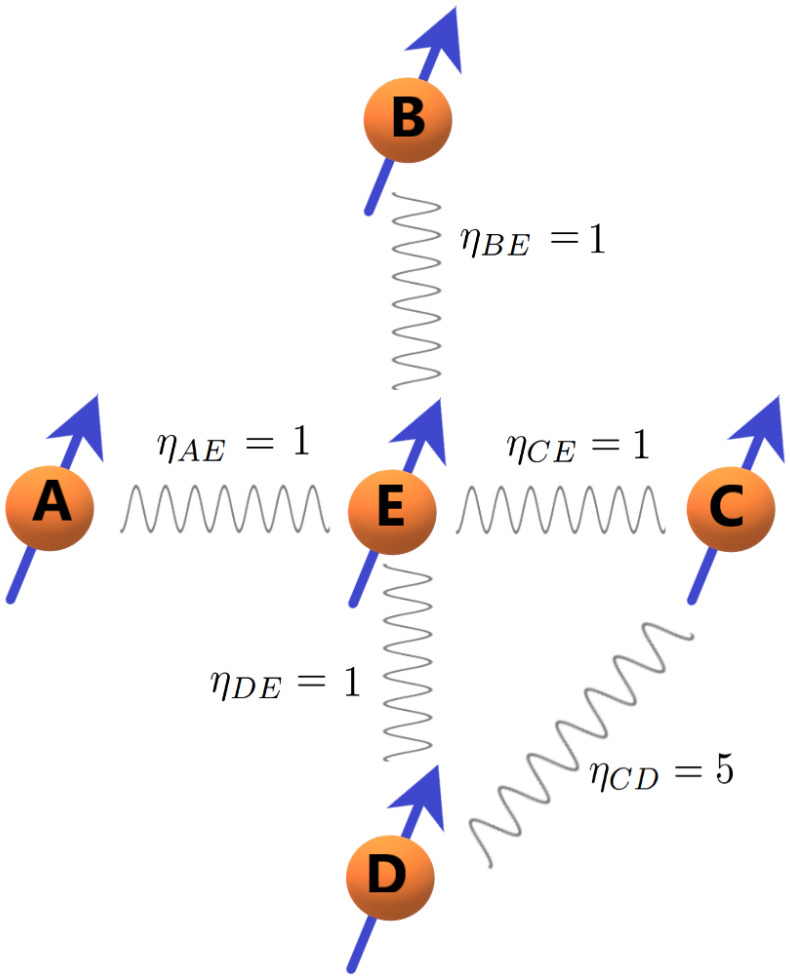

Fig. 4.5 **schematic diagram:** A,B couples solely with E, while C,D also interacts with each other. $\eta_{DE} = \eta_{CE} = \eta_{BE} = \eta_{AE} = 1$, $\eta_{CD} = 5$

With this additional interaction term, the cumulative information flow from each sending qubit to E is plotted in Fig. 4.4b. Comparing Fig. 4.4b to Fig. 4.4a, the additional interaction term between C, D greatly reduces the transmitted uncertainty from qubit C (D) to qubit E, while increasing that from qubit A (B) to qubit E. After time $t \sim 0.49$, $\mathbb{T}_{C\to E}$ reaches negative value, that is, the presence of qubit C (D) reduces the uncertainty of qubit E. The uncertainty from qubit C (D) now has two routes to propagate, either towards E or D (C). Also, the relative coupling strength η_{CD} is 5 times stronger than η_{CE}, η_{DE}. The strongly coupled route connecting C and D then diverts the uncertainty propagation away from the original path between C (D) and E, so that $\mathbb{T}_{C\to E}(\mathbb{T}_{D\to E})$ decrease. Qubits A and B now have less competition from qubits C and D to propagate uncertainty towards qubit E. Then, $\mathbb{T}_{A\to E}(\mathbb{T}_{B\to E})$ increases. The presence of certain coupling can thus be used to preserve information. Although beyond the scope of this proof of principle work, we point out that this methodology could be exploited to design robust quantum circuits. Take variational

quantum algorithms on Noisy Intermediate-Scale Quantum computers for instance [126]. The parameters of a quantum circuit are optimized to give a minimum cost function. Ground state energy is typically the choice of cost function in many cases (eg. solving quantum many-body systems). One can add to this the average Quantum Liang information flow, for instance, from one node to another as a supplementary cost function. In that case the optimized circuit will be more robust against single node failure.

4.6 Application: Two-qubit system in bosonic bath

Let A and B indicate two non-interacting qubits with ground and excited states $|0\rangle$, $|1\rangle$, embedded in a common zero-temperature bosonic reservoir labeled C. We wish to compare the information flow between the two qubits. The Hamiltonian governing the mechanism is given by $H_{SB} = H_0 + H_{int}$, with:

$$\begin{aligned} H_0 &= \omega_0 \sigma_+^A \sigma_-^A + \omega_0 \sigma_+^B \sigma_-^B + \sum_k \omega_k b_k^\dagger b_k \\ H_{int} &= \alpha_A \sigma_+^A \sum_k g_k b_k + \alpha_B \sigma_+^B \sum_k g_k b_k + h.c. \end{aligned} \tag{4.26}$$

where $\sigma_\pm^{A(B)}$ and ω_0 are the inversion operator and transition frequency of qubit $A(B)$. $b_k, b_k^\dagger$ are annihilation and creation operator of the environment C. $\alpha_{A(B)}$ measures the coupling between each qubit and the reservoir. In the limit α_B or α_A goes to 0, that is, when one of the qubit decouples from the setup, then ρ_A and ρ_{AB} obeys the same equation of motion and $\rho_A(t) = \rho_{AB}(t)$. Therefore, $T_{B\to A} = T_{A\to B} = 0$.

We adopt the lossy cavity model given in Ref[62]. The two-qubit dynamics is solved exactly at zero temperature. Take initial state $\rho_{AB}(0) = |\psi_0\rangle\langle\psi_0|$, where $|\psi_0\rangle = \frac{1}{\sqrt{3}}(|01\rangle + \sqrt{2}|10\rangle)$. Set λ and $\hbar$ equal to unity, $\alpha_A/\alpha_B = 10/1$ and take strong coupling limit $R = 10$, where λ defines the spectral width of the coupling and R determines the collective coupling strength. The rate of information flow with respect to scaled time t from B to A versus that from A to B is plotted in Fig. 4.6a. The cumulative information flow is shown in Fig. 4.6b. From Fig. 4.6a, we see that the rate of information flow from the weakly coupled qubit (B) towards the strongly coupled qubit (A) possesses a higher peak than that from A to B. On the other hand, as shown in Fig. 4.6b, the cumulative information flow from A to B grows steadily and surpasses that from B to A as the system approaches equilibrium. Note that the information flow formalism is generically asymmetric $T_{\to A} \neq T_{A\to B}$, as opposed to most quantum correlation measures.

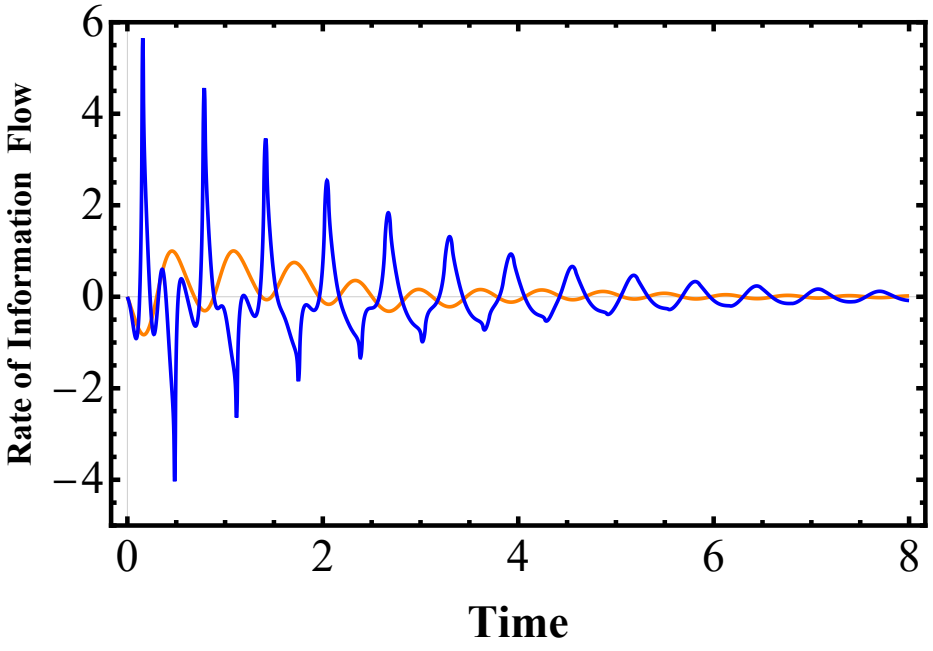

(a)

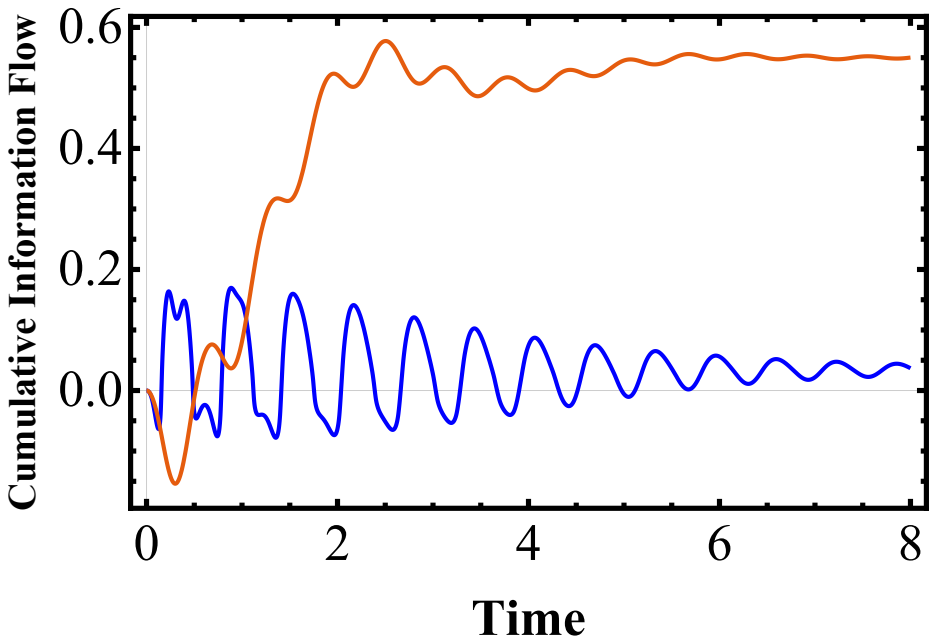

(b)

Fig. 4.6 **Two-qubit system in a lossy cavity** Blue curves: From B to A. Orange curves: From A to B. Coupling strength ratio: $\alpha_A/\alpha_B = 10/1$. (a) Rate of information flow (bits per unit time) (b) Cumulative information flow (bits).

4.7 Summary

We have generalized Liang's theory/methodology for classical systems to quantify causality in quantum networks. In quantum networks, the growth of entropy of a node can be attributed to: (1) uncertainty propagation, (2) growth of entanglement. It is found that the information flow between two qubits through a common bath could be nontrivial: the weakly coupled qubit has higher rate of information flow, while in the long run, the strongly coupled qubit has more impact. Another non-trivial result obtained for a 5-qubit network reveals that an additional strong coupling diverts the directions of uncertainty propagation. The information flow based causal measure may have applications in parallel with its classical counterparts [105, 106, 109, 110, 166, 84, 73, 159, 32, 83].

Chapter 5

Causal analysis with respect to quantum relative entropy

5.1 Introduction

The original Liang-Kleeman analysis is formulated with respect to Shannon entropy. Following the same logistic, Liang then extended the formalism with respect to relative entropy [107]. Relative entropy provides a better measure of predictability than Shannon entropy in certain cases [153, 91]. It is invariant under nonlinear transformation and consistent with the second law of thermodynamics [91, 93, 92]. The Liang information flow with respect to relative entropy is shown to be equivalent to the Shannon entropy-based formalism for non-linear stochastic systems [107]. Properties of the Shannon entropy-based formalism, including the nil causality principle [106], are also shared with the relative entropy-based formalism. Furthermore, the latter is found invariant under nonlinear transformation under weak assumptions. The relative entropy-based formalism also captures underlying causal relations and it is shown that the influence of one component to another changes rapidly when white noise is introduced.

In quantum information theory, quantum relative entropy also inherits advantages from its classical counterpart. The inequalities quantum relative entropy satisfies is a "parent" of many theorems of information processing. It also has the interpretation in terms of statistical distinguishability between two states, which is similar to distance measure. In this paper, we formulate the quantum Liang information flow formalism with respect to quantum relative entropy.

5.2 Definition

For density operators ρ, σ, the quantum relative entropy $S(\rho||\sigma)$ is defined as:

$$S(\rho||\sigma) = Tr[\rho \log \rho - \rho \log \sigma] \tag{5.1}$$

Consider a multipartite state ρ evolve under unitary operator $U(t)$ generated from Hamiltonian function H. Reduced density state of subsystems of ρ AB, A, B is then denoted ρ_{AB}, ρ_A, ρ_B. Following the methodology of its classical counterpart [107], quantum Liang information flow with respect to relative entropy is then

$$T^r_{B\to A} = \frac{dS(\rho_A||\sigma)}{dt} - \frac{dS(\rho_{A\not B}||\sigma)}{dt} \tag{5.2}$$

the cumulative information flow is then

$$\mathbb{T}^r_{B\to A} = \int T^r_{B\to A} dt = \Delta S(\rho_A||\sigma) - \Delta S(\rho_{A\not B}||\sigma) \tag{5.3}$$

where σ is an arbitrary constant density state and the superscript r is used to denote that the formalism is based on relative entropy. Here $\rho_{A\not B}$ again refers to the density state of A evolving with B frozen. The frozen mechanism is adopted from the original von Neumann entropy-based formalism by removing terms relevant to subsystem B in the Hamiltonian function H [182].

5.3 Interpretations and properties

Interpretation of this information flow formalism follows directly from the interpretations of quantum relative entropy. The quantum Sanov's theorem claims that the quantum relative entropy gives the asymptotic distinguishability of two density states by measurements. Suppose ρ_x and ρ_y are two possible states of a quantum system and we prepare n identical copies of the system. A measurement is then performed to test if the state is ρ_x, the probability of passing the test with state ρ_y in the asymptotic limit $n \to \infty$ is

$$p(n) \simeq 2^{-nS(\rho_x||\rho_y)} \tag{5.4}$$

Therefore, the quantum Liang information flow Eq. 5.2 and Eq. 5.3 can then be interpreted as quantifying how much would the distinguishability of subsystem A and a fixed constant state σ change if subsystem B is frozen throughout the evolution. If the information flow measure

is positive, the interpretation is that the presence of B in the interaction causes A to be more distinguishable from the reference state σ and vice versa for negative measure. The choice of σ depends on the information processing task of interest. For simplicity, one may pick the initial state of the target node A, $\sigma = \rho_A(0)$. When the evolution of subsystem A models a noisy quantum channel where A interacts with its environment, the distinguishability of subsystem A at time t and at time 0: $S(\rho_A(t)||\rho_{A(0)})$ then quantifies the decoherence and memory effects.

von Neumann entropy can be interpreted in terms of quantification of computational resources, for instance entanglement, in information processing tasks. Quantum relative entropy plays a similar role. To name a few [128],

$$I_\rho = \min_{\pi\in\mathscr{P}} S(\rho||\pi) = S(\rho||\pi_\rho) \tag{5.5}$$

$$E_\rho = \min_{\omega\in\mathscr{S}} S(\rho||\omega) \tag{5.6}$$

$$D_\rho = \min_{\chi\in\mathscr{C}} S(\rho||\chi) \tag{5.7}$$

$$Q_\omega = \min_{\chi_\omega\in\mathscr{C}} S(\omega||\chi_\omega) \tag{5.8}$$

where I_ρ is the total mutual information of ρ, $\pi \in \mathscr{P}$ is a product density state, and $\pi_\rho = \pi_1 \otimes ...\pi_n$ with π_i the ith reduced density state of ρ. Eq5.5 states that the total information of ρ is given by the distance with its closest product state π_ρ, which is the tensor product of its reduced state. E_ρ is the entanglement of ρ, given by the distance with its closet separable state ω. $\mathscr{S}$ denotes the set of separable states. D_ρ is the discord of state ρ, which is a quantum correlation weaker than entanglement. It is given by the distance of ρ with its closest classical state $\chi \in \mathscr{C}$. Quantum dissonance, denoted Q, is the distance between ω and the closest classical state χ_ω. It quantifies the rest of quantum correlations after entanglement is "excluded" from ρ. The central role of relative entropy in quantum information science provides versatility to the relative entropy-based information flow formalism by changing the reference state σ in Eq. 5.2 and Eq. 5.3.

A special choice of σ is the identity matrix I. This reflects the probability of confusing any density matrix from maximally mixed (completely random) state. For the model considered in Ref [107], the classical relative entropy-based formalism is equivalent to its absolute entropy-based alternative up to a minus sign. The quantum extension inherits this feature. It should be immediately obvious by checking the definition of relative entropy Eq. 5.1. In the

case where the reference state $\sigma = I$,

$$\begin{aligned} Tr[\rho \log I] &= 0 \\ S(\rho||\sigma) &= Tr[\rho \log \rho] = -S(\rho) \end{aligned} \tag{5.9}$$

The same equation $S(\rho||\sigma) = -S(\rho)$ also holds when σ is pure since $\log \sigma$ is defined as 0 for pure states. For instance, one may be interested in the distance of a qubit A and its initial state after evolution $S(\rho_A(t)||\rho_A(0))$ and the initial state $\rho_A(0)$ can be taken as a pure state. Then the relative entropy-based formalism would be no different from its absolute entropy-based counterpart. In this sense, the von Neumann entropy-based formalism is a special case of its relative entropy-based alternative.

One may also be interested in $S(\rho_A(t)||\rho_{A\not{B}}(t))$, which quantifies the distance between the evolution of system A with or without freezing the component system B. This is also a special case of the information flow formalism Eq. 5.2, Eq. 5.3 by picking $\sigma = \rho_{A\not{B}}(t)$. Since $S(\rho_{A\not{B}}||\rho_{A\not{B}}(t)) = 0$,

$$T^r_{B\to A} = \frac{dS(\rho_A||\rho_{A\not{B}})}{dt} \tag{5.10}$$

$$\mathbb{T}^r_{B\to A} = \Delta S(\rho_A||\rho_{A\not{B}}) \tag{5.11}$$

Certain basic features of the original quantum Liang information flow formalism are inherited by the relative-entropy based alternative. The principle of nil causality states that the information flow measure vanishes when the evolution of A and B are independent [106]. This property can be directly observed from Eq. 5.2 and Eq. 5.3. Let the rest of the system denoted by letter C, if the unitary operator acting on system ABC, $U_{ABC}(t)$ is separable: $U_{ABC}(t) = \mathscr{M}_A \otimes \mathscr{N}_{BC}$ or $U_{ABC}(t) = \mathscr{O}_{AC} \otimes \mathscr{Q}_B$, where $\mathscr{M}, \mathscr{N}, \mathscr{O}, \mathscr{Q}$ are all unitary, then $\rho_A(t) = \rho_{A\not{B}}(t)$. Hence

$$T^r_{B\to A} = 0 \tag{5.12}$$

$$\mathbb{T}^r_{B\to A} = 0 \tag{5.13}$$

Bipartite system However, new opportunities are brought into the relative entropy-based formalism by the freedom of choice of the reference state σ in Eq. 5.2, 5.3. For pure bipartite state AB under unitary evolution U, the reduced density state ρ_A and ρ_B share the same eigenvalues, therefore, $S_A = S_B$ at all times. The original quantum Liang information flow

formalism then reduces to:

$$T_{B\to A} = \frac{dS_A}{dt} - \frac{dS_{A\not B}}{dt} = \frac{dS_A}{dt} = \frac{dS_B}{dt} = T_{A\to B} \tag{5.14}$$

where in the second equal sign, we have exploited the unitary invariance of von-Neumann entropy. The evolution of A with B frozen $\rho_{A\not B}(t)$ is governed by a unitary operation acting on A, so, $\frac{dS_{A\not B}}{dt} = 0$. The third equal sign is a direct outcome of Schmidt decomposition. Such simple reduction does not occur in the relative-entropy based formalism. First, $\frac{dS(\rho_{A\not B}||\sigma)}{dt} \neq 0$. The unitary transformation

$$\rho_A(0) \to \rho_{A\not B}(t) = U(t)\rho_A(0)U^\dagger(t) \tag{5.15}$$

does not preserve the distance between system A and reference state σ in general. Furthermore, Schmidt decomposition of pure bipartite system does not guarantee the relative entropy between system A and σ is the same as that between system B and σ:

$$\frac{dS(\rho_A||\sigma)}{dt} \neq \frac{dS(\rho_B||\sigma)}{dt} \tag{5.16}$$

Though ρ_A and ρ_B share the same eigenvalues, their eigenvectors are not necessarily identical. So their distances between σ are not always the same. To build some intuition of the relative entropy-based information flow formalism, we exemplify with a few toy models.

5.3.1 Application: XY spin chain

Consider a 5-qubit spin chain system emerged in a heat reservoir with temperature T, the interaction term between any two interacting qubits in the Hamiltonian function is given in Eq. 4.16. To break the symmetry between $|0\rangle$ and $|1\rangle$, we also apply a uniform magnetic field on each spin along the z-axis. The Hamiltonian of the 5 qubit spin chain is then:

$$\begin{aligned} H_{int,5spins} &= \sum_{i=1\ldots5} \eta_{i,i+1}(\sigma_{+(i)}\sigma_{-(i+1)} \\ &+ \sigma_{-(i)}\sigma_{+(i+1)}) + \mathscr{B}\sigma_{z(i)} \end{aligned} \tag{5.17}$$

where $\sigma_+ = 1/\sqrt{2}(\sigma_x + i\sigma_y)$, $\sigma_- = 1/\sqrt{2}(\sigma_x - i\sigma_y)$, $\mathscr{B}$ is magnetic field strength, η_{ij} is the relative coupling between the i^{th} and j^{th} spin. The value of i runs through the first 4 spins $\{A,B,C,D\}$. Set the relative coupling strength and magnetic field strength to unity without loss of generality $\eta_{ij} = 1$, $\mathscr{B} = 1$. The value of η, $\mathscr{B}$ and time t here is again scaled with respect to unit relative coupling strength.

To apply the relative entropy-based information flow formalism, one has to pick a reference state σ. Here we investigate the information flow towards the end qubit E. Pick $\sigma = \rho_{0E}$, where $\rho_{0E} = Tr_{ABCD}[\rho_0]$ is the reduced density state of the thermal equilibrium state of the 5-qubit spin chain $\rho_0 = e^{\beta H}/Tr[e^{\beta H}]$ and $\beta = 1/kT$. The information flow formalism Eq. 5.2, 5.3 is then a measure of change in the relative distance between qubit E and the reduced thermal equilibrium state ρ_{0E} upon freezing a qubit in the chain. Note that relative entropy has a interpretation in terms of free energy [54]. The relative entropy-based information flow measure towards qubit E is then related to extractable work from the system.

The cumulative information flow formalism reads:

$$\mathbb{T}^r_{i\to E} = \Delta S(\rho_E||\rho_{0E}) - \Delta S(\rho_{Ei}||\rho_{0E}) \tag{5.18}$$

where $i \in \{A,B,C,D\}$. Setting the initial state an equal superposition of base states in the standard 5 qubit basis with each qubit spanned by $\{|0\rangle,|1\rangle\}$ so that the initial configuration weights each qubit equally:

$$|\psi_i\rangle = |+\rangle^{\otimes n} = \frac{1}{2^{n/2}} \sum_{x=0}^{2^n-1} |x\rangle \tag{5.19}$$

where $|+\rangle = \frac{1}{\sqrt{2}}(|0\rangle + |1\rangle)$, $n = 5$ is the number of qubits and $\{|x\rangle\}$ is a set of binary state, for instance, $|x = 0\rangle = |00000\rangle$. This choice of initial state is typical in quantum computational protocols[130].

The cumulative information flow from individual qubit to E is plotted in Fig. 5.1. Note that each qubit is only interacting with its adjacent qubits, so freezing a qubit in the middle essentially divide the chain in half. The information flow from a spin, say B, towards E is then equivalent to that obtained by freezing B and all qubits before B (qubit A in this case). The information flow from D to E, in particular, is equivalent to collective information flow from A, B, C, D to E (By freezing A,B,C,D altogether) $\mathbb{T}^r_{D\to E} = \mathbb{T}^r_{ABCD\to E}$.

The information flow is plotted over a time period of $t \sim 300$ in Fig. 5.1. The reason for choosing such a large time interval in comparison to the time needed for influence to reach from one end of the chain to another ($\sim 5/\eta = 5$) is that we want to identify the influence per se without the effect of propagation speed. The averaged cumulative information flow over the duration is -0.0447, -0.1246, -0.233 and -0.7932 bits from A, B, C, D to E respectively. The variance is also computed to be 0.062, 0.1795, 0.1217, 0.0581 bit^2 from each qubit to E.

The first observation from the plot is that the influence from a qubit farther away takes longer time to reach the target qubit E. For the farthest qubit A, it takes $t \sim 18$ to influence E,

the next one qubit B takes about $t \sim 12$, qubit C takes time around $t \sim 2$. This is expected as there will be a speed of propagation in the system. This result validates the interpretation of our formalism as an information flow measure. The influence from the adjacent qubit D towards E takes effect immediately at $t \sim 0$. This is a reflection of the fact that the simplified model Eq. 5.18 does not involve explicit terms of coherent mediators. For a more rigorous account of propagation speed, one may adopt a quantum field theoretical model.

The second observation is that the natural dynamics of the chain should take the subsystem E closer to equilibrium. This is modulo the fact we have considered very small chain in this preliminary study so that the thermalizing effects of the dynamics can be trusted only for small times, and have a finite size effects giving long term oscillations. We see that farther the qubit, the less it affects the departure from equilibrium, as evidenced also from the decreasing of the mean value magnitude.

Another observation is that influence from closest qubit D (or, equivalently, the rest of the chain) forms a lower bound on the information flow from other qubits. This is a reflection of the intuition that the influence from a component is no larger than the entire chain except the target qubit. Note also that the mean value of the influence is negative for all the qubits, indicating that overall, they all play a role in the equilibration of the target system (bringing the target closer to equilibrium).

5.3.2 Application: Ergodic Ising spin chain

The Hamiltonian given in Eq. 5.18 is non-ergodic so that its subsystems do not thermalize, although they equilibrate. For the same reason, we also investigate the Hamiltonian

$$H_{\text{int,5spins2}} = \sum_{i=1\ldots5} \eta_{i,i+1}\sigma_{z(i)}\sigma_{z(i+1)} + \mathscr{B}_x\sigma_{x(i)} + \mathscr{B}_z\sigma_{z(i)} \tag{5.20}$$

where the interaction term between qubit i, j is now described by $\sigma_{z(i)}\sigma_{z(j)}$ and a magnetic field is applied along both x and z components.

The above Hamiltonian is ergodic, so that its subsystems should fully thermalize in the long chain thermodynamic limit given enough time. We have also plotted the information flow for this model in Fig. 5.2 to see whether, even at this level of short chain length (5 qubits), any difference can be spotted between ergodic and non-ergodic evolution towards equilibration.

The information flow is plotted again over a time period of $t \sim 300$ in Fig. 5.2. The averaged cumulative information flow over the duration is -0.0256, -0.1124, -0.1217 and -0.9908 bits from A, B, C, D to E respectively. The variance is also computed to be 0.0378, 0.0842, 0.1635, 0.0355 bit^2 from each qubit to E.

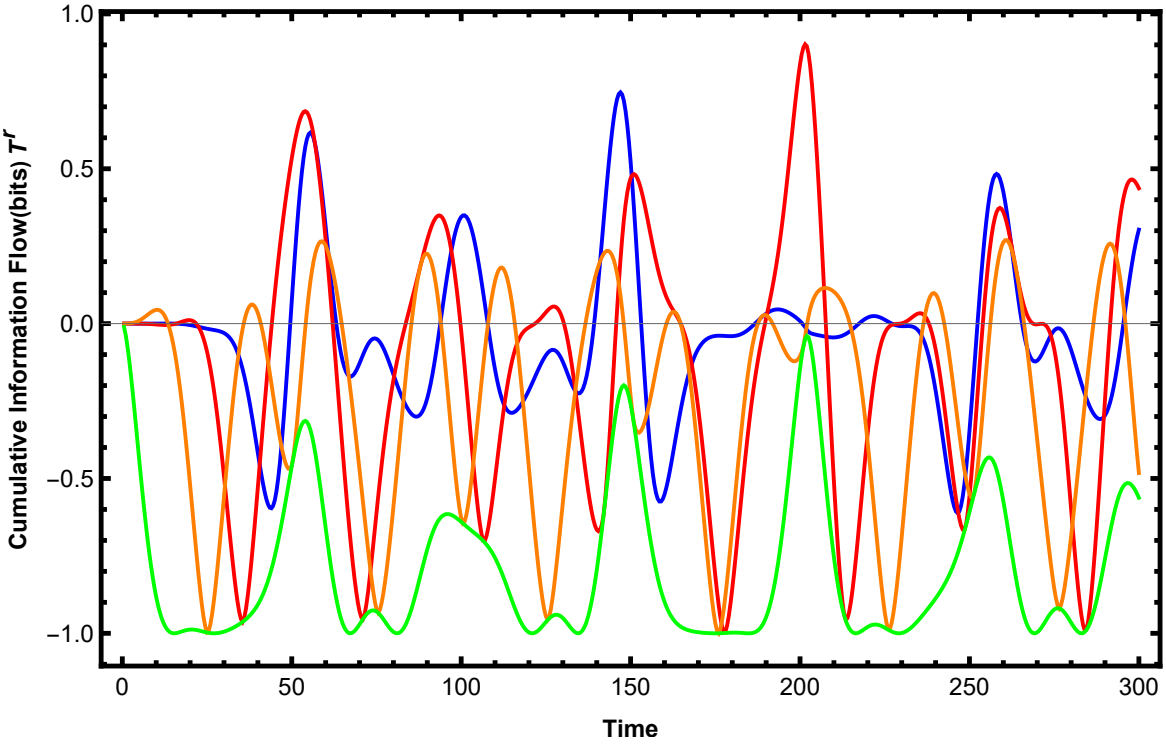

Fig. 5.1 **Non-ergodic model: Cumulative Information flow towards qubit E (in Bits)** The initial state is set to be equal superposition state in the standard $\{|0\rangle, |1\rangle\}$ basis: $|\psi_i\rangle = |+\rangle^{\otimes n} = \frac{1}{2^{n/2}} \sum_{x=0}^{2^n-1} |x\rangle$. Blue: $\mathbb{T}^r_{A\to E}$, Red: $\mathbb{T}^r_{B\to E}$, Orange: $\mathbb{T}^r_{C\to E}$, Green: $\mathbb{T}^r_{D\to E}$

If one compares the ergodic and non-ergodic models, we see from the mean value of cumulative information flow over a long time that the collective influence of the chain on thermalization (influence from D to E) is more for the ergodic than the non-ergodic model. On the other hand, influence from parts of the chain to E is more for non-ergodic than ergodic model. This is a reflection of the fact that the equilibration in ergodic systems is a delocalized process involving all qubits more equally than in non-ergodic systems. The variance, on the other hand, are comparable in both models, and the middle qubits have greater variance than the qubits at the ends. This result implies that information flow is more stable from end to end than middle to end. We do not yet have a good explanation of the trend but we realize that it is parallel to the behavior of entropy between complementary blocks in a typical state of a spin chain [3] (block entropy peaks when the partition reaches the middle of the chain). This is not immediately relatable to our variances as it involves differences arising from the act of freezing a qubit as well as the fluctuations in the dynamics.

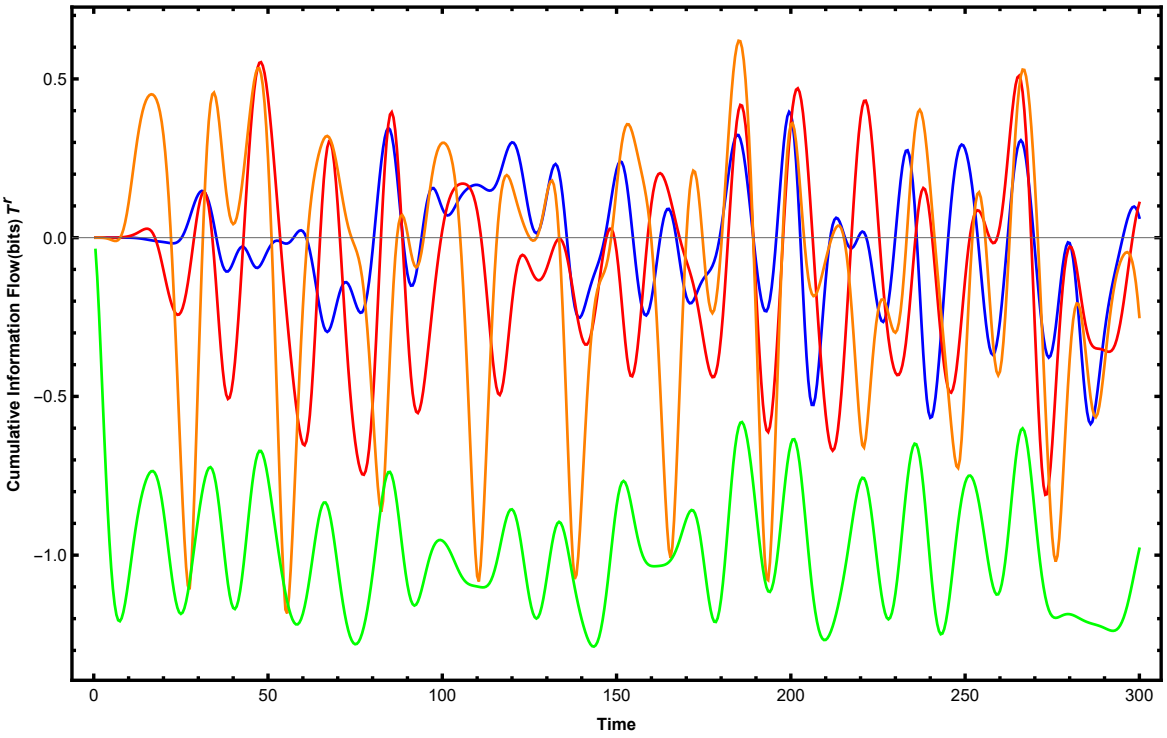

Fig. 5.2 **Ergodic model: Cumulative Information flow towards qubit E (in Bits)** The initial state is set to be equal superposition state in the standard $\{|0\rangle, |1\rangle\}$ basis: $|\psi_i\rangle = |+\rangle^{\otimes n} = \frac{1}{2^{n/2}} \sum_{x=0}^{2^n-1} |x\rangle$. Blue: $\mathbb{T}^r_{A\to E}$, Red: $\mathbb{T}^r_{B\to E}$, Orange: $\mathbb{T}^r_{C\to E}$, Green: $\mathbb{T}^r_{D\to E}$

5.4 Conclusion

Liang information flow based on Shannon entropy has been applied to various schemes in classical dynamic systems to analyze causal relations and it has been generalized to the quantum regime with respect to von Neumann entropy. However, von Neumann entropy does not always quantify the computational resource of interest in various information processing tasks. Relative entropy, on the other hand, plays a "parent" role in quantifying computational resource in general protocols. In particular, it has a statistical interpretation in terms of distinguishing states. Motivated by this, in the current chapter, we have adopted relative entropy as the entity in generalizing Liang information to the quantum setting. In particular, the freedom of choosing a reference state in the formalism gives us a tool for looking at different aspects of a quantum process. For example, here we looked at thermalization in ergodic versus non-ergodic systems, albeit with very small sized models. We found that, consistent with expectations, information propagates at finite speed during thermalizing/equilibrating dynamics. More distant qubits initializing influence at a later time and to a lesser extent even if given a very long time. The formalism also agrees with the more delocalized and collective influence of all spins in the dynamics of ergodic systems

as opposed to non-ergodic systems. The fact that differences can be found for such short chains using our formalism is interesting to note. For the type of case studied, even a single qubit tomography will suffice to measure ρ_E thereby find out the information flow in the many-body system. So it will be attractive to implement this in a quantum simulator.

Chapter 6

Summary and outlook

In this chapter, I will start with a summation of the projects conducted during my PhD studies. Then, I will give concluding remarks on these works and an outlook of future studies. This thesis consists of two parts: Massive spatial qubits and Quantum Liang information flow.

6.1 Massive spatial qubit

The first part of the thesis is centered around a novel methodology to encode qubits with the spatial superposition state of nano-micro objects. It is an open challenge to evidence nonclassicality in the behaviour of the center of mass of a large object, thereby extending the boundaries of quantum physics. Here we combine ideas from photonic quantum information processing and levitated quantum objects to encode and readout a qubit encoded in the spatial degree of freedom of a free mass. The scheme consists only the free evolution of a superposed state followed by spatial detection at particular position. Simplicity of the scheme avoids unnecessary interaction that induces decoherence such as passing through beam-splitters in Mach-Zhender type interferometer. However, one of its downside is that the Pauli-z measurement needs to be performed at a time earlier than Pauli-x and y measurement (an ensemble of particles are considered). For applications where all Pauli-measurements need to be conducted at approximately same time, squeezing technique may be exploited to shorten the difference in time. This massive spatial qubit methodology avoids a Mach-Zehnder interferometer. The tunneling probability is increasingly small when the size of the objects enlarges. For nano-objects, the standard beam splitters in Mach-Zehnder type interferometers becomes infeasible. The qubit encoding scheme can be simulated with cold atoms before being applied to nano-objects.

We fist applied this methodology to verify the nonclassicality inherent in a Stern-Gerlach state before the final stage of the measurement in which the deflection of the mass that bears

the spin is recorded. The Stern-Gerlach state is usually written down as a quantum entangled state of a spin and the position, but there is no direct test of this yet. Such Stern-Gerlach states have been created with atoms [114, 117] and the coherence of the spatial part alone has been verified by interferometry after selecting a specific spin state. An alternative is to verify the coherence by undoing the Stern-Gerlach splitting, which, while it would scale to large masses, is extremely difficult[116]. However, there are, as yet, no protocols to verify the nonclassicality directly from correlation measurements of spin and position thereby verifying their entanglement. We show that this can be accomplished via the violation of a Bell's inequality in which the spin and the positions of the mass are measured, even when the positions are measured sufficiently imprecisely. This violation will also prove the nonclassicality of a large mass in terms of quantum contextuality[1, 80].

The second application is to test the quantum nature of Casimir interaction. The scheme witnesses the entanglement created between two neutral nano-crystal masses through their Casimir interaction (a minor additional squeezing operation has to be appended). This has two types of foundational imports: (a) It shows that the Casimir interaction has a quantum origin – it is mediated by virtual photons – the quantum nature of these is the cause of entanglement between the masses (if the agent going between the masses was classical it would not entangle). Though there have been numerous experiments on Casimir forces, recently even for torques on nanocrystals[181], they do not "qualitatively" identify it as a quantum force, only via a quantitative matching of the magnitude of the force as derived from quantum field theory. (b) As the entangled state is generated by starting from superpositions of distinct localized (Gaussian) states, it is highly non-Gaussian in nature, and will be a simplest unique example of how to generate and verify such a state for two nano-crystals (mass $\sim 10^{-19}$kg). While there are several ideas to date for the generation of Gaussian entangled states of massive systems (e.g., [140, 174] for nano-objects) where the familiar EPR criterion [155] to witness entanglement can be applied, there are hardly any schemes to either generate or witness non-Gaussian entangled states of nano-crystals. The realization of a Casimir induced entanglement will thus be a significant milestone in the entanglement frontier of nano-crystals.

Finally, we looked at the potential of applying this methodology to witness the quantum nature of gravitational interaction. The original scheme to test quantum gravity[28] exploits spin degree of freedom, which involves spin-embedded mass and a standard Stern-Gerlach interferometer. The challenge is that the spin-entanglement scheme requires an precise overlap of the wavepackets in the two interferometric arms to complete SGIs. The spin degree of freedom also introduces additional source of decoherence. The massive spatial qubit approach provides a spinless alternative, but also arises its own challenges. The

scheme consists of two spatially superposed masses $m \sim 10^{-15}kg$, which propagates and interacts through gravitational interaction. A *Faraday* shielding scheme is incorporated to block unwanted electromagnetic interaction between the masses. The requirement for the wavepacket spreading to dominate over the displacement due to Casimir force imposes constraint on the minimum distance to the screen, which, in turn, implies a minimum separation between the initial state of the two masses so that in-negligible relative phase can be induced during the propagation stage. The protocol requires all Pauli-Z,X and Y measurement to readout the potential entanglement due to quantum gravity. In order to shorten the time difference between Pauli-Z and Pauli-X,Y measurement, one squeezes the wavepacket width immediately after observable relative phase has been induced among the superposition components. The proposed scheme requires spatial squeezing of the wavepacket by 7 orders of magnitude, which can hardly be achieved. Magnetic field generated from current-carrying wire may be used for squeezing such massive objects. Decoherence due to random field fluctuations place strict upper bound on the force noise spectrum. If the proposed spatial superposition state can be prepared and the above requirements can be met, evidencing quantum gravity nurtured entanglement between two test masses can be achieved solely through spatial measurements.

As the next step, there are a number of interesting avenues to investigate. The most important is to have a comparison between spinful(as in reference [28]) and spinless (as in this thesis) scenarios in terms of various achievable decoherence values. Decoherence in our works have been introduced heuristically (of course, with magnitudes taken from realistic calculations), without incorporating it into the dynamics while the Hamiltonian creating the superpositions, squeezings and wavefunction spreadings are simultaneously acting. That is a master equation approach using system dynamics as well as decoherence is important. This will help to really understand whether spinful or spinless approach is better and indeed, compare them with approaches based on Gaussian states[97]. In particular, even the preparation of the superposed quantum state, if it can be achieved without spins, using double slits manufactured from other electromagnetic sources, will be an important thing to study. Usage of massive spatial qubits as quantum sensors, as well as their extension to qudits (quantum multi-dimensional systems), can also be interesting directions to study.

6.2 Quantum information flow-based causality analysis

The second part of the thesis addresses causality in quantum physics from the perspective of information flow. Quantification of causation between dynamical events is of enormous interest in various subjects. In classical physics, the recent developments of causality theory

have been widely applied to various disciplines, e.g., climate science, finance, turbulence, etc. In quantum physics, the discussion of causality can be traced back to the paradigmatic Bell experiment, in which it shows causal structure places constraints on correlation generation. In light of the intimate relation between causation and correlation, multiple attempts have been made to estimate causal influences in certain types of quantum environments. Yet, a generic measure of causation in quantum physics is still lacking.

Here we adopt a new methodology from classical physics (Liang information flow) to propose a generic quantification of causation in quantum dynamical systems. The relative causal influence is assessed by an entropic quantity measured in Bits per unit time. When the target and sending nodes evolve independently, this measure vanishes. This information flow-based formalism ascertain causality from one node to another in a network by simply subtracting the former from the mechanism, which is what an experimentalist would naturally employ. In classical information, the increase in Shannon entropy is a result of uncertainty propagation. The quantum counterpart, on the other hand, can be a result of both uncertainty propagation and entanglement generation. We verified the formalism through some toy models. We considered two qubits interact through a common bath. The information flow from the weakly coupled qubit to the other one has a higher rate. But in the long run, the strongly coupled qubit has more influence towards the weakly coupled one. We also considered information flow from the end qubits towards the center qubit in a 3 qubit spin chain system. The strongly coupled qubit exerts a stronger impact towards the center than the weakly coupled one. The information flow formalism also depends on the initial configuration. We considered two set of initial configurations in the 3 qubit spin chain system. The evolution mechanism entangles one initial configuration but not the other. As a result, the setup, in which entanglement is generated, manifests a greater causal influence from one end of the chain to the other end. Next, we examined quantum superexchange, where a magnetic field is applied to the center qubit in the 3 qubit spin chain system. Information flow from one end of the chain to the other end is studied. It is found that as the strength of magnetic field increases, the energy rise of the center qubit gradually blocks the information transmission between the two ends of the chain. Finally, we looked at a 5-qubit network with one qubit in the center connecting the other 4 qubits. The information flow from the 4 qubits at the end towards the center is studied. When we turn on an additional coupling between any two qubits at the end, this additional coupling diverts the direction of uncertainty propagation.

This project proposes a generic concept of causation quantifier for any quantum dynamical system. It may be exploited to investigate quantum versus classical behavior from a fundamental aspect or aid the design of robust quantum network for practical purposes. This proof-of-principle work provides a picturization of causal relations in a complex quantum

network in terms of information flow. This formalism is based on a) full knowledge of the dynamics and b) an intervention applied upon the system. For classical information, the analytical expression has been obtained for linear systems and can be estimated with local measurements. This result greatly enhances the applicability of this information flow-based causality analysis. To what extent can the quantum version be estimated without knowing the dynamics apriori remains a subject of investigation for future studies.

Next, we extended the von-Neumann entropy-based causal analysis to relative entropy. von-Neumann entropy possess the interpretation of quantifying resources in information tasks. Relative entropy plays similar role in quantum information science. Quantum correlations can be expressed in terms of relative entropy and the inequalities satisfied by relative entropy act as a "parent" of various theorems in quantum information science. Here we have generalized quantum Liang information flow with respect to relative entropy. The new information flow measure quantifies how much would the distance between the state of interest and a fixed reference state (as quantified by relative entropy) change upon freezing a subsystem. This relative entropy-based formalism incorporates the von-Neumann entropy based formalism as a special case by choosing a maximally mixed reference state. The principle of nil causality is inherited. That is, if the evolution of two subsystems are independent, the information flow measure from one subsystem to another vanishes. This result is intuitive in the sense that if the evolution is separable, the act of freezing a component would not lead to any change on the other one. This formalism is then applied to thermalization in non-ergodic and ergodic short spin chain systems. We observed, in both cases, the influence from one qubit to the target qubit is consistent with a finite speed propagation. The farther the qubit, the longer it takes to start influencing the target, also a lesser impact averaged over a long time duration. The calculated information flow is also consistent with the knowledge that equilibration in ergodic systems is delocalized, which exhibits more collective behavior of all qubits than in non-ergodic systems.

For future studies, from a fundamental aspect, one may also be interested in a possible connection with the thermodynamics of causal structures, given the key-role played by entropic arguments in this manuscript. The Liang-Kleeman analysis is linked to the Horowitz-Esposito analysis[32]. The latter concerns entropic balance arguments in the study of information transfer in complex dynamical systems[83]. How the current formalism is connected with the thermodynamics of causal structures is also of interest for future exploration. From a practical side, one may be interested in applying the quantum Liang causal analysis to certain information processing tasks. For instance, quantum spatial search is a quantum computational problem of finding a marked site in a structured database[42]. It is shown that, in real complex network, hubs in the network as target nodes tend to have low

success probability[115]. Such phenomenon may be interpreted in terms of quantum Liang information flow. Further, the formalism maybe applied to reveal features of networks, which lead to robustness against failure of nodes.

References

[1] (2016). https://www.youtube.com/watch?v=0Fv-0k13s_k. Accessed 1/11/22.

[2] Åberg, J., Nery, R., Duarte, C., and Chaves, R. (2020). Semidefinite tests for quantum network topologies. *Physical Review Letters*, 125(11):110505.

[3] Abolfazl, B., Sougato, B., and Henrik, J. (2022). Entanglement in spin chains.

[4] Aimet, S., Chevalier, H., and Kim, M. (2022). Gravity mediated entanglement between light beams as a table-top test of quantum gravity. *arXiv preprint arXiv:2210.12713*.

[5] Armour, A., Blencowe, M., and Schwab, K. C. (2002). Entanglement and decoherence of a micromechanical resonator via coupling to a cooper-pair box. *Physical Review Letters*, 88(14):148301.

[6] Arndt, M. and Hornberger, K. (2014). Testing the limits of quantum mechanical superpositions. *Nature Physics*, 10(4):271–277.

[7] Arndt, M., Hornberger, K., and Zeilinger, A. (2005). Probing the limits of the quantum world. *Physics world*, 18(3):35.

[8] Aspect, A., Grangier, P., and Roger, G. (1982). Experimental realization of einstein-podolsky-rosen-bohm gedankenexperiment: a new violation of bell's inequalities. *Physical review letters*, 49(2):91.

[9] Azzini, S., Mazzucchi, S., Moretti, V., Pastorello, D., and Pavesi, L. (2020). Single-particle entanglement. *Advanced Quantum Technologies*, 3(10):2000014.

[10] Bar-Gill, N., Pham, L. M., Jarmola, A., Budker, D., and Walsworth, R. L. (2013). Solid-state electronic spin coherence time approaching one second. *Nature communications*, 4(1):1–6.

[11] Barker, P. and Shneider, M. (2010). Cavity cooling of an optically trapped nanoparticle. *Physical Review A*, 81(2):023826.

[12] Barnett, L., Barrett, A. B., and Seth, A. K. (2009). Granger causality and transfer entropy are equivalent for gaussian variables. *Physical review letters*, 103(23):238701.

[13] Barrett, J., Lorenz, R., and Oreshkov, O. (2019). Quantum causal models. *arXiv preprint arXiv:1906.10726*.

[14] Bassi, A., Großardt, A., and Ulbricht, H. (2017). Gravitational decoherence. *Classical and Quantum Gravity*, 34(19):193002.

[15] Bassi, A., Lochan, K., Satin, S., Singh, T. P., and Ulbricht, H. (2013). Models of wave-function collapse, underlying theories, and experimental tests. *Reviews of Modern Physics*, 85(2):471.

[1] Basu, S., Bandyopadhyay, S., Kar, G., and Home, D. (2001). Bell's inequality for a single spin-1/2 particle and quantum contextuality. *Physics Letters A*, 279(5-6):281–286.

[17] Bateman, J., Nimmrichter, S., Hornberger, K., and Ulbricht, H. (2014). Near-field interferometry of a free-falling nanoparticle from a point-like source. *Nature communications*, 5(1):1–5.

[18] Belenchia, A., Wald, R. M., Giacomini, F., Castro-Ruiz, E., Brukner, Č., and Aspelmeyer, M. (2018). Quantum superposition of massive objects and the quantization of gravity. *Physical Review D*, 98(12):126009.

[19] Bell, J. S. (1964). On the einstein podolsky rosen paradox. *Physics Physique Fizika*, 1(3):195.

[20] Benjamin, S. C. and Bose, S. (2004). Quantum computing in arrays coupled by "always-on" interactions. *Physical Review A*, 70(3):032314.

[21] Bennett, C. H., DiVincenzo, D. P., Fuchs, C. A., Mor, T., Rains, E., Shor, P. W., Smolin, J. A., and Wootters, W. K. (1999). Quantum nonlocality without entanglement. *Physical Review A*, 59(2):1070.

[22] Bennett, C. H., DiVincenzo, D. P., Smolin, J. A., and Wootters, W. K. (1996). Mixed-state entanglement and quantum error correction. *Physical Review A*, 54(5):3824.

[23] Bezruchko, B. P. and Smirnov, D. A. (2010). *Extracting knowledge from time series: An introduction to nonlinear empirical modeling*. Springer Science & Business Media.

[24] Biswas, D., Bose, S., Mazumdar, A., and Toroš, M. (2022). Gravitational optomechanics: Photon-matter entanglement via graviton exchange. *arXiv preprint arXiv:2209.09273*.

[25] Bose, S. (2006). Qubit assisted probing of coherence between mesoscopic states of an apparatus. *Physical review letters*, 96(6):060402.

[26] Bose, S., Home, D., and Mal, S. (2018). Nonclassicality of the harmonic-oscillator coherent state persisting up to the macroscopic domain. *Physical review letters*, 120(21):210402.

[27] Bose, S., Jacobs, K., and Knight, P. L. (1999). Scheme to probe the decoherence of a macroscopic object. *Physical Review A*, 59(5):3204.

[28] Bose, S., Mazumdar, A., Morley, G. W., Ulbricht, H., Toroš, M., Paternostro, M., Geraci, A. A., Barker, P. F., Kim, M., and Milburn, G. (2017). Spin entanglement witness for quantum gravity. *Physical review letters*, 119(24):240401.

[29] Bose, S., Mazumdar, A., Schut, M., and Toroš, M. (2022). Mechanism for the quantum natured gravitons to entangle masses. *Physical Review D*, 105(10):106028.

[30] Bunn, D. W. and Fezzi, C. (2007). Interaction of european carbon trading and energy prices.

[31] Cabello, A. (2008). Experimentally testable state-independent quantum contextuality. *Physical review letters*, 101(21):210401.

[32] Cafaro, C., Ali, S. A., and Giffin, A. (2016). Thermodynamic aspects of information transfer in complex dynamical systems. *Physical Review E*, 93(2):022114.

[33] Cafaro, C., Lord, W. M., Sun, J., and Bollt, E. M. (2015). Causation entropy from symbolic representations of dynamical systems. *Chaos: An interdisciplinary journal of nonlinear science*, 25(4):043106.

[34] Calabrese, P., Cardy, J., and Tonni, E. (2012). Entanglement negativity in quantum field theory. *Physical review letters*, 109(13):130502.

[35] Carlesso, M. and Bassi, A. (2016). Decoherence due to gravitational time dilation: Analysis of competing decoherence effects. *Physics Letters A*, 380(31-32):2354–2358.

[36] Carney, D. (2022). Newton, entanglement, and the graviton. *Physical Review D*, 105(2):024029.

[37] Casimir, H. B. and Polder, D. (1948). The influence of retardation on the london-van der waals forces. *Physical Review*, 73(4):360.

[38] Chang, D. E., Regal, C., Papp, S., Wilson, D., Ye, J., Painter, O., Kimble, H. J., and Zoller, P. (2010). Cavity opto-mechanics using an optically levitated nanosphere. *Proceedings of the National Academy of Sciences*, 107(3):1005–1010.

[39] Chaves, R., Majenz, C., and Gross, D. (2015). Information–theoretic implications of quantum causal structures. *Nature communications*, 6(1):1–8.

[40] Chevalier, H., Paige, A., and Kim, M. (2020a). Witnessing the nonclassical nature of gravity in the presence of unknown interactions. *Physical Review A*, 102(2):022428.

[41] Chevalier, H., Paige, A. J., and Kim, M. S. (2020b). Witnessing the nonclassical nature of gravity in the presence of unknown interactions. *Phys. Rev. A*, 102:022428.

[42] Childs, A. M. and Goldstone, J. (2004). Spatial search by quantum walk. *Physical Review A*, 70(2):022314.

[43] Christensen, B. G., McCusker, K. T., Altepeter, J. B., Calkins, B., Gerrits, T., Lita, A. E., Miller, A., Shalm, L. K., Zhang, Y., Nam, S. W., et al. (2013). Detection-loophole-free test of quantum nonlocality, and applications. *Physical review letters*, 111(13):130406.

[44] Christodoulou, M., Di Biagio, A., Aspelmeyer, M., Brukner, Č., Rovelli, C., and Howl, R. (2022). Locally mediated entanglement through gravity from first principles. *arXiv preprint arXiv:2202.03368*.

[45] Christodoulou, M. and Rovelli, C. (2019). On the possibility of laboratory evidence for quantum superposition of geometries. *Physics Letters B*, 792:64–68.

[46] Clauser, J. F., Horne, M. A., Shimony, A., and Holt, R. A. (1970). Proposed experiment to test local hidden variable theories. *Phys. Rev. Lett.*, 24:549–549.

[47] Costa, F. and Shrapnel, S. (2016). Quantum causal modelling. *New Journal of Physics*, 18(6):063032.

[48] Danielson, D. L., Satishchandran, G., and Wald, R. M. (2022). Gravitationally mediated entanglement: Newtonian field versus gravitons. *Physical Review D*, 105(8):086001.

[49] Delić, U., Reisenbauer, M., Dare, K., Grass, D., Vuletić, V., Kiesel, N., and Aspelmeyer, M. (2020). Cooling of a levitated nanoparticle to the motional quantum ground state. *Science*, 367(6480):892–895.

[50] Di Franco, C., Paternostro, M., and Palma, G. (2008). A deeper insight into quantum state transfer from an information flux viewpoint. *International Journal of Quantum Information*, 6(supp01):659–665.

[51] Di Franco, C., Paternostro, M., Palma, G., and Kim, M. (2007). Information-flux approach to multiple-spin dynamics. *Physical Review A*, 76(4):042316.

[52] Diósi, L. (1989). Models for universal reduction of macroscopic quantum fluctuations. *Physical Review A*, 40(3):1165.

[53] Docquier, D., Vannitsem, S., Ragone, F., Wyser, K., and Liang, X. S. (2021). Causal links between arctic sea ice and its potential drivers based on the rate of information transfer.

[54] Donald, M. J. (1987). Free energy and the relative entropy. *Journal of statistical physics*, 49(1):81–87.

[55] Donoghue, J. F. (1995). Introduction to the effective field theory description of gravity. *Advanced school on effective theories: Almunecar, Granada, Spain*, 26:217–240.

[56] Englert, B., Schwinger, J., and Scully, M. (1988a). Is spin coherence like humpty-dumpty? i. simplified treatment. *Found Phys*, 18:1045–1056.

[57] Englert, B.-G., Schwinger, J., and Scully, M. O. (1988b). Is spin coherence like humpty-dumpty? i. simplified treatment. *Foundations of physics*, 18(10):1045–1056.

[58] Fein, Y. Y., Geyer, P., Zwick, P., Kiałka, F., Pedalino, S., Mayor, M., Gerlich, S., and Arndt, M. (2019). Quantum superposition of molecules beyond 25 kda. *Nature Physics*, 15(12):1242–1245.

[59] Feinberg, G. and Sucher, J. (1970). General theory of the van der waals interaction: A model-independent approach. *Physical Review A*, 2(6):2395.

[60] Fitzsimons, J. F., Jones, J. A., and Vedral, V. (2015). Quantum correlations which imply causation. *Scientific reports*, 5(1):1–7.

[61] Flühmann, C., Nguyen, T. L., Marinelli, M., Negnevitsky, V., Mehta, K., and Home, J. (2019). Encoding a qubit in a trapped-ion mechanical oscillator. *Nature*, 566(7745):513–517.

[62] Franco, R. L., Bellomo, B., Maniscalco, S., and Compagno, G. (2013). Dynamics of quantum correlations in two-qubit systems within non-markovian environments. *International Journal of Modern Physics B*, 27(01n03):1345053.

[63] Freedman, S. J. and Clauser, J. F. (1972). Experimental test of local hidden-variable theories. *Physical Review Letters*, 28(14):938.

[64] Fritz, T. (2016). Beyond bell's theorem ii: Scenarios with arbitrary causal structure. *Communications in Mathematical Physics*, 341(2):391–434.

[65] Gachechiladze, M., Miklin, N., and Chaves, R. (2020). Quantifying causal influences in the presence of a quantum common cause. *Physical Review Letters*, 125(23):230401.

[66] Gerlich, S., Eibenberger, S., Tomandl, M., Nimmrichter, S., Hornberger, K., Fagan, P. J., Tüxen, J., Mayor, M., and Arndt, M. (2011). Quantum interference of large organic molecules. *Nature communications*, 2(1):1–5.

[67] Ghosh, D., Jennewein, T., Kolenderski, P., and Sinha, U. (2018). Spatially correlated photonic qutrit pairs using pump beam modulation technique. *OSA Continuum*, 1(3):996–1011.

[68] Gieseler, J., Deutsch, B., Quidant, R., and Novotny, L. (2012a). Subkelvin parametric feedback cooling of a laser-trapped nanoparticle. *Phys. Rev. Lett.*, 109:103603.

[69] Gieseler, J., Deutsch, B., Quidant, R., and Novotny, L. (2012b). Subkelvin parametric feedback cooling of a laser-trapped nanoparticle. *Physical review letters*, 109(10):103603.

[70] Giustina, M., Mech, A., Ramelow, S., Wittmann, B., Kofler, J., Beyer, J., Lita, A., Calkins, B., Gerrits, T., Nam, S. W., et al. (2013). Bell violation using entangled photons without the fair-sampling assumption. *Nature*, 497(7448):227–230.

[71] Gottesman, D., Kitaev, A., and Preskill, J. (2001). Encoding a qubit in an oscillator. *Physical Review A*, 64(1):012310.

[72] Granger, C. (1969). Investigating casual relations by econometric models and cross spectral.

[73] Hagan, D. F. T., Wang, G., Liang, X. S., and Dolman, H. A. (2019). A time-varying causality formalism based on the liang–kleeman information flow for analyzing directed interactions in nonstationary climate systems. *Journal of Climate*, 32(21):7521–7537.

[74] Hahs, D. W. and Pethel, S. D. (2011). Distinguishing anticipation from causality: Anticipatory bias in the estimation of information flow. *Physical review letters*, 107(12):128701.

[75] Hasegawa, Y., Loidl, R., Badurek, G., Baron, M., and Rauch, H. (2006). Quantum contextuality in a single-neutron optical experiment. *Phys. Rev. Lett.*, 97:230401.

[76] Hensen, B., Bernien, H., Dréau, A. E., Reiserer, A., Kalb, N., Blok, M. S., Ruitenberg, J., Vermeulen, R. F., Schouten, R. N., Abellán, C., et al. (2015). Loophole-free bell inequality violation using electron spins separated by 1.3 kilometres. *Nature*, 526(7575):682–686.

[77] Henson, J., Lal, R., and Pusey, M. F. (2014). Theory-independent limits on correlations from generalized bayesian networks. *New Journal of Physics*, 16(11):113043.

[78] Hollands, S. and Wald, R. M. (2010). Axiomatic quantum field theory in curved spacetime. *Communications in Mathematical Physics*, 293(1):85–125.

[79] Home, D., Pan, A. K., Ali, M. M., and Majumdar, A. (2007). Aspects of nonideal stern–gerlach experiment and testable ramifications. *Journal of Physics A: Mathematical and Theoretical*, 40(46):13975.

[80] Home, D. and Sengupta, S. (1984). Bell's inequality and non-contextual dispersion-free states. *Physics Letters A*, 102(4):159–162.

[81] Hornberger, K., Sipe, J. E., and Arndt, M. (2004). Theory of decoherence in a matter wave talbot-lau interferometer. *Physical Review A*, 70(5):053608.

[82] Horodecki, M., Horodecki, P., and Horodecki, R. (2001). Separability of n-particle mixed states: necessary and sufficient conditions in terms of linear maps. *Physics Letters A*, 283(1-2):1–7.

[83] Horowitz, J. M. and Esposito, M. (2014). Thermodynamics with continuous information flow. *Physical Review X*, 4(3):031015.

[84] Hristopulos, D. T., Babul, A., Babul, S., Brucar, L. R., and Virji-Babul, N. (2019). Disrupted information flow in resting-state in adolescents with sports related concussion. *Frontiers in human neuroscience*, 13:419.

[85] Janszky, J. and Adam, P. (1992). Strong squeezing by repeated frequency jumps. *Physical Review A*, 46(9):6091.

[86] Kafri, D. and Taylor, J. (2013). A noise inequality for classical forces. *arXiv preprint arXiv:1311.4558*.

[87] Kafri, D., Taylor, J., and Milburn, G. (2014). A classical channel model for gravitational decoherence. *New Journal of Physics*, 16(6):065020.

[88] Keil, M., Machluf, S., Margalit, Y., Zhou, Z., Amit, O., Dobkowski, O., Japha, Y., Moukouri, S., Rohrlich, D., Binstock, Z., et al. (2020). Stern-gerlach interferometry with the atom chip. *arXiv preprint arXiv:2009.08112*.

[89] Kiefer, C. (2006). Quantum gravity: general introduction and recent developments. *Annalen der Physik*, 15(1-2):129–148.

[90] Kiss, T., Adam, P., and Janszky, J. (1994). Time-evolution of a harmonic oscillator: jumps between two frequencies. *Physics Letters A*, 192(5):311–315.

[91] Kleeman, R. (2002). Measuring dynamical prediction utility using relative entropy. *Journal of the atmospheric sciences*, 59(13):2057–2072.

[92] Kleeman, R. (2008). Limits, variability, and general behavior of statistical predictability of the midlatitude atmosphere. *Journal of the atmospheric sciences*, 65(1):263–275.

[93] Kleeman, R. and Majda, A. (2005). Predictability in a model of geophysical turbulence. *Journal of the atmospheric sciences*, 62(8):2864–2879.

[94] Kolenderski, P., Sinha, U., Youning, L., Zhao, T., Volpini, M., Cabello, A., Laflamme, R., and Jennewein, T. (2011). Aharon-vaidman quantum game with a young-type photonic qutrit. *Physical Review A*, 86.

[95] Kolenderski, P., Sinha, U., Youning, L., Zhao, T., Volpini, M., Cabello, A., Laflamme, R., and Jennewein, T. (2012). Aharon-vaidman quantum game with a young-type photonic qutrit. *Physical Review A*, 86(1):012321.

[96] Kovachy, T., Asenbaum, P., Overstreet, C., Donnelly, C., Dickerson, S., Sugarbaker, A., Hogan, J., and Kasevich, M. (2015). Quantum superposition at the half-metre scale. *Nature*, 528(7583):530–533.

[97] Krisnanda, T., Paterek, T., Paternostro, M., and Liew, T. C. (2022). Quantum neuromorphic approach to efficient sensing of gravity-induced entanglement. *arXiv preprint arXiv:2209.14565*.

[98] Krisnanda, T., Tham, G. Y., Paternostro, M., and Paterek, T. (2020). Observable quantum entanglement due to gravity. *npj Quantum Information*, 6(1):1–6.

[99] Krisnanda, T., Zuppardo, M., Paternostro, M., and Paterek, T. (2017). Revealing nonclassicality of inaccessible objects. *Physical review letters*, 119(12):120402.

[100] Lamoreaux, S. K. (2012). The casimir force and related effects: The status of the finite temperature correction and limits on new long-range forces. *Annual Review of Nuclear and Particle Science*, 62:37–56.

[101] Landig, A. J., Koski, J. V., Scarlino, P., Müller, C., Abadillo-Uriel, J. C., Kratochwil, B., Reichl, C., Wegscheider, W., Coppersmith, S. N., Friesen, M., et al. (2019). Virtual-photon-mediated spin-qubit–transmon coupling. *Nature communications*, 10(1):1–7.

[102] Leggett, A. J. (2002). Testing the limits of quantum mechanics: motivation, state of play, prospects. *Journal of Physics: Condensed Matter*, 14(15):R415.

[103] Leng, Y., Li, R., Kong, X., Xie, H., Zheng, D., Yin, P., Xiong, F., Wu, T., Duan, C.-K., Du, Y., et al. (2021). Mechanical dissipation below 1 μ hz with a cryogenic diamagnetic levitated micro-oscillator. *Physical Review Applied*, 15(2):024061.

[104] Liang, X. S. (2008). Information flow within stochastic dynamical systems. *Physical Review E*, 78(3):031113.

[105] Liang, X. S. (2014). Unraveling the cause-effect relation between time series. *Physical Review E*, 90(5):052150.

[106] Liang, X. S. (2016). Information flow and causality as rigorous notions ab initio. *Physical Review E*, 94(5):052201.

[107] Liang, X. S. (2018). Causation and information flow with respect to relative entropy. *Chaos: An Interdisciplinary Journal of Nonlinear Science*, 28(7):075311.

[108] Liang, X. S. (2021a). The causal interaction between complex subsystems. *Entropy*, 24(1):3.

[109] Liang, X. S. (2021b). Measuring the importance of individual units in producing the collective behavior of a complex network. *Chaos: An Interdisciplinary Journal of Nonlinear Science*, 31(9):093123.

[110] Liang, X. S. (2021c). Normalized multivariate time series causality analysis and causal graph reconstruction. *Entropy*, 23(6):679.

[111] Liang, X. S. and Kleeman, R. (2005). Information transfer between dynamical system components. *Physical review letters*, 95(24):244101.

[112] Liang, X. S., Xu, F., Rong, Y., Zhang, R., Tang, X., and Zhang, F. (2021). El niño modoki can be mostly predicted more than 10 years ahead of time. *Scientific reports*, 11(1):1–14.

[113] Lu, X., Liu, K., Lai, K. K., and Cui, H. (2022). Transmission between eu allowance prices and clean energy index. *Procedia Computer Science*, 199:1327–1331.

[114] Machluf, S., Japha, Y., and Folman, R. (2013). Coherent stern–gerlach momentum splitting on an atom chip. *Nature Communications*, 4:2424.

[115] Malmi, J., Rossi, M. A., García-Pérez, G., and Maniscalco, S. (2022). Spatial search by continuous-time quantum walks on renormalized internet networks. *arXiv preprint arXiv:2205.02137*.

[116] Margalit, Y., Dobkowski, O., Zhou, Z., Amit, O., Japha, Y., Moukouri, S., Rohrlich, D., Mazumdar, A., Bose, S., Henkel, C., et al. (2020). Realization of a complete stern-gerlach interferometer: Towards a test of quantum gravity. *arXiv preprint arXiv:2011.10928*.

[117] Margalit, Y., Zhou, Z., Dobkowski, O., Japha, Y., Rohrlich, D., Moukouri, S., and Folman, R. (2018). Realization of a complete stern-gerlach interferometer. *arXiv preprint arXiv:1801.02708*.

[118] Margalit, Y., Zhou, Z., Machluf, S., Japha, Y., Moukouri, S., and Folman, R. (2019). Analysis of a high-stability stern–gerlach spatial fringe interferometer. *New Journal of Physics*, 21(7):073040.

[119] Marletto, C. and Vedral, V. (2017). Gravitationally induced entanglement between two massive particles is sufficient evidence of quantum effects in gravity. *Physical review letters*, 119(24):240402.

[120] Marshall, W., Simon, C., Penrose, R., and Bouwmeester, D. (2003). Towards quantum superpositions of a mirror. *Physical Review Letters*, 91(13):130401.

[121] Marshman, R. J., Mazumdar, A., and Bose, S. (2020a). Locality and entanglement in table-top testing of the quantum nature of linearized gravity. *Physical Review A*, 101(5):052110.

[122] Marshman, R. J., Mazumdar, A., Folman, R., and Bose, S. (2022). Constructing nano-object quantum superpositions with a stern-gerlach interferometer. *Physical Review Research*, 4(2):023087.

[123] Marshman, R. J., Mazumdar, A., Morley, G. W., Barker, P. F., Hoekstra, S., and Bose, S. (2020b). Mesoscopic interference for metric and curvature & gravitational wave detection. *New Journal of Physics*, 22(8):083012.

[124] Matsko, A. B., Vyatchanin, S. P., and Yi, L. (2020). On mechanical motion damping of a magnetically trapped diamagnetic particle. *Physics Letters A*, 384(26):126643.

[125] Maziarz, M. (2015). A review of the granger-causality fallacy. *The journal of philosophical economics: Reflections on economic and social issues*, 8(2):86–105.

[126] McClean, J. R., Romero, J., Babbush, R., and Aspuru-Guzik, A. (2016). The theory of variational hybrid quantum-classical algorithms. *New Journal of Physics*, 18(2):023023.

[127] Milburn, G. (1991). Intrinsic decoherence in quantum mechanics. *Physical Review A*, 44(9):5401.

[128] Modi, K., Paterek, T., Son, W., Vedral, V., and Williamson, M. (2010). Unified view of quantum and classical correlations. *Physical review letters*, 104(8):080501.

[129] Neumeier, L., Ciampini, M. A., Romero-Isart, O., Aspelmeyer, M., and Kiesel, N. (2022). Fast quantum interference of a nanoparticle via optical potential control. *arXiv preprint arXiv:2207.12539*.

[130] Nielsen, M. A. and Chuang, I. (2002). Quantum computation and quantum information.

[131] Oppenheim, J. (2018). A post-quantum theory of classical gravity? *arXiv preprint arXiv:1811.03116*.

[132] Oppenheim, J. and Weller-Davies, Z. (2022). The constraints of post-quantum classical gravity. *Journal of High Energy Physics*, 2022(2):1–39.

[133] Oriti, D. (2009). *Approaches to quantum gravity: Toward a new understanding of space, time and matter*. Cambridge University Press.

[134] Osnaghi, S., Bertet, P., Auffeves, A., Maioli, P., Brune, M., Raimond, J.-M., and Haroche, S. (2001). Coherent control of an atomic collision in a cavity. *Physical Review Letters*, 87(3):037902.

[135] Pearl, J. et al. (2000). Models, reasoning and inference. *Cambridge, UK: Cambridge-UniversityPress*, 19.

[136] Pedernales, J. S., Morley, G. W., and Plenio, M. B. (2020). Motional dynamical decoupling for interferometry with macroscopic particles. *Physical Review Letters*, 125(2):023602.

[137] Penrose, R. (1996). On gravity's role in quantum state reduction. *General relativity and gravitation*, 28(5):581–600.

[138] Pino, H., Prat-Camps, J., Sinha, K., Venkatesh, B. P., and Romero-Isart, O. (2018). On-chip quantum interference of a superconducting microsphere. *Quantum Science and Technology*, 3(2):025001.

[139] Pisarczyk, R., Zhao, Z., Ouyang, Y., Vedral, V., and Fitzsimons, J. F. (2019). Causal limit on quantum communication. *Physical review letters*, 123(15):150502.

[140] Qvarfort, S., Bose, S., and Serafini, A. (2020). Mesoscopic entanglement through central–potential interactions. *Journal of Physics B: Atomic, Molecular and Optical Physics*, 53(23):235501.

[141] Rahman, A. A., Frangeskou, A., Kim, M., Bose, S., Morley, G., and Barker, P. (2016). Burning and graphitization of optically levitated nanodiamonds in vacuum. *Scientific reports*, 6(1):1–7.

[142] Rashid, M., Tufarelli, T., Bateman, J., Vovrosh, J., Hempston, D., Kim, M., and Ulbricht, H. (2016). Experimental realization of a thermal squeezed state of levitated optomechanics. *Physical review letters*, 117(27):273601.

[143] Rengaraj, G., Prathwiraj, U., Sahoo, S. N., Somashekhar, R., and Sinha, U. (2018). Measuring the deviation from the superposition principle in interference experiments. *New Journal of Physics*, 20(6):063049.

[144] Romero-Isart, O. (2011). Quantum superposition of massive objects and collapse models. *Physical Review A*, 84(5):052121.

[145] Romero-Isart, O., Juan, M. L., Quidant, R., and Cirac, J. I. (2010). Toward quantum superposition of living organisms. *New Journal of Physics*, 12(3):033015.

[146] Romero-Isart, O., Pflanzer, A. C., Blaser, F., Kaltenbaek, R., Kiesel, N., Aspelmeyer, M., and Cirac, J. I. (2011). Large quantum superpositions and interference of massive nanometer-sized objects. *Physical review letters*, 107(2):020405.

[147] Rosenfeld, E., Riedinger, R., Gieseler, J., Schuetz, M., and Lukin, M. D. (2021). Efficient entanglement of spin qubits mediated by a hot mechanical oscillator. *Physical Review Letters*, 126(25):250505.

[148] Rowe, M. A., Kielpinski, D., Meyer, V., Sackett, C. A., Itano, W. M., Monroe, C., and Wineland, D. J. (2001). Experimental violation of a bell's inequality with efficient detection. *Nature*, 409(6822):791–794.

[2] Sadana, S., Sanders, B. C., and Sinha, U. (2019). Double-slit interferometry as a lossy beam splitter. *New Journal of Physics*, 21(11):113022.

[150] Sawant, R., Samuel, J., Sinha, A., Sinha, S., and Sinha, U. (2014). Nonclassical paths in quantum interference experiments. *Physical review letters*, 113(12):120406.

[151] Scala, M., Kim, M., Morley, G., Barker, P., and Bose, S. (2013). Matter-wave interferometry of a levitated thermal nano-oscillator induced and probed by a spin. *Physical review letters*, 111(18):180403.

[152] Schlosshauer, M. A. (2007). *Decoherence: and the quantum-to-classical transition*. Springer Science & Business Media.

[153] Schneider, T. and Griffies, S. M. (1999). A conceptual framework for predictability studies. *Journal of climate*, 12(10):3133–3155.

[154] Schreiber, T. (2000). Measuring information transfer. *Physical review letters*, 85(2):461.

[155] Simon, R. (2000). Peres-horodecki separability criterion for continuous variable systems. *Physical Review Letters*, 84(12):2726.

[156] Smirnov, D. A. (2013). Spurious causalities with transfer entropy. *Physical Review E*, 87(4):042917.

[157] Spirtes, P., Glymour, C. N., Scheines, R., and Heckerman, D. (2000). *Causation, prediction, and search*. MIT press.

[158] Staniek, M. and Lehnertz, K. (2008). Symbolic transfer entropy. *Physical review letters*, 100(15):158101.

[159] Stips, A., Macias, D., Coughlan, C., Garcia-Gorriz, E., and Liang, X. S. (2016). On the causal structure between co 2 and global temperature. *Scientific reports*, 6(1):1–9.

[160] Strogatz, S. H. (2001). Exploring complex networks. *nature*, 410(6825):268–276.

[161] Sun, J. and Bollt, E. M. (2014). Causation entropy identifies indirect influences, dominance of neighbors and anticipatory couplings. *Physica D: Nonlinear Phenomena*, 267:49–57.

[162] Taguchi, G., Dougakiuchi, T., Yoshimoto, N., Kasai, K., Iinuma, M., Hofmann, H. F., and Kadoya, Y. (2008). Measurement and control of spatial qubits generated by passing photons through double slits. *Physical Review A*, 78(1):012307.

[163] Tebbenjohanns, F., Frimmer, M., Militaru, A., Jain, V., and Novotny, L. (2019). Cold damping of an optically levitated nanoparticle to microkelvin temperatures. *Physical review letters*, 122(22):223601.

[164] Toroš, M., van de Kamp, T. W., Marshman, R. J., Kim, M., Mazumdar, A., and Bose, S. (2020). Relative acceleration noise mitigation for entangling masses via quantum gravity. *arXiv preprint arXiv:2007.15029*.

[165] van de Kamp, T. W., Marshman, R. J., Bose, S., and Mazumdar, A. (2020). Quantum gravity witness via entanglement of masses: Casimir screening. *Physical Review A*, 102(6):062807.

[166] Vannitsem, S., Dalaiden, Q., and Goosse, H. (2019). Testing for dynamical dependence: Application to the surface mass balance over antarctica. *Geophysical Research Letters*, 46(21):12125–12135.

[167] Vastano, J. A. and Swinney, H. L. (1988). Information transport in spatiotemporal systems. *Physical Review Letters*, 60(18):1773.

[168] Vovrosh, J., Rashid, M., Hempston, D., Bateman, J., Paternostro, M., and Ulbricht, H. (2017). Parametric feedback cooling of levitated optomechanics in a parabolic mirror trap. *JOSA B*, 34(7):1421–1428.

[169] Walker, L., Robb, G., and Daley, A. (2019). Measurement and feedback for cooling heavy levitated particles in low-frequency traps. *Physical Review A*, 100(6):063819.

[170] Wan, C., Scala, M., Morley, G., Rahman, A. A., Ulbricht, H., Bateman, J., Barker, P., Bose, S., and Kim, M. (2016). Free nano-object ramsey interferometry for large quantum superpositions. *Physical review letters*, 117(14):143003.

[171] Wang, J.-F., Yan, F.-F., Li, Q., Liu, Z.-H., Liu, H., Guo, G.-P., Guo, L.-P., Zhou, X., Cui, J.-M., Wang, J., et al. (2020). Coherent control of nitrogen-vacancy center spins in silicon carbide at room temperature. *Physical review letters*, 124(22):223601.

[172] Weinberg, S. (1995). *The quantum theory of fields*, volume 2. Cambridge university press.

[173] Weinberg, S. (2012). Collapse of the state vector. *Phys. Rev. A*, 85:062116.

[174] Weiss, T., Roda-Llordes, M., Torrontegui, E., Aspelmeyer, M., and Romero-Isart, O. (2020). Large quantum delocalization of a levitated nanoparticle using optimal control: Applications for force sensing and entangling via weak forces. *arXiv preprint arXiv:2012.12260*.

[175] Weiss, T., Roda-Llordes, M., Torrontegui, E., Aspelmeyer, M., and Romero-Isart, O. (2021). Large quantum delocalization of a levitated nanoparticle using optimal control: applications for force sensing and entangling via weak forces. *Physical Review Letters*, 127(2):023601.

[176] Whittle, C., Hall, E. D., Dwyer, S., Mavalvala, N., Sudhir, V., Abbott, R., Ananyeva, A., Austin, C., Barsotti, L., Betzwieser, J., et al. (2021). Approaching the motional ground state of a 10-kg object. *Science*, 372(6548):1333–1336.

[177] Wilde, M. M. (2013). *Quantum information theory*. Cambridge University Press.

[178] Wolfe, E., Pozas-Kerstjens, A., Grinberg, M., Rosset, D., Acín, A., and Navascués, M. (2021). Quantum inflation: A general approach to quantum causal compatibility. *Physical Review X*, 11(2):021043.

[179] Wood, B., Bose, S., and Morley, G. (2022). Spin dynamical decoupling for generating macroscopic superpositions of a free-falling nanodiamond. *Physical Review A*, 105(1):012824.

[180] Xu, Z., Gao, X., Bang, J., Jacob, Z., and Li, T. (2021). A casimir diode. *arXiv preprint arXiv:2102.12857*.

[181] Xu, Z. and Li, T. (2017). Detecting casimir torque with an optically levitated nanorod. *Physical Review A*, 96(3):033843.

[182] Yi, B. and Bose, S. (2022). Quantum liang information flow as causation quantifier. *Physical Review Letters*, 129(2):020501.

[183] Yi, B., Sinha, U., Home, D., Mazumdar, A., and Bose, S. (2021). Massive spatial qubits for testing macroscopic nonclassicality and casimir induced entanglement. *arXiv preprint arXiv:2106.11906*.

[184] Yin, Z.-q., Li, T., Zhang, X., and Duan, L. (2013). Large quantum superpositions of a levitated nanodiamond through spin-optomechanical coupling. *Physical Review A*, 88(3):033614.

[185] Yung, M.-H., Leung, D. W., and Bose, S. (2003). An exact effective two-qubit gate in a chain of three spins. *arXiv preprint quant-ph/0312105*.

[186] Zheng, D., Leng, Y., Kong, X., Li, R., Wang, Z., Luo, X., Zhao, J., Duan, C.-K., Huang, P., Du, J., et al. (2020). Room temperature test of the continuous spontaneous localization model using a levitated micro-oscillator. *Physical Review Research*, 2(1):013057.

[187] Zhou, J.-W., Wang, P.-F., Shi, F.-Z., Huang, P., Kong, X., Xu, X.-K., Zhang, Q., Wang, Z.-X., Rong, X., and Du, J.-F. (2014). Quantum information processing and metrology with color centers in diamonds. *Frontiers of Physics*, 9(5):587–597.

[188] Zhou, R., Marshman, R. J., Bose, S., and Mazumdar, A. (2022a). Catapulting towards massive and large spatial quantum superposition. *arXiv preprint arXiv:2206.04088*.

[189] Zhou, R., Marshman, R. J., Bose, S., and Mazumdar, A. (2022b). Mass independent scheme for large spatial quantum superpositions. *arXiv preprint arXiv:2210.05689*.

Appendix A

Massive Spatial Qubits

A.1 Efficacy of the Pauli-Z measurement as a function of measurement time

The system freely propagates for a time t, the final state may be written, for an initial state $|+\rangle$, as:

$$\begin{aligned}\langle x|\Psi(t)\rangle =& \frac{1}{[2\pi\sigma^2]^{1/4}}\sqrt{\frac{1}{\frac{1}{s}-i\frac{\hbar t}{2m}}} \\ &\times\left\{\exp[-\frac{(x-\frac{d}{2\sigma_d^2 s})^2}{4(\frac{1}{s}-i\frac{\hbar t}{2m})}]+\exp[-\frac{(x+\frac{d}{2\sigma_d^2 s})^2}{4(\frac{1}{s}-i\frac{\hbar t}{2m})}]\right\}\end{aligned} \tag{A.1}$$

where $s\equiv\frac{i4\phi}{\sigma^2}+\frac{1}{\sigma^2}+\frac{1}{\sigma_d^2}$, ϕ is global phase added during the propagation.

Note that Eq. A.1 consists of two terms tracing which path the object passes through, effectively the predefined Young qubit. σ_z measurement requires that the wave packets are well separated upon measurement. The condition maybe formulated by demanding the probability distribution P_0 (P_1) of $|0\rangle$ ($|1\rangle$) state alone confined in the $x<0$ ($x>0$) regime:

$$\varepsilon = 1-\frac{\int_{-\infty}^{0}P_0 dx}{\int_{-\infty}^{\infty}P_0 dx}\ll 1 \tag{A.2}$$

Substituting Eq. A.1, the fraction term can be evaluated at the σ_z measurement time $t = t^z_{meas}$:

$$\frac{\int_{-\infty}^{0} P_0 dx}{\int_{-\infty}^{\infty} P_0 dx} = \frac{\int_{-\infty}^{0} \exp[-\frac{(x+\frac{d}{2\sigma_d^2 s})^2 \frac{1}{s}}{\frac{2}{s^2}+\frac{\hbar^2 t^2}{8m^2}}]dx}{\int_{-\infty}^{\infty} \exp[-\frac{(x+\frac{d}{2\sigma_d^2 s})^2 \frac{1}{s}}{\frac{2}{s^2}+\frac{\hbar^2 t^2}{8m^2}}]dx} \tag{A.3}$$

where the normalization factor in the probability distribution, independent of x, cancels out in the calculation.

Let us take $\sigma_d : d = 1 : 50$ and $t^z_{meas} \approx$ one-tenth of the overlapping time $\frac{d(2\sigma_d m)}{\hbar}$. We then get $\varepsilon \sim (1 - 4.7 \times 10^{-7})$. We may thus claim that for the above choice of parameters the left and right Gaussian wavepackets are well separated, and Pauli-Z measurement has a good fidelity.

A.2 Efficacy of the Pauli-X and Pauli-Z measurement for various parameters

We take $t = t^{x,y}_{\text{meas}} \sim \frac{2\sigma_d m d}{\hbar}$ as the time of σ_x, σ_y measurement, and evaluate how accurate this measurement is for various ratios $\sigma_d : d$ using the full time evolution as in A.1. Our target is to check how accurately the interference pattern is reproduced at correct positions as given by $x = \frac{\hbar k_x t^{x,y}_{\text{meas}}}{m}$. For an initial state $|0\rangle + |1\rangle$, if $\sigma_d : d = 1 : 10$ the first peak of the interference pattern adjacent to the central peak (corresponding to $\theta = 2\pi$) locates at $x \sim 11.797\sigma_d$. If $\sigma_d : d = 1 : 100$, $x \sim 12.559\sigma_d$. If $\sigma_d : d = 1 : 50$, $x \sim 12.536\sigma_d$. While assumption $x = \frac{\hbar k_x t^{x,y}_{\text{meas}}}{m}$ gives a value of $x = 4\pi\sigma_d \sim 12.566\sigma_d$, which is $>\sim 99.94\%$ accurate for $\frac{\sigma_d}{d} \leq \frac{1}{100}$, $>\sim 99.76\%$ accurate for $\frac{\sigma_d}{d} \leq \frac{1}{50}$. Therefore, the σ_x, σ_y measurements have a good fidelity in the $\frac{\sigma_d}{d} \leq \frac{1}{50}$ setting, which we shall use.

A.3 Methods of computation with effective Pauli operators including uncertainties, and the incorporation of decoherence

Let $\tilde{\sigma}$ denotes the measured Pauli operator, parameterized by uncertainty in phase angle $\delta\theta$. Then,

$$\begin{aligned} \tilde{\sigma}_x &= \frac{1}{\delta\theta}\begin{pmatrix} 0 & -ie^{i\frac{\delta\theta}{2}} + ie^{-i\frac{\delta\theta}{2}} \\ -ie^{i\frac{\delta\theta}{2}} + ie^{-i\frac{\delta\theta}{2}} & 0 \end{pmatrix} \\ &= g(\delta\theta)\sigma_x \end{aligned} \tag{A.4}$$

where $g(\delta\theta) = -ie^{i\frac{\delta\theta}{2}} + ie^{-i\frac{\delta\theta}{2}} = \frac{2}{\delta\theta}cos(\frac{\pi-\delta\theta}{2})$. $g(\delta\theta)$ goes to 1 as $\delta\theta \to 0$. Similarly,

$$\tilde{\sigma}_y = g(\delta\theta)\sigma_y \tag{A.5}$$

Therefore, for arbitrary density state ρ

$$\begin{aligned} Tr(\tilde{\sigma}_x\rho) &= g(\delta\theta)Tr(\sigma_x\rho) \\ Tr(\tilde{\sigma}_y\rho) &= g(\delta\theta)Tr(\sigma_y\rho) \end{aligned} \tag{A.6}$$

In particular, let $\rho_{x+}(\rho_{y+})$ denotes the positive eigenstate of $\sigma_x(\sigma_y)$, and $\rho_{x+} = \frac{1}{2}\begin{pmatrix} 1 & 1 \\ 1 & 1 \end{pmatrix}$, $\rho_{y+} = \frac{1}{2}\begin{pmatrix} 1 & -i \\ i & 1 \end{pmatrix}$. Then,

$$Tr(\tilde{\sigma}_x\rho_{x+}) = Tr(\tilde{\sigma}_y\rho_{y+}) = g(\delta\theta) \tag{A.7}$$

Furthermore, if decoherence is considered, let $\tilde{\rho} = \begin{pmatrix} \rho_{00} & \rho_{01}e^{-\gamma t} \\ \rho_{10e^{-\gamma t}} & \rho_{11} \end{pmatrix}$, where γ denotes dephasing rate, then we have:

$$\begin{aligned} Tr(\tilde{\sigma}_x\tilde{\rho}) &= g(\delta\theta)Tr(\sigma_x\rho)e^{-\gamma t} \\ Tr(\tilde{\sigma}_y\tilde{\rho}) &= g(\delta\theta)Tr(\sigma_y\rho)e^{-\gamma t} \end{aligned} \tag{A.8}$$

A.4 Decoherence in probing the entanglement of the Stern-Gerlach state

Consider the state $\phi^+ = \frac{1}{\sqrt{2}}(|\uparrow,R\rangle + |\downarrow,L\rangle)$, where the spatial qubit undergoes decoherence. The density state can be written as

$$\tilde{\rho}(\phi^+) = \frac{1}{2}\begin{pmatrix} 0 & 0 & 0 & 0 \\ 0 & 1 & e^{-\gamma t} & 0 \\ 0 & e^{-\gamma t} & 1 & 0 \\ 0 & 0 & 0 & 0 \end{pmatrix} \tag{A.9}$$

$$\begin{aligned} Tr(\sigma_x \otimes \sigma_x \tilde{\rho}(\phi^+)) &= Tr(\sigma_y \otimes \sigma_y \tilde{\rho}(\phi^+)) = e^{-\gamma t} \\ Tr(\sigma_x \otimes \sigma_y \tilde{\rho}(\phi^+)) &= Tr(\sigma_y \otimes \sigma_x \tilde{\rho}(\phi^+)) = 0 \end{aligned} \tag{A.10}$$

Therefore,

$$|\langle ab\rangle + \langle ab'\rangle + \langle a'b\rangle - \langle a'b'\rangle| = |2\sqrt{2}g(\delta\theta)e^{-\gamma t}| \leq 2\sqrt{2} \tag{A.11}$$

References

[1] Basu, S., Bandyopadhyay, S., Kar, G. & Home, D. Bell's inequality for a single spin-1/2 particle and quantum contextuality. *Physics Letters A*. **279**, 281-286 (2001)

[2] Sadana, S., Sanders, B. & Sinha, U. Double-slit interferometry as a lossy beam splitter. *New Journal Of Physics*. **21**, 113022 (2019)

Appendix B

Quantum gravity induced phase

B.1 time delayed induction

In the following, we will take into account the propagation time of quantum mediators. The system would not entangle before the virtual gravitons reach the corresponding superposition component. The state evolution, therefore, consists of four periods:

$$
\begin{gathered}
t < \frac{D-d}{c},\ \phi_{RL} = 0\ \phi = 0\ \phi_{LR} = 0 \\
\frac{D-d}{c} < t < \frac{D}{c},\ \phi_{RL} = \phi'_{RL}\ \phi = 0\ \phi_{LR} = 0 \\
\frac{D}{c} < t < \frac{D+d}{c},\ \phi_{RL} = \phi'_{RL}\ \phi = \phi'\ \phi_{LR} = 0 \\
t > \frac{D+d}{c},\ \phi_{RL} = \phi'_{RL}\ \phi = \phi'\ \phi_{LR} = \phi'_{LR}
\end{gathered}
$$

the (delayed) induced phase is given by:

$$
\begin{aligned}
\phi'_{RL} &\sim \frac{Gm_1m_2}{\hbar(D-d)}(t-\frac{D-d}{c}) \\
\phi'_{LR} &\sim \frac{Gm_1m_2}{\hbar(D+d)}(t-\frac{D+d}{c}) \\
\phi' &\sim \frac{Gm_1m_2}{\hbar D}(t-\frac{D}{d})
\end{aligned}
\tag{B.1}
$$

Take $m \sim 10^{-14}kg, D \sim 450\mu m, d \sim 250\mu m$. The timescale, at which the phase evolution threshold occurs, is of order of magnitude $10^{-12}s$.With these parameters, the induced phase Eq. B.1 at this timescale is of order of magnitude 10^{-13}rad. The entanglement witness

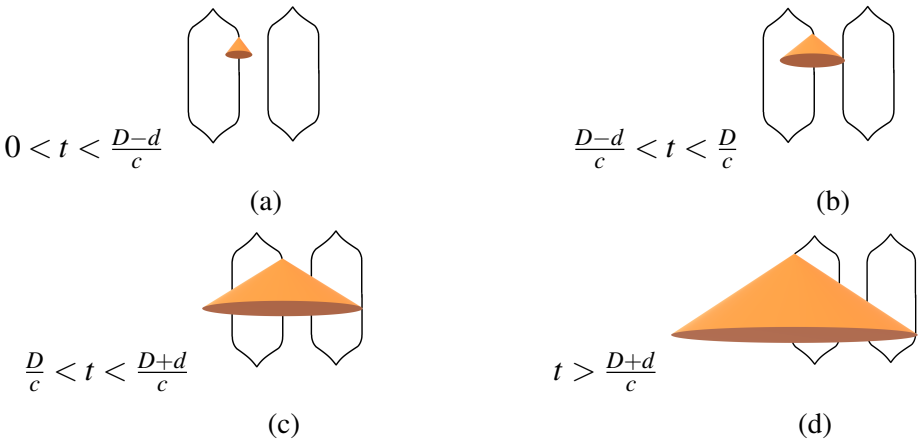

Fig. B.1 **Illustrative light cone structure for one superposition component:** B.1a Before $t = \frac{D-d}{c}$, no quantum mediator emitted has reached the other mass. B.1b Immediately after $t = \frac{D-d}{c}$, mediators emitted from the left(right) component of the right(left) mass reaches the right(left) component of the left(right) test mass. B.1c,B.1d Immediately after $t = \frac{D}{c}$, and consecutively $\frac{D+d}{c}$, superposition components separated by distance D, and $D+d$, also establishes quantum communication.

$\langle \mathscr{W} \rangle$ as a function of time is plotted below. Note that the graph takes four regions, $t < \frac{D-d}{c}$, $\frac{D-d}{c} < t < \frac{D}{c}$, $\frac{D}{c} < t < \frac{D+d}{c}$, $t > \frac{D+d}{c}$.

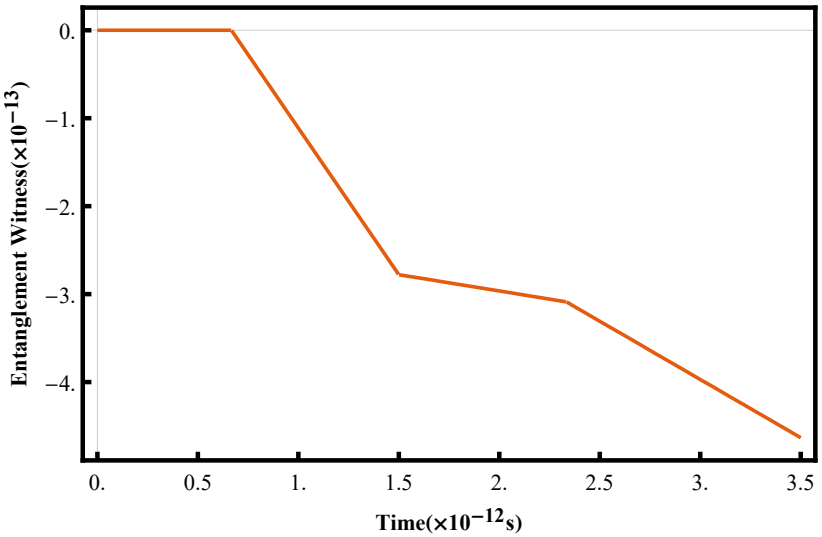

Fig. B.2 **g**ravitational interaction: witness versus time.

We expect that the entanglement witness reaches negative value immediately after $t = \frac{D-d}{c}$. This is when the closest superposition components of the two test masses encounter the edge of each other's light cone.

Similarly, entanglement entropy $E(\rho_{12})$ also generates at different rates in four regions $t < \frac{D-d}{c}$, $\frac{D-d}{c} < t < \frac{D}{c}$, $\frac{D}{c} < t < \frac{D+d}{c}$, $t > \frac{D+d}{c}$. This is attributed to the transmission time of

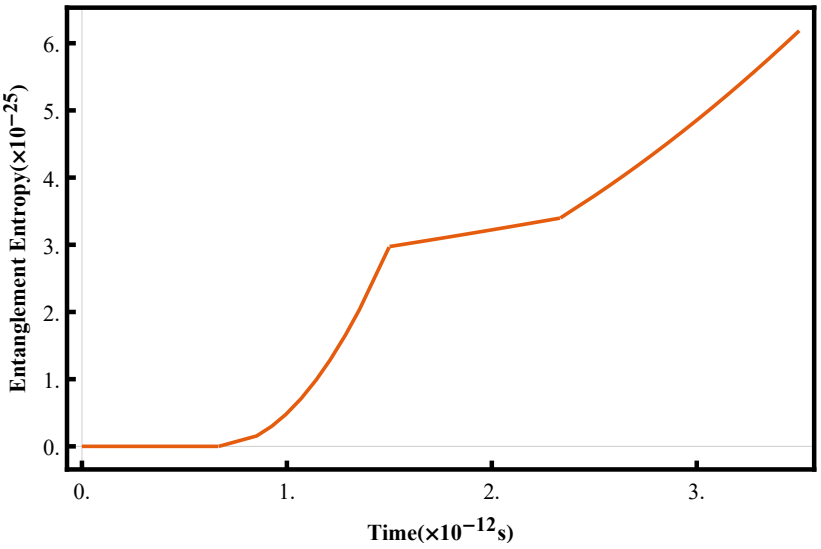

Fig. B.3 **G**ravitational interaction: entropy versus time

gravitons. Each junction point in the figure corresponds to when the light cone of a given superposition component of one test mass reaches that of another mass. The magnitude of entropy at this timescale ($\sim 10^{-12}s$) is of order of magnitude $\sim 10^{-25}$, the detection of which is unattainable with current technology.

decoherence The time span of our proposal ($\sim 10^{-12}$s) is much smaller than the typical coherence time of mesoscopic masses($\sim$ 1s) [28, 165, 144]. The major source of decoherence for orbital degree of freedom is collision with air molecules as well as emission and absorption of blackbody radiation [81, 144, 35, 152]. Take air pressure $\sim 10^{-15}$Pa and temperature 0.15K, the collisional decoherence time is of order of magnitude $\sim$ 1s for test mass $\sim 10^{-14} - 10^{-15}$kg in superposition state with size $\sim 10^{-4}$m. Decoherence due to thermal noise is negligible in comparison with collisional noise. The proposal also requires spin degree of freedom to remain coherent. Coherence time of 1s may be achieved with micro-diamond below 77K [10]. Since the time span of our proposal is much smaller, effects due to decoherence shall be neglected.